



Vurdering av grovpartikkelutskiller ved Elkem Thamshavn

Martin Birger Midthun

Master i produktutvikling og produksjon

Innlevert: juni 2013

Hovedveileder: Erling Næss, EPT

Norges teknisk-naturvitenskapelige universitet
Institutt for energi- og prosessteknikk

EPT-M-2013-83

MASTEROPPGAVE

for

Stud.techn. Martin Birger Midthun

Våren 2013

Vurdering av grovpartikkelutskiller ved Elkem Thamshavn

*Evaluation of course particle separator at Elkem Thamshavn***Bakgrunn og målsetting**

I Elkem Thamshavns silisiumproduksjon genereres store mengder avgasser som inneholder partikler av ulik opprinnelse, kjemisk sammensetning og størrelse. Partiklene separeres fra gasstrømmen i et gassrensesystem og transporteres videre for deponi eller lagring/pakking. Et viktig moment i dette er utskillingen salgbar finfraksjon av partiklene. I denne forbindelsen skal det undersøkes hvorvidt utskillingen av finfraksjon av partikler kan skje mer effektivt i prosessen enn tilfellet er i dag, samt hvordan partikkelutskillingen er i anleggets grovutskiller/radiklon påvirkes av ulike driftsparametre. Arbeidet foregår i samarbeid med Alfsen og Gunderson AS og ElkemThamshavn.

Oppgaven bearbeides ut fra følgende punkter

1. Den eksisterende grovpartikkelutskilleren ved Elkem Thamshavn skal beskrives. Geometri, virkemåte, dimensjoner og nåværende ytelse skal presenteres. Teoretisk underlag for ytelsesberegninger skal presenteres og diskuteres.
2. Det skal utarbeides en beregningsmodell for ytelsesberegninger av grovpartikkelutskilleren. Modellen skal inkludere effekten av relevante driftsparametre. Modellen skal beskrives, og eventuelle begrensninger i modellen skal påpekes og diskuteres.
3. Det skal gjennomføres et måleprogram ved Elkem Thamshavn for å kartlegge hvordan den eksisterende grovpartikkelutskillerens operasjonskarakteristika. Måleprogrammet fastlegges i samarbeid med Elkem Thamshavn AS og Instituttet. Instrumenteringen samt måleprogrammet presenteres. Måleresultatene presenteres, diskuteres og sammenliknes med beregninger fra modellen utviklet i oppgavens pkt. 2.
4. Tiltak for videre optimalisering av driften av grovutskilleren, evt. modifikasjoner på denne for å bedre ytelsen, samt videre utvikling av teoretiske beregningsmodeller skal utarbeides.

Senest 14 dager etter utlevering av oppgaven skal kandidaten levere/sende instituttet en detaljert fremdrift- og eventuelt forsøksplan for oppgaven til evaluering og eventuelt diskusjon med faglig ansvarlig/veiledere. Detaljer ved eventuell utførelse av dataprogrammer skal avtales nærmere i samråd med faglig ansvarlig.

Besvarelsen redigeres mest mulig som en forskningsrapport med et sammendrag både på norsk og engelsk, konklusjon, litteraturliste, innholdsfortegnelse etc. Ved utarbeidelsen av teksten skal kandidaten legge vekt på å gjøre teksten oversiktlig og velskrevet. Med henblikk på lesning av besvarelsen er det viktig at de nødvendige henvisninger for korresponderende steder i tekst, tabeller og figurer anføres på begge steder. Ved bedømmelsen legges det stor vekt på at resultatene er grundig bearbeidet, at de oppstilles tabellarisk og/eller grafisk på en oversiktlig måte, og at de er diskutert utførlig.

Alle benyttede kilder, også muntlige opplysninger, skal oppgis på fullstendig måte. For tidsskrifter og bøker oppgis forfatter, tittel, årgang, sidetall og eventuelt figurnummer.

Det forutsettes at kandidaten tar initiativ til og holder nødvendig kontakt med faglærer og veileder(e). Kandidaten skal rette seg etter de reglementer og retningslinjer som gjelder ved alle (andre) fagmiljøer som kandidaten har kontakt med gjennom sin utførelse av oppgaven, samt etter eventuelle pålegg fra Institutt for energi- og prosesssteknikk.

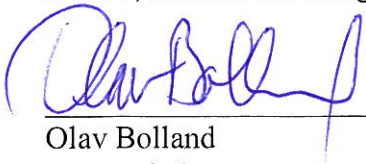
Risikovurdering av kandidatens arbeid skal gjennomføres i henhold til instituttets prosedyrer. Risikovurderingen skal dokumenteres og inngå som del av besvarelsen. Hendelser relatert til kandidatens arbeid med uheldig innvirkning på helse, miljø eller sikkerhet, skal dokumenteres og inngå som en del av besvarelsen. Hvis dokumentasjonen på risikovurderingen utgjør veldig mange sider, leveres den fulle versjonen elektronisk til veileder og et utdrag inkluderes i besvarelsen.

I henhold til "Utfyllende regler til studieforskriften for teknologistudiet/sivilingeniørstudiet" ved NTNU § 20, forbeholder instituttet seg retten til å benytte alle resultater og data til undervisnings- og forskningsformål, samt til fremtidige publikasjoner.

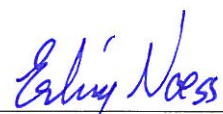
Besvarelsen leveres digitalt i DAIM. Et faglig sammendrag med oppgavens tittel, kandidatens navn, veileders navn, årstall, institutt navn, og NTNUs logo og navn, leveres til instituttet som en separat pdf-fil. Etter avtale leveres besvarelse og evt. annet materiale til veileder i digitalt format.

- Arbeid i laboratorium (vannkraftlaboratoriet, strømningsmeknikk, varmeteknikk)
 Feltarbeid

NTNU, Institutt for energi- og prosesssteknikk, 14. januar 2013


Olav Bolland
Instituttleder

2


Erling Næss
Faglig ansvarlig/veileder

Medveileder(e): Bjørn Saugestad, Elkem Thamshavn

Preface

This report is written in cooperation with NTNU, Department of Energy and Process Engineering and Elkem.

I would like to express my sincere thanks to Bjørn Saugestad and Jørund Vangskåsen for making this project possible. And for taking the time to assist me despite a hectic time at the Thamshavn plant. I would also like to thank Arne Jovik for helping me create this project and for his counseling during the early phase. Final appreciation is given to Erling Næss for providing guidance and support during this whole project. And for driving 30 minuets in -10°C on a motorcycle to discuss my assignment last fall.

"Nothing is less predictable than the development of an active scientific field."
-Charles Francis Richter

Trondheim 01.06.2013

Martin B. Midthun

Abstract

At Elkem Thamshavn, filter south, the gas/particle separation goes through two separation stages. The first one is called a radiclone. This consists of a cyclone and a pre-separator, which object is to pass good quality microsilica to the next separation stage. To create microsilica with 971 quality, the product specification states that $<0.5\%$ of the particles is required to have a diameter of $45\ \mu\text{m}$. The object for this report was to create a model to calculate performance of the radiclone and verify the model with experimental results. This has been used to investigate the amount of fine particles lost in the radiclone, and the amount of coarse particles sent to the next separation stage.

A theoretical study of cyclone efficiency models has been performed. Based on this, an analytical model has been developed to calculate radiclone efficiency by using static particle theory and timed flight theory. Complicated calculations have been avoided by creating an equivalent cylindrical cyclone volume. The developed model assumes a uniform particle concentration in radial direction which eliminates all turbulent features.

Gathered dust samples have been analyzed to obtain the particle size distribution at the radiclone inlet and radiclone dust outlet. This was used to document the current separation efficiency. The developed model was compared to the experimental values for verification. Based on this, further model development has been suggested.

Flow in the radiclone is influenced by adjusting two dampers. One for controlling flow into the cyclone and one for controlling flow from the cyclone to the pre-separator. By creating a factorial experimental set up, the effect of damper positions with respect to performance has been documented.

To recover the fine particles lost in the radiclone, an additional cyclone was installed by Elkem. Introducing pressured air at the bottom of this cyclone makes it possible to control performance. A theoretical study has been performed for similar solutions, and the amount of air flow to obtain wanted performance was calculated based on this.

Sammendrag

Ved Elkem Thamshavn, filter sør, blir partikler separert fra støvholdig gas gjennom to separasjonstrinn. I det først trinnet blir gassen sendt gjennom en radiklon. Denne består av en forutskiller og en syklon. Funksjonen til radiklonen er å fjerne grove partikler slik at microsilica med høy kvalitet blir sendt til neste separasjons trinn. 971 kvalitets microsilica må ifølge produktspesifikasjonen inneholde <0.5 % partikler med en partikkeldiameter på 45 μ m. Målet for denne oppgaven var å utarbeide en beregningsmodell for ytelsesberegninger av radiklonen for så å sammenligne med eksperimentelle resultater. Dette har blitt brukt til å undersøke finfraksjonen av partikler som går tapt i radiklonen og grovfraksjonen som sendes til neste separeringstrinn.

Det har blitt utført et litteraturstudie på beregningsmodeller for syklon ytelse. På bakgrunn av dette har det blitt utarbeidet en beregningsmodell basert på statisk partikkelteori og residenstidteori. Kompliserte beregninger ble unngått ved å regne ut et ekvivalent, sylindrisk syklon volum. Beregningsmodellen antar uniform støvkonsentrasjon i radiell retning slik at turbulente faktorer blir neglisjert.

Partikkelstørrelsesfordelingen ved radiklon inngangen og ved støv utgangen, har blitt funnet ved å analysere støvprøver. Resultatene har blitt brukt for å dokumentere nåværende ytelse. De har også blitt sammenlignet med beregningsmodellen. Basert på dette er det foreslått tiltak for videreutvikling av beregningsmodellen.

Strømningen i radiklonen kan påvirkes ved å endre på to spjeld. Et for å kontrollere gassmengden inn i syklonen og et for å kontrollere gassmengden fra syklonen til forutskilleren. Et faktorielt måleprogram har blitt designet for å avgjøre spjeldposisjonenes effekt på radiklonytelse.

For å minske finfraksjonen av partikler som går tapt i radiklonen, har Elkem installert en ekstra syklon. Fire spjeld ved syklonbunnen gir mulighet til å tilføre falskluft og dermed påvirke ytelsen. Et litteraturstudie har blitt gjennomført på lignende løsninger. Basert på dette har mengden falskluft, nødvendig for ønsket ytelse, blitt beregnet.

Table of Content

Preface	I
Abstract	II
Sammendrag	III
Table of Content	IV
List of Figures	V
List of Tables	VII
Nomenclature	VIII
1 Introduction	1
1.1 Background	1
1.2 Objective and Method	1
1.3 Structure and Limitations	2
2 Basic Principles for a Cyclone	4
2.1 Performance	5
2.2 Cyclone Applications	8
3 A Theoretical Study of Cyclone	
Efficiency Models	11
3.1 Collection Efficiency	13
3.2 Velocity Profile	17
3.3 Residence Time	21
3.4 Pressure Drop	23
4 Filter South - Elkem Thamshavn	28
5 Radiclone at Filter South	31
5.1 Functionality	31
5.2 Dimensions	37
5.3 Theoretical Basis for Performance	38
5.4 Current Performance	41
6 An Analytical Model for Predicting Radiclone Efficiency	45
6.1 Radiclone Velocity Profile	45
6.1.1 Radial Particle Velocity	45
6.1.2 Tangential Particle Velocity	50
6.2 Radiclone Grade Efficiency	52
6.3 Model Parameters	57
6.4 Result - Radiclone Model	59
6.5 Verification and Validation	59

7	Optimizing the Radiclone Performance	62
7.1	Method	62
7.2	Radiclone Damper Experiment	64
7.2.1	Results	65
7.2.2	Evaluating Data	66
7.2.3	Recommended Measures	69
7.3	Radiclone Damper Post Experiment	70
7.3.1	Results	70
7.3.2	Evaluating Post Experiment Data	71
8	Additional Separation Stage at Filter South - Cyclone With Air Injection	73
8.1	A Theoretical Study of Cyclones With Additional Streams	73
8.2	New Cyclone Description	77
8.3	Calculating Optimal Volumetric Flow Into the New Cyclone	78
8.4	Discussion	80
8.5	Recommended Measures	81
9	Conlusion	82
10	Further Research	83
	Appendix	87
A	Technical Drawings of the Radiclone	88
B	Microsilica Grade 971	94
C	MatLab Codes for Cyclone Performance	95
D	Articles	99
	Processes Use Many Collector Types [1]	99
	The Cyclone Efficiency of Cyclone Type Particle Collectors [2]	103
E	Pitot Calculations	109

List of Figures

2.1	Reverse flow cyclone	4
2.2	Different inlet arrangements	5
2.3	Typical particle size distribution	6
2.4	A selection of various industrial cyclone solutions	9
2.5	Cyclones for commercial use	10
3.1	Dimensions of a tangential inlet cyclone	11

3.2	Schematic diagram of flow rate through the collection zone with modified cyclone design	12
3.3	Collection efficiency of a cyclone based on the cut-size diameter . . .	13
3.4	Grade efficiency curve characteristics	14
3.5	Particle trajectories influenced by wall boundary layer	16
3.6	Velocity profile in a tangential inlet cyclone	18
3.7	Tangential velocity distribution in a Cyclone	19
3.8	Cylindrical shaped vortexes caused by the theoretical shift from the outer to the inner cyclone vortex.	20
4.1	Filter south layout	28
4.2	Single chamber pulse-jet filter	29
4.3	Dust sampling locations	30
5.1	Radiclone at filter south	31
5.2	Cell feeder (left) and vibrator (right)	32
5.3	Radiclone at filter south from above	32
5.4	Inlet of the radiclone	33
5.5	Inlet gas transport duct	33
5.6	Gas path in pre-separator	34
5.7	Upper knife damper position handle	34
5.8	Lower knife damper position handle	35
5.9	Gas path in the cyclone	35
5.10	Over head duct and the associated damper	36
5.11	Radiclone gas outlet	36
5.12	Radiclone dimensions	37
5.13	Top (left) and bottom (right) radiclone plate	37
5.14	Overhead duct dimensions	38
5.15	Diagram to determine cyclone size	40
5.16	Particle size distribution	41
5.17	Particle size distribution	42
5.18	Total mass flow into the radiclone versus particle diameter	43
5.19	Mass flow into the radiclone and mass flow at the radiclone dust outlet versus particle diameter	43
5.20	Grade efficiency curve	44
6.1	Particle path when the centrifugal forces exceeds drag forces	46
6.2	Curvilinear motion	47
6.3	Drag coefficient of a spherical particle	48
6.4	Three different scenarios of particle trajectory within the cyclone . . .	50
6.5	Control volume for calculating the tangential gas velocity	51
6.6	Control volume for particle separation model	53
6.7	Volumes used for calculating t_{res}	55

6.8	Location for taking pitot samples at the overhead duct	57
6.9	Grade efficiency curve, radiclone filter south	59
6.10	Present model compared to a selection of other models	60
6.11	Comparing model to experimental results	61
7.1	Radiclone dampers	62
7.2	CS-2000 Carbon/Sulfur Determinator	63
7.3	Sieving with 45 μm mesh size	63
7.4	Radiclone experiment 14/02-15/02	65
7.5	Dust production	65
7.6	Correlation between μ_{45} and C	66
7.7	Correlation between μ_{45} and DP	67
7.8	Correlation between C and DP	67
7.9	2x2 factorial analysis performed in Minitab	68
7.10	Regression fit for μ_{45} and C	69
7.11	Dust samples taken from filter south	70
7.12	Dust samples taken from filter south	70
7.13	Dust samples taken from filter south	71
7.14	Dust samples taken from filter south	71
8.1	Test cyclone, seen from above with two clean air inlets	73
8.2	Showing F_c / F_d versus radial distance	74
8.3	Double inlet cyclone. Seen from above	75
8.4	Experimental cyclones used by Yoshida et al.	76
8.5	The new cyclone	77
8.6	The new cyclone	77

List of Tables

3.1	Critical and cut-off diameter derived with various methods	17
3.2	Standard designs for tangential inlet cyclones	25
3.3	Different cyclone efficiency models	27
6.1	A mathematical model to predict grade efficiency	56
6.2	Pitot measurements in overhead duct	58
6.3	Radiclone parameters	58
7.1	Damper positions	64
7.2	2x2 factorial design setup	64
7.3	Statistical data for the three different sampling sessions	72
8.1	Radiclone parameters	79

Nomenclature

a_p	particle acceleration
a_{pr}	radial particle acceleration
$a_{\theta p}$	tangential particle acceleration
c	particle concentration
c_0	initial particle concentration
d_{50}	cut-size (cut-off) diameter - particles collected with 50 % efficiency
d_{100}	critical particle diameter - particles collected with 100 % efficiency
d_p	spherical particle diameter
D	cyclone body diameter
D_c	cyclone particle outlet diameter
D_e	cyclone gas outlet diameter (vortex finder diameter)
D_l	radiclone scaling parameter
Eu	Euler number
f	particle frequency distribution
f_c	frequency distribution of coarse particles collected by the cyclone
f_f	frequency distribution of fine particles escaping the cyclone with the gas
F_c	centrifugal force
F_d	drag force
F_p	pressure force
g	gravitational constant
h	control volume 1 height
H	cyclone inlet height
ΔH_{vh}	cyclone velocity heads
\mathbf{i}, \mathbf{j}	cartesian unit vector for x and y direction respectively
K	Bøckmans pressure factor
l	natural vortex length
L^*	modified cyclone height
L_b	cyclone body length
L_c	cyclone cone length
m_p	particle mass
M	total solid mass flow rate entering the cyclone
M_c	solid mass flow rate of coarse particles collected by the cyclone
M_f	solid mass flow rate of fine particles escaping the cyclone with the gas
n	vortex exponent
N	number of effective turns
p	pressure
p_{dyn}	dynamic pressure
p_{static}	static pressure

p_{tot}	total pressure
Δp	pressure drop
Q	incoming volumetric flow to cyclone
Q_O	volumetric flow from the oven
r	radial polar (cylindrical) coordinate
r_i	radial distance from cyclone axis to innermost particle at entry
R	cyclone body radius
R^*	modified cyclone radius
R_e	cyclone vortex finder radius
Re	gas Reynolds number based on gas velocity
Re_p	particle Reynolds number based on particle terminal velocity
S	gas outlet duct length
Stk_{50}	Stokes number based on particle cut-size diameter
t	time variable
t_∞	residence time calculated from terminal velocity
\bar{t}_{res}	average residence time
t_{res}	residence time
T	temperature
T_0	ambient temperature
$\mathbf{u}_r, \mathbf{u}_\theta$	polar unit vector for r and θ direction respectively
v_r	radial gas velocity
v_θ	tangential gas velocity
$v_{\theta \max}$	maximum tangential gas velocity
$v_{\theta R}$	tangential particle velocity at the cyclone wall
v_p	particle velocity
v_{rp}	radial particle velocity
v_R	radial particle velocity at the cyclone wall
$v_{\theta p}$	tangential particle velocity
v_t	terminal particle velocity
V_c	cyclone inlet velocity
W	cyclone inlet width
z	axial cylindrical coordinate

Greek letters

α	control volume 1 angle
η	grade efficiency
η_T	total efficiency
θ	tangential polar (cylindrical) coordinate
μ	gas viscosity
ρ_g	gas density
ρ_p	particle density
ϕ	cyclone cone angle

1 Introduction

This section is dedicated to give a brief explanation of the background for this assignment. Further, the objective and method for this assignment is described, and finally the structure and limitations is listed.

1.1 Background

The silicon production at Elkem Thamshavn produces large quantities of dust laden off-gas. This dust is made up from particles with different origin, chemical composition and size. A significant part of the plants revenue comes from selling microsilica, which is one type of particles contained in the off-gas. To capture microsilica, the off-gas goes through a separation process. Two such separation processes are present at Thamshavn, and are labeled filter south and filter north. Early in the process of filter south, a coarse particle separator is used to remove unwanted particles. The coarse particle separator is called a radiclone which is a cyclone with a pre-separator. All the unwanted particles are thrown away after removal which makes the radiclone to generate a lot of waste. Dust analysis by Elkem has shown that this waste contains a significant fraction of good quality microsilica. The main focus of this report is to determine current performance of the radiclone in order to find out if separation can be more efficient.

1.2 Objective and Method

The main objective of this report is to investigate the possibility of running the radiclone more efficiently. The following secondary objectives are included in the report:

1. Describe the radiclone at Elkem Thamshavn, filter south.
2. Investigate performance prediction models for similar equipment.
3. Develop a prediction model for radiclone performance.
4. Investigate current performance of the radiclone.
5. Assist with the installation of an additional cyclone.

Secondary objective 1 was divided into two smaller objectives:

- Acquire technical drawings of the radiclone from Elkem.

- Gather all information regarding the calculations of radiclone performance by Elkem.

Secondary objective 2 was based on passive research. This was done by gathering and systemizing the results of others which is given in the reference list.

Secondary objective 3 was divided into three smaller objectives:

- Gather suited information from secondary objective 2 for the model.
- Obtain relevant operational parameters from Elkem.
- Determine unknown parameters by doing measurements.

Secondary objective 4 was divided into three smaller objectives:

- Analyzing dust samples to determine separation efficiency.
- Investigate how changes in operation influences performance.
- Suggest efficient operation criteria.

Secondary objective 5 could be done when the plant had a steady operation.

1.3 Structure and Limitations

The most significant part of the radiclone is a cyclone. This is where the actual separation occurs. This report is therefore structured by presenting a general overview of how a cyclone works in section 2. This section also includes some basic principles for calculating cyclone performance.

Section 3 is a theoretical study of the cyclone mechanics. This also sums up different analytical performance models developed over the years. Much weight has been given to research done from 1950-2000. The cyclone mechanics has been known for a long time, and when it comes to analytical models, many of the earlier results is still used. The theoretical study discusses the results of many scientists, but emphasizes those results that is used in the analytical model in a later section.

Section 4 gives a short introduction to how filter south operates. Most weight has been given to describe the pulse-jet filter as this the main separation stage. This section also includes a description of where dust samples for analysis was taken.

Section 5 describes the radiclone in detail. The primary focus of this section is to describe the gas/particle path through this separation stage. Because of

secret/limited information provided by Elkem, the part about presenting actual calculations done when building the radiclone, was given less weight. The section also includes a description of current performance based on information from Elkem and analyzed dust samples. This part is given most focus because the information is valuable to Elkem and it is used to validate the analytical performance model.

Section 6 gives the derivation of the analytical model suggested for calculating radiclone performance. The section gives much focus to the actual derivation and assumptions used. A comparison with the current performance results from the previous section, are done to check the model validation. The model parameters were also used with other cyclone models for comparison.

Section 7 describes an experiment conducted to improve radiclone performance. The experiment was limited to regulate gas flow by varying the positions of two dampers. This section also includes an analysis of dust samples gathered at a later time. This was to determine the effect of the new damper positions.

Section 8 gives a short overview of the research done for controlling cut-off diameter in a cyclone. This is followed by a calculation of volumetric flow into the cyclone to achieve the wanted effect. Most focus has been given to the fact that this is very hard to do analytically, and why.

It was originally intended that secondary objective 5 would be weighted the most. Because of several production stops at Thamshavn, the installation of the additional cyclone was postponed until july. Because of this, more weight has been given to the analytical model and the theoretical study. The small theoretical study of cyclones with air injections, in addition to the simple calculations in section 8, was also added to the report because of this.

2 Basic Principles for a Cyclone

A cyclone (or cyclone separator) is used in industry to remove solid particles from a gas or a liquid without the use of filters. This report will focus on the gas-solid separation, although the basic principles of operation are the same. Cyclones were first used to remove dust from gases in the 1880's and are still used due to its many advantages. They are simple, inexpensive to make, economical to operate and can be used in a wide variety of operating conditions such as high temperature, high pressure and high dust concentration.

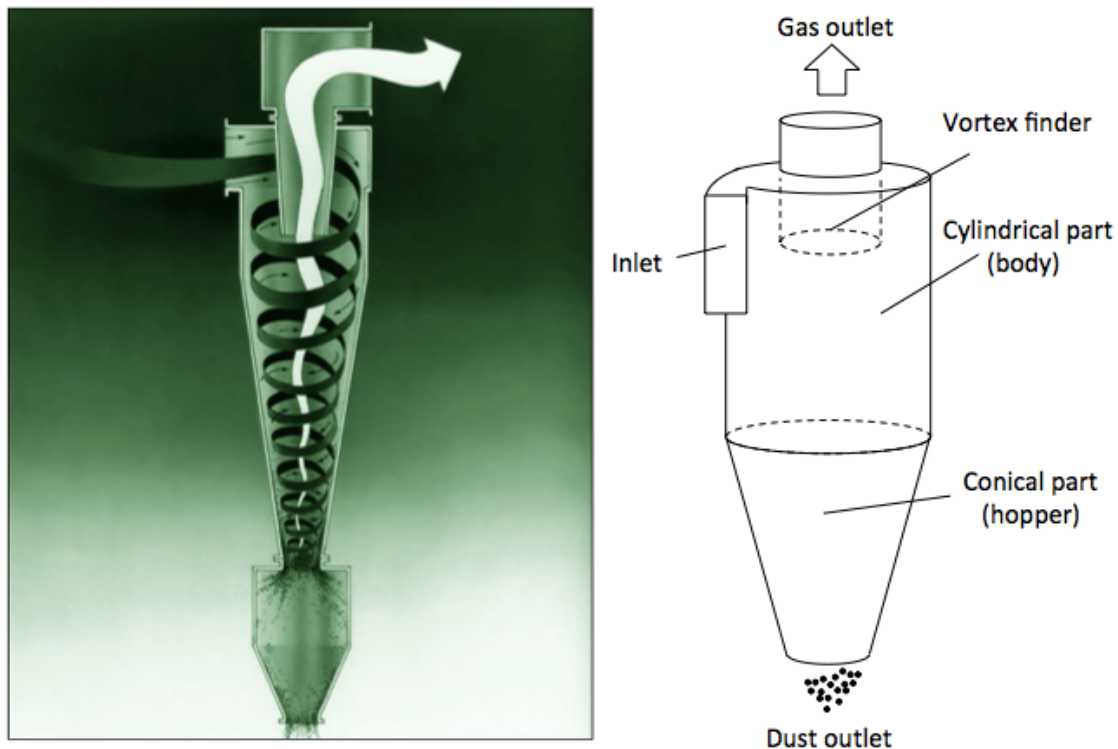


Figure 2.1: Tangential inlet reverse flow cyclone. Left picture shows a simplified flow pattern [3]

Over the years, many cyclone designs have been suggested and manufactured. For industrial gas cleaning however, the "reverse-flow" cyclone is the most common. This is made up by a cylindrical part on top and a conical part at the bottom as showed in figure 2.1. There are many different inlet arrangements. This report will focus on inlet type (a) from figure 2.2. For this design, a gas-solid mixture is brought tangentially into the cyclone body through the inlet. Typically the

gas is pulled through the cyclone by a fan located further downstream in the process. After entering, the gas forms a vortex with a helical pattern caused by the circular geometry. This is labeled the "outer vortex". This is where the separation occurs. Due to the increasing gas velocity, particles within the gas experience large centrifugal forces caused by the outer vortex, and are pushed radially towards the cyclone wall. This happens to all the particles that are sufficiently dense such that the centrifugal forces exceeds the drag from the vortex. Once a particle collides with the wall it is slowed down by frictional forces. The particles will therefore be separated from the main gas stream and pushed down towards the conical part by the downward component of the gas velocity. Gravity has been shown to have little effect. The centrifugal forces is a function (among others) of particle mass, hence heavier particles is collected more easily. The separated solid particles leaves the cyclone at the dust outlet. When the gas reaches the conical part bottom the rotation changes direction and a reverse vortex is created, labeled "inner vortex". This rotates about the cyclone axis and moves upwards and through the gas outlet.

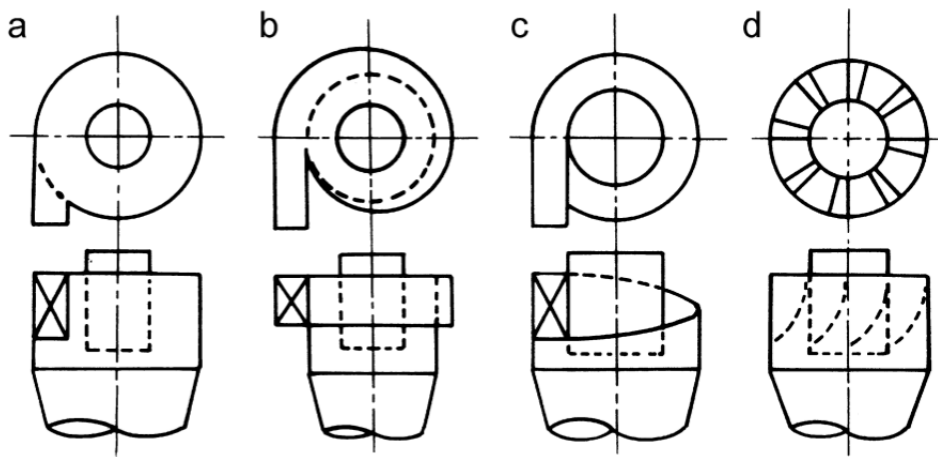


Figure 2.2: Different inlet arrangements (a) tangential, (b) scoll, (c) helicoidal, (d) axial [4]

2.1 Performance

There are several measures that describe the operational performance of a cyclone. The most common are: Total efficiency, grade efficiency, cut-off diameter and pressure-drop.

Particle Size Distribution

Industrial dust contain particles of many sizes. The basis for many particle

separation theories is to determine the particle size distribution. This is a continuous mathematical function that defines the relative amount of particles according to particle size. Figure 2.3 shows a typical particle size distribution with one mode. The cumulative distribution is denoted as F and the frequency distribution as $dF/dx = f(x)$.

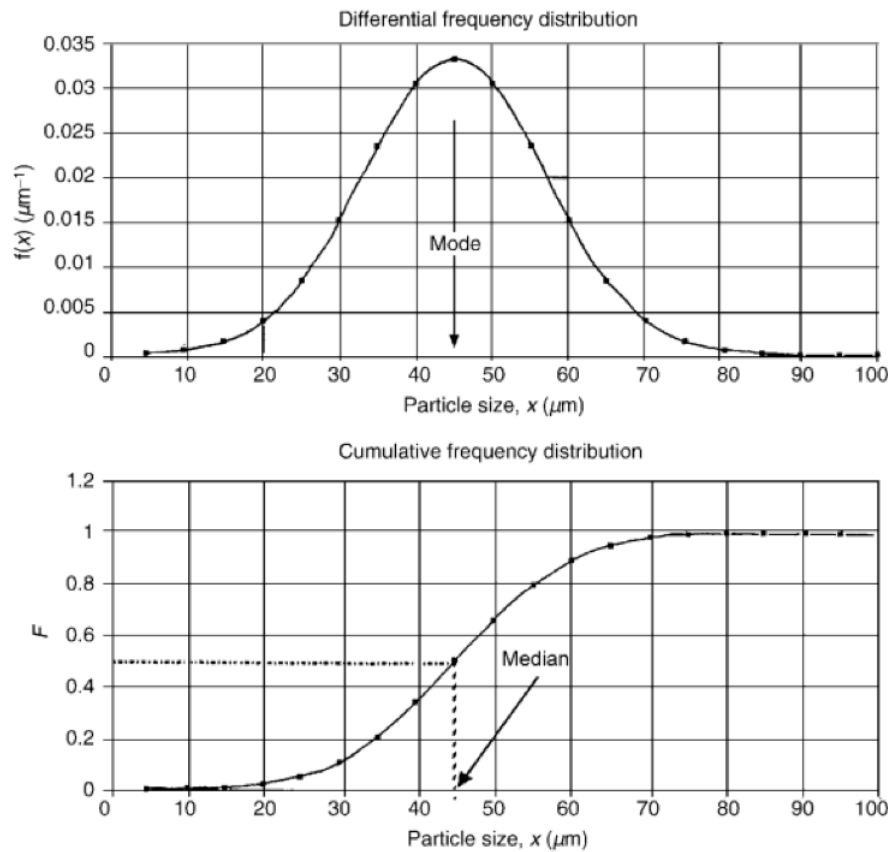


Figure 2.3: Typical particle size distribution. Given as differential and cumulative frequency [5]

Total efficiency

The total efficiency of a cyclone is based on the mass of solid particles that are separated from the gas. Consider a cyclone where the total flow rate of solid mass is M . From this total mass flow, a fraction is collected by the cyclone. It is therefore convenient to split the solid mass flow rate into two components:

$$M = M_f + M_c \quad (2.1)$$

M_c is the mass flow rate of coarse particles that are collected by the cyclone. And M_f is the mass flow rate of fine particles that escapes with the gas. This can also be expressed for each particle size x using the notation from figure 2.3:

$$Mf(x) = M_f f_f(x) + M_c f_c(x) \quad (2.2)$$

The total efficiency of a cyclone is then defined as:

$$\eta_T = \frac{M_c}{M} \quad (2.3)$$

η_T can also be calculated by multiplying the fraction of particles with size x by the efficiency of this particle size. The sum of all the products gives the total efficiency.

$$\eta_T = \int_0^1 \eta(x) df \quad (2.4)$$

where f is the differential frequency dF/dx .

Grade efficiency

As mentioned earlier, particles with a bigger mass is collected more easily. The fraction of collected mass is therefore a function of the particle size distribution. By using this concept, that each particle size has a separate efficiency, the grade efficiency defined is as

$$\eta(x) = \frac{\text{mass of solids of size } x \text{ in coarse product}}{\text{mass of solids of size } x \text{ entering the cyclone}} \quad (2.5)$$

or (based on equation 2.2):

$$\eta(x) = \frac{M_c f_c(x)}{M f(x)} \quad (2.6)$$

Combining this equation with 2.3 gives a relationship between total and grade efficiency.

$$\eta(x) = \eta_T \frac{f_c(x)}{f(x)} \quad (2.7)$$

This can also be given in terms of the particle concentration c at a given time after entering the cyclone, and the initial concentration c_0 which is M per cubic meter of gas entering the cyclone.

$$\eta = 1 - \frac{c}{c_0} \quad (2.8)$$

A spherical particle shape is usually assumed so that $x = d =$ particle diameter. For better approximation, spherical equivalent diameters could be applied instead. In this report, all particles are assumed to have a spherical shape so: $x = d_p =$ the spherical particle radius.

Grade efficiency is very close to 1 for particles with $d_p = 100 \mu m$ and decreases to very small values for $d_p < 1 \mu m$ [5].

Cut-off diameter

Cut-off (d_{50}) is the particle diameter that is collected with a 50 % efficiency. As the cut-off diameter increases the total efficiency decreases.

Critical diameter

This is the particle diameter that is collected with 100 % efficiency (d_{100}). Since collection efficiency increases gradually with increasing particle diameter and approaches 100 % only as a limit, this value is usually determined analytically.

Pressure drop

Pressure drop over the cyclone is an important performance parameter because it is directly proportional to the energy consumption. There are generally a trade-off between pressure drop and total efficiency. Higher pressure drop means higher collection efficiency, but more energy consumption.

2.2 Cyclone Applications

Cyclones are usually divided into two main categories. "High efficiency"- and "high rate"-cyclones. High efficiency cyclones has a small gas inlet and outlet. They also have long bodies, and they have high recovery rate. High rate cyclones however, are usually shorter and have large gas inlet and outlet. They perform with medium recovery rate, but can handle much bigger loads.

Cyclone separators are used in many applications. Both in industry and private. Simple bag less vacuum cleaners (figure 2.5) and a wide variety of landscaping equipment are a couple of examples of cyclone technology utilization. In bag less vacuum cleaners, many small cyclones would be working in a parallel system. This

is to save space while conserving efficiency. For industrial purposes, cyclones are for instance used to extract airborne sawdust particles from the air in wood products workplace environments. They are also used in many combustion processes. Such processes produce fine particles and fuel ashes that cannot be discharged to the environment. In these situations, cyclones would collect these particles before the gas is let out in the atmosphere. Another use is to control dust from cement kilns. Un-processed particles are sent back to the kilns, and the exhaust gas is efficiently cooled down before discharging. For such processes, usually 1-6 cyclones operate in series to achieve maximum efficiency. Another use is in professional kitchen ventilation systems. Cyclones is then used to separate grease from air. Cyclones can also be very small. The small ones are used in the field of medicine for biomedical and micro chemical processes. Researches are currently looking at the possibility to use cyclones as micro separation techniques for detection of cancer cells.



Figure 2.4: A selection of various industrial cyclone solutions [6] [7]

Cyclones can also be used with fluids as working medium. It is then referred to as hydro-clones, and a pump is usually used instead of a fan. The principles are the same, but the solid particles are carried in a fluid, for instance oil or water. Hydro-clones are usually used to supply a primary separation stage that cannot handle large particles. One application is to separate solid waste from water in a sewage treatment plant. Hydro-clones are also used to separate oil from gas in oil refineries. For hydro-clones that are not powered by a pump, the liquid is poured down into the cyclone and a rotating object inside causes the fluid motion. The principles are the same, and particles are pushed towards the wall. This kind of arrangement requires a vertically placed hopper as the fluid will exit at the bottom. One type of hydro-clone is used at Ringnes E.C. Dahls brewery in Trondheim.

After the fermentation process, the remaining hops and malt particles are separated from the beer. Using a hydro-clone for this purpose is a cheap and efficient solution.



Figure 2.5: Cyclones for commercial use [8]

3 A Theoretical Study of Cyclone Efficiency Models

Analytical investigations of cyclone performances started in the early 1930's. Even though the basic principles are well understood, the turbulent features occurring in the cyclone is hard to generalize. Due to the vast complexity of this problem, a general satisfactory model has not yet been developed. However, if the analytical model is customized to fit a specific physical cyclone, trustworthy predictions is obtainable.

Figure 3.1 shows a standard way to label the dimensions of a cyclone.

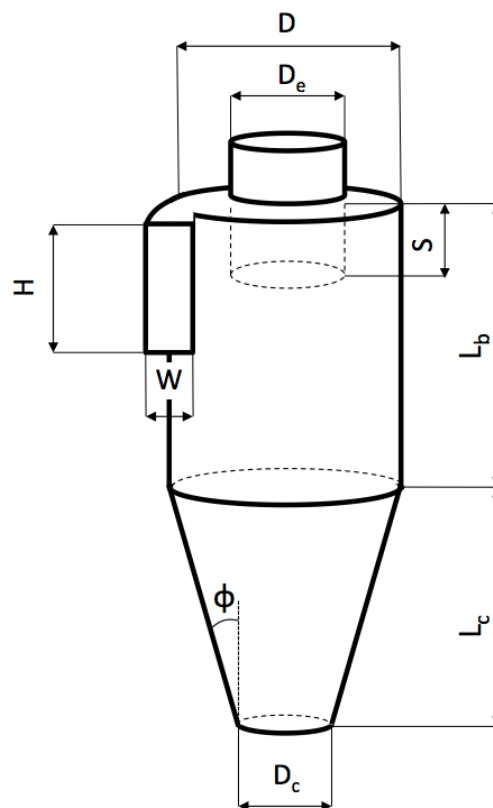


Figure 3.1: Dimensions of a tangential inlet cyclone

To avoid the non-uniform effect from the cyclone cone, thus making calculations simpler, it is common to calculate an equivalent cyclone radius R^* , and an equivalent cyclone height L^* . This height and radius generates a modified cylindrical design that is used as an approximation to the cyclone geometry. This is usually derived

using the principle of conservation of effective volume. The idea of an equivalent cyclone radius was originally proposed by Leith and Licht [2]

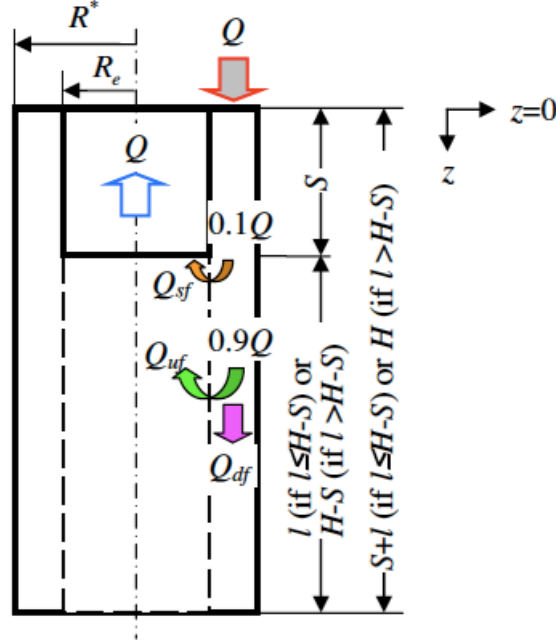


Figure 3.2: Schematic diagram of flow rate through the collection zone with modified cyclone design. The distribution of Q is explained further in section 3.3. In the figure $H = L_c + L_b$ [9]

There are many different ways of calculating R^* and L^* . The one suggested by Leith and Licht [2] gives the height of this equivalent geometry based on the natural vortex length (see section 3.2). If this natural vortex length l exceeds the height of the cyclone, l is the height of the equivalent cylinder. If not, $L_c + L_b$ is the height. This is because collection primary occurs within the range of l . R^* is found from the following calculations:

$$R^* = \left[\frac{V_{cs}}{\pi(S+l)} \right]^{1/2} \quad \text{for } l \leq L_c + L_b - S \quad (3.1)$$

where

$$V_{cs} = \frac{\pi D^2 L_b}{4} + \frac{\pi D^2 (S+l-L_b)}{4} \left[1 + \frac{D_0}{D} + \left(\frac{D_0}{D} \right)^2 \right] \quad (3.2)$$

$$D_0 = D - \frac{(D-D_c)(S+l-L_b)}{L_c} \quad (3.3)$$

or

$$R^* = \left[\frac{V_{cs}}{\pi(L_b + L_c)} \right]^{1/2} \quad \text{for } l > L_c + L_b - S \quad (3.4)$$

where

$$V_{cs} = \frac{\pi D^2 L_b}{4} + \frac{\pi D^2 L_c}{4} \frac{1}{3} \left[1 + \frac{D_e}{D} + \left(\frac{D_e}{D} \right)^2 \right] \quad (3.5)$$

3.1 Collection Efficiency

The first collection efficiency models was very simple and produced the cut-size diameter only. This gave a discontinuous function where any particle below d_{50} had a 0 % collection and every particle above d_{50} is collected with a 100 % efficiency (figure 3.3). In reality, the discontinuous jump is replaced by a gradually growth before d_{50} and a gradually decrease after. The limits remain the same at 0 and 1 which causes an overall s-shaped curve.

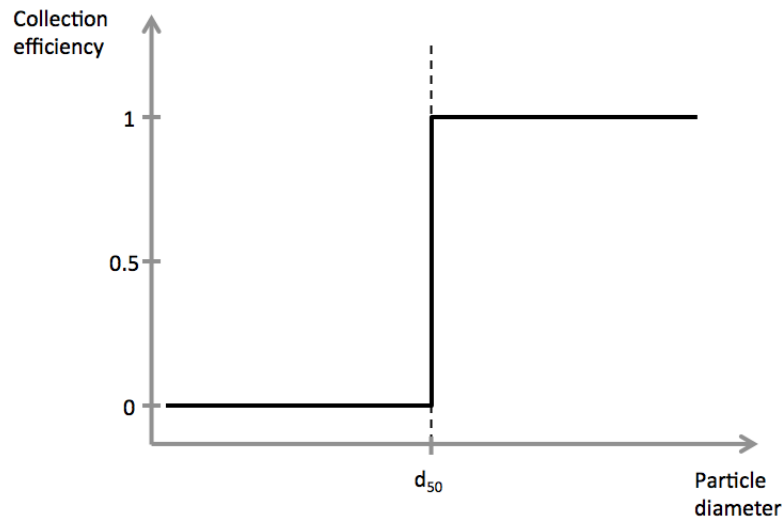


Figure 3.3: Collection efficiency of a cyclone based on the cut-size diameter

One of the first collection efficiency theories that produced a grade efficiency curve, was developed by Lapple [1]. Even though the model is fairly simple and with few parameters, many other scientists have based their research on Lapple's work. He suggested that the cyclone efficiency depended on how many times the gas rotated around the outer vortex axis before reaching the bottom. This was determined by

an empirical relation and named “the number of effective turns”. Further he used a particle force balance. The drag force from the gas was set equal to the centrifugal force caused by the vortex. When these two forces are equal there is 50 % chance that the particle will be collected by the cyclone. Based on this fact the cut-off diameter (d_{50}) was calculated, and then the grade efficiency η . Later research by Wang [10] showed that the calculated number of effective turns was only accurate for a very limited number of cyclone designs.

Barth (read in [11], originally from [12]) derived an expression for particle acceleration in the cyclone by using curvilinear motion theory. Using this acceleration in a force balance together with the terminal settling velocity calculated from Stokes Law, he developed a model to predict grade efficiency. For any particle size, the collection efficiency is determined from the ratio of its terminal velocity to the terminal velocity of the static particle. This model has been shown to return very different results for increasing cyclone diameter. In addition, this model proves unable to predict collection efficiency for cyclones with diameter over a certain limit. Ioza and Leith [13] improved Barth’s model by suggesting new empirical equations to estimate diameter, cyclone axis length, maximum tangential velocity and how these parameters are affected by the remaining cyclone dimensions.

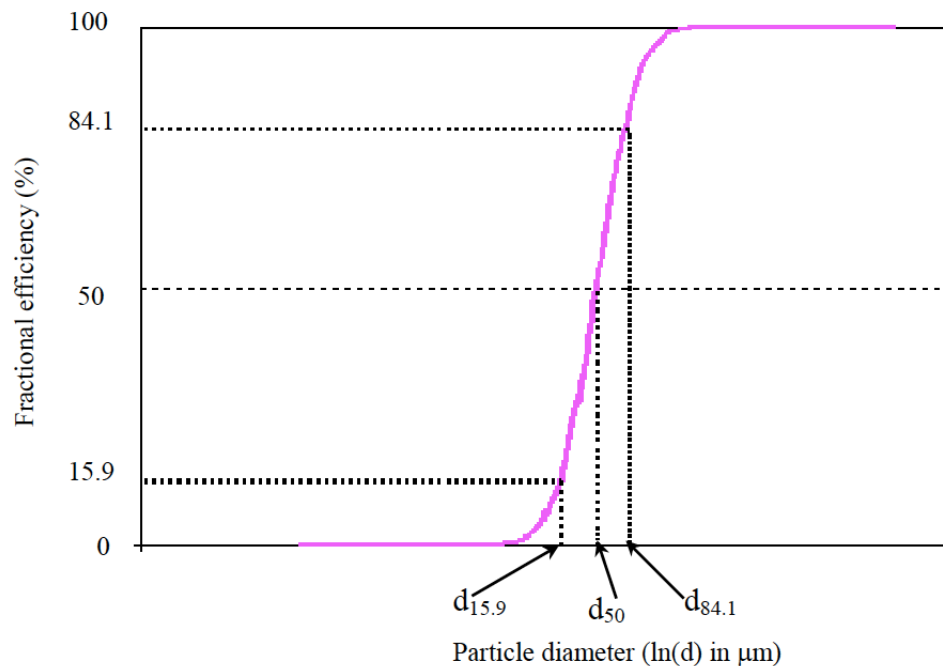


Figure 3.4: Grade efficiency curve characteristics [10]

In her dissertation, Wang [10] came up with many interesting results. First she

pointed out that the most common shape for a grade efficiency curve obtained by various models, has a cumulative lognormal shape. She also found that a good approximation for such a curve had the slope = $d_{84.1}/d_{50} = d_{50}/d_{15.9}$. This is shown in figure 3.4.

She also argued that 1D3D and 2D2D cyclones gives the highest total efficiency for dust laden gas with particles under $100 \mu m$. (An xDyD cyclone has dimensions $L_b = x \cdot D$ and $L_c = y \cdot D$). Among other scientist, she pointed out some of the flaws with the Lapple model and suggested a new way of determining the number of effective turns. Using this with Barth's particle acceleration she derived a new model for grade efficiency and d_{50} .

Parnell [14] documented that each cyclone design has one optimum inlet velocity when it comes to collection efficiency. The Lapple model did not account for inlet velocity, which was pointed out by Parnell, among other flaws. He therefore suggested an alternative model, based on many of the same principles. The idea was that an engineer could chose a wanted inlet velocity and then calculate all the cyclone dimensions from this one parameter. However, this model is not able to calculate either cut-off diameter or grade efficiency which therefore limits its uses.

The Lapple model also has many similarities to the one proposed by Alexander (read in [9], originally from [15]). Instead of using the number of effective turns he introduced the concept of "natural vortex length". This is defined as the vertical length from the bottom of the vortex finder to the transition point where the vortex changes direction. Alexanders natural vortex length is given by the empirical relation:

$$l = 2.3D_e \left(\frac{D^2}{HW} \right)^{1/3} \quad (3.6)$$

where all the parameters is given in figure 3.1. This result led to a discussion on whether the vortex length was dependent on inlet velocity or not, and other empirical relations were suggested to implement this parameter [16]. It was later shown that the effect of inlet velocity was only significant for small cyclones. When calculating the performance of an industrial cyclone by using natural vortex length, Alexander's model is in most cases applied [9].

Zhao has contributed a lot to cyclone research the last years. In 2005 [17] he developed a model to predict grade efficiency based on flow pattern, critical particle separation theory and boundary layer separation theory. One limitation is the assumption of a particle size distribution with one mode. Later [9] he proposed a different model which he labeled: "A time-of-flight model". Using the concepts

of Leith and Licht he developed different expressions for the gas residence time depending on the natural vortex length for given cyclone designs. This model also accounts for the short-circuit flow that is absorbed by the vortex finder.

The previously discussed models are just a few of the cyclone models out there. However, most of the models are derived around three different school of thoughts: Static particle theory, timed flight theory or boundary layer theory. Table 3.1 shows several results based on these methods.

Static particle theory

The calculations are based on the tangential velocity at the edge of the core (all the axial positions in the cyclone body at $r = R_e$). It is the maximum tangential velocity which sets an upper limit to the particle size that can remain in the outer vortex. This is found by balancing the drag force with the centrifugal force of the particle. This “static particle” will then remain suspended at the edge of the core. The static particle will then remain stationary which leads to the assumption that there is no radial acceleration or velocity.

Timed flight theory

Collection efficiency is based on the time a particle is suspended in the cyclone. This time is labeled “residence time” and is calculated from cyclone dimensions and inlet velocity. This is explained further in section 3.3.

Boundary layer theory

The boundary layer starts to become more important as the cyclone size decreases. Depending on the velocity developing near the walls, particle movement will be influenced by the boundary layer as showed in figure 3.5.

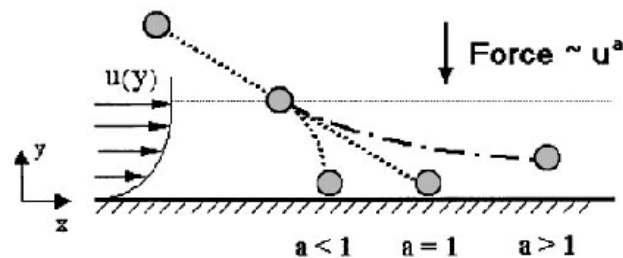


Figure 3.5: Particle trajectories influenced by wall boundary layer [18]

The cyclone is divided into two regions: Core region and the boundary layer region. First, the particle flux distribution into the boundary layer is calculated, then the collection of particles on the wall. Perfect radial mixing is assumed in the boundary layer i.e. no concentration gradient.

Source	Equation
Static particle theory	
Ioza and Leith [13]	$d_{50} = \left(\frac{9Q\mu}{\pi N \rho_p v_{\theta_{\max}}^2} \right)^{1/2}$
Barth [19]	$d_{50} = \left(\frac{9\mu D_e v_R}{\rho_p v_{\theta R}^2} \right)$
Barth [19]	$d_{100} = \left(\frac{9Q\mu}{\pi(L_b + L_c - S)\rho_p v_{\theta_{\max}}^2} \right)^{1/2}$
Time of flight theory	
Lapple [1]	$d_{50} = \left(\frac{9\mu W}{2\pi \rho_p V_c N} \right)^{1/2}$
Lapple and Shepherd [20]	$d_{100} = \left(\frac{9\mu D_e}{2\pi \rho_p V_c N} \right)^{1/2}$
Fayed and Otten [19]	$d_{100} = \left[\frac{9\mu D^2 \left(1 - \frac{2r_i}{D}\right)^{2n+2}}{4(n+1)V_c^2 \rho_p t_{\text{res}}} \right]^{1/2}$

Table 3.1: Critical and cut-off diameter derived with various methods

3.2 Velocity Profile

Early investigations by Sheperd and Lapple [20] showed that the velocity profile in a cyclone consists of a inner and a outer vortex. The vortexes was observed with helical shapes. Because of this, it was found most convenient to use cylindrical coordinates when describing velocity profile. The three components are denoted v_r (radial velocity), v_{θ} (tangential velocity) and v_z (axial velocity). The components are usually calculated for the gas and for the particles separately.

In the outer vortex Sheperd and Lapple found that the flow was irrotational. The transfer of fluids between the two vortexes originates at the bottom of the gas exit duct (the vortex finder) and continues to the cyclone bottom. Their results for the tangential velocity component is presented in figure 3.7. From the figure it can be seen that $v_{\theta_{\max}}$ occurs at the edge of the vortex finder.

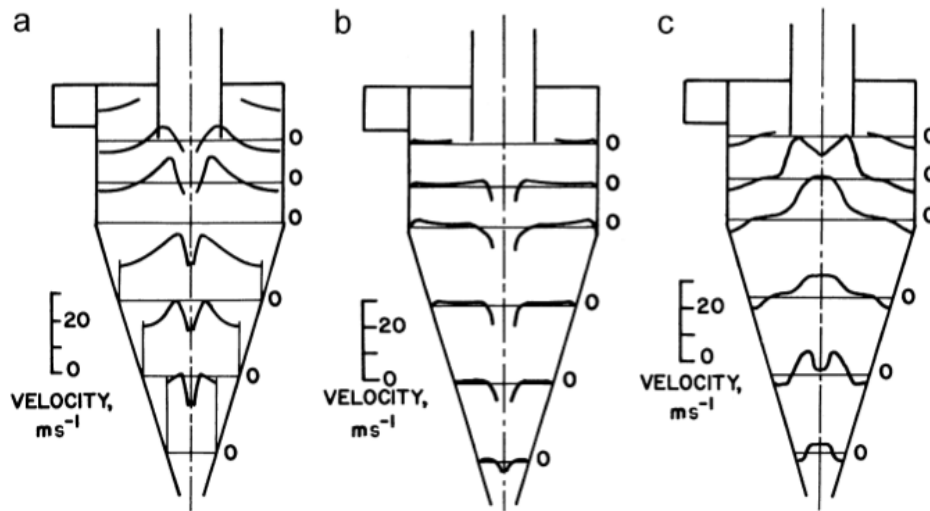


Figure 3.6: Velocity profile in a tangential inlet cyclone, (a) tangential, (b) radial, (c) axial [4]

In the outer vortex the tangential velocity distribution was found by Sheperd and Lapple to obey the equation

$$v_{\theta} r^n = C \quad (3.7)$$

where C is a constant, r is the radial position and n is the vortex exponent, which depends on r . This is the most widely used model for tangential velocity in analytical cyclone models. In the outer vortex, n approaches 1 as r closes the wall, and behaves like a free vortex. Near the cyclone axis n is close to -1, which makes it a forced vortex. The definition of a free vortex is that the shear stress is so low that viscosity is negligible close to the wall. In practice, this is not the case for cyclones and the tangential velocity in the outer vortex is better correlated using n in the range 0.4-0.8. According to this model, v_{θ} decreases as r increases, thus making the tangential velocity fairly small close to the wall. Factors like wall friction, and particle concentration are not included in this model. Both factors directly influence the strength of the vortex which shows that there is still much work remaining in modeling of tangential velocity.

Mothes and Löffler [21] developed an analytical expression for $v_{\theta\max}$ by dividing the cyclone into four characteristic regions. This has been shown to give a good approximation [17], but contains many parameters which are difficult to determine and some that must be determined experimentally. This includes a wall friction coefficient and a parameter of momentum exchange between gas and the wall.

For similar cyclone designs, Mothes and Löffler's experimental values can be used. Unfortunately, the parameters changes rapidly with velocity, particle density and concentration.

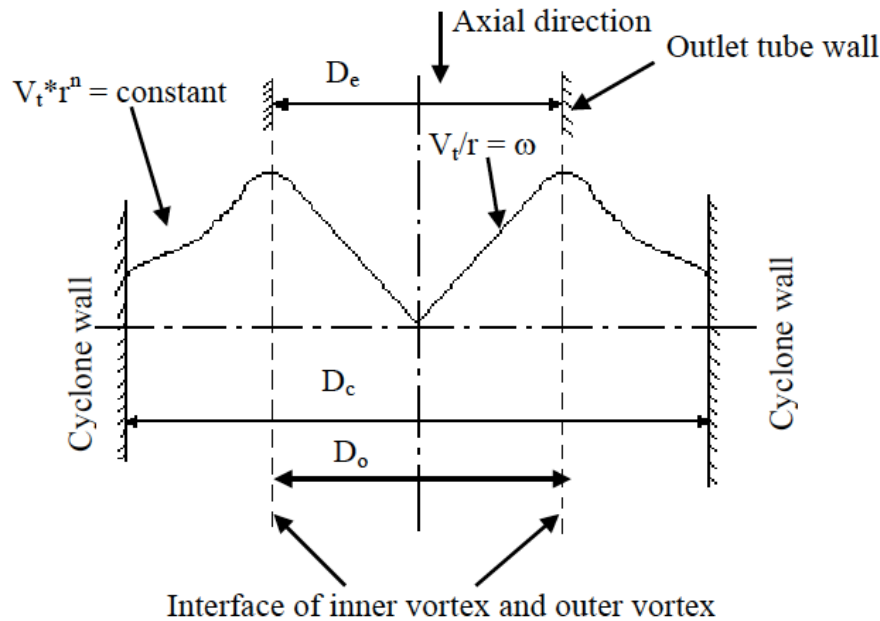


Figure 3.7: Tangential velocity distribution in a Cyclone [10]

Using equation 3.7, Wang [10] derived an expression for the tangential velocity in the cyclone cone. She studied cyclones with big inlets, which gave room for the assumption that the tangential velocity in the cyclone body was equal to the inlet velocity. From the work of Sheperd and Lapple, and assuming a free vortex flow in the cone, she found the following relation:

$$v_{\theta} = \frac{R \cdot V_c}{R_e + z \cdot \tan(\phi)} \quad (3.8)$$

It is common to assume that the tangential particle velocity is equal to the tangential gas velocity. This assumption causes the movement of particles towards the wall to be influenced by radial and axial velocity components.

In the outer vortex, the radial velocity is the component with fewest assumptions, and is the one most easily found. Because of the vortex behavior it is common

to assume that the radial gas velocity is zero. The radial velocity component will therefore govern the rate at which particles move out of the vortex and towards the wall. This is usually found from a force balance including drag, centrifugal, gravity and buoyancy forces. In the inner vortex this is more tricky. The radial velocity increases greatly as approaching the core, with direction inward. This fact conflicts with the assumption that radial velocity can be neglected due to small magnitude compared to the other components.

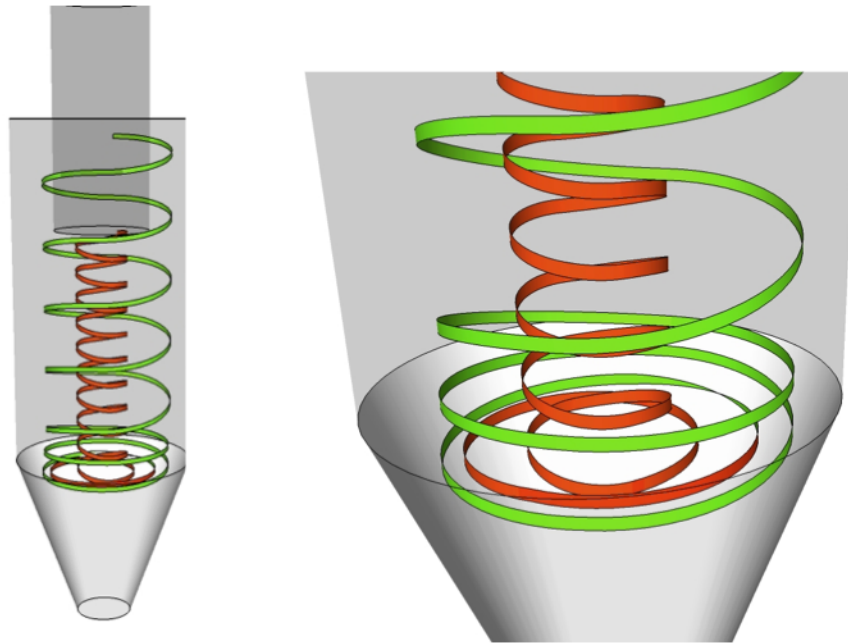


Figure 3.8: Cylindrical shaped vortices caused by the theoretical shift from the outer to the inner cyclone vortex.

The axial velocity component is more responsible for the downward transport of particles than gravity. A simple model for axial velocity suggests radially constant downward velocity for the outer vortex. For the double vortex structure to stay intact, a radially constant upward velocity is assumed for the inner vortex. The two vortices are usually modeled as perfect cylinders (figure 3.8), and these radially constant axial velocities must even each other out at the shifting point. From figure 3.6 it can be seen that the axial velocity exhibits a W-shaped profile, with a maximum at the symmetry axis. Sometimes, this momentum drop is so strong that instabilities arise which causes even stronger turbulent features [4]. From this fact the vortex shape cannot be a cylinder if continuity is to be satisfied.

3.3 Residence Time

Leith and Licht [2] based their collection theory on the residence time. Residence time indicates how long a particle is suspended in the cyclone. In other words, this is the available time a particle has to reach the collection zone. Increasing residence time will increase the probability of collection. This has been derived in many different ways, but it is usually based on an effective volume divided by an effective volumetric flow. The residence time can also be defined in terms of the "number of effective turns" N . Increasing cyclone diameter and length increases the residence time. From the definition it would appear that increasing residence time in such a fashion will result in better collection efficiency. However, an increase in cyclone diameter will cause a drop in the centrifugal forces so there is a trade-off.

Szekely and Carr (from Saruchera [22]) attempted to measure the residence time experimentally. They used a reversed flow cyclone with height 330 mm and mass flow M . At first they tried to measure it by hand. Single particles were let into the cyclone and a stopwatch was used to determine the residence time. Unfortunately this led to big uncertainty errors. Another attempt was to suddenly isolate the cyclone inlet and outlet. By doing so, they could determine the mass $\sum m_p$ of all the particles trapped inside the cyclone. An average residence time could then be calculated:

$$\bar{t}_{\text{res}} = \frac{\sum m_p}{M} \quad (3.9)$$

It is questionable whether the calculated residence time is representable for other materials. Particle trajectories are influenced by many factors and could contribute to change the outcome of this experiment.

Lede et al. [23] attempted to model the residence time as a function of the Reynolds number. The Reynolds number used, was based on the free fall terminal velocity and the centrifugal forces was neglected. The suggested empirical relation is

$$t_{\text{res}} = t_{\infty} + 4.5 \cdot 10^{-5} Re_p^{1.09}, \quad 400 < Re_p < 250000 \quad (3.10)$$

where t_{∞} is the residence time calculated from terminal velocity. The range of validity indicates that large particles were used to obtain this empirical relation. For such high Reynolds numbers it is doubtful that the centrifugal forces are negligible compared to gravitational forces.

Kang et al. [24] measured the residence time by coating glass particles with KCl. The cyclone hopper was exchanged with a cylindrical sampling tube that was

divided many layers. After a given period of time the bottom layer was closed, then the next layer and so on. By timing the whole operation and then measure the KCl concentration of each layer, they were able to determine the residence time. The following correlation was suggested:

$$\frac{t_{\text{res}}}{\bar{t}_{\text{res}}} = 0.032 Re_p^{0.13} \left(\frac{V_c - v_t}{v_t} \right)^{0.70} \left(\frac{\rho_p - \rho_g}{\rho_g} \right)^{0.42} \left(\frac{L_b + L_c}{L_c} \right)^{-1.76} \quad (3.11)$$

$$\bar{t}_{\text{res}} = \frac{V_c}{Q} \quad (3.12)$$

Saruchera [22] wanted to document cyclone characteristics that influenced the residence time. To measure the residence time, he injected the cyclone feed with tracer particles. The tracer particles was monitored using a traveling microscope with image grabbing software. He found that the residence time:

- decrease with increase in air flow into the cyclone
- increase with increase in density of the particle
- increase with increase in cyclone diameter and length for a given cone geometry
- is strongly influenced by cone angle

Leith and Licht assumed that turbulence causes a uniform radial dust concentration for a given horizontal cyclone plane. This assumption makes the residence time related to the amount of time a particle uses to travel in the radial and axial direction towards the wall. Later research has showed that there is in fact a concentration gradient in the radial direction [17].

For a tangential inlet cyclone, approximately 4-16 % of the incoming Q becomes short-circuit flow (flow that travels unhindered into the inner vortex) and exits the cyclone. On average this is 10 %. These assumptions is showed in figure 3.2. The residence time (t_{res}) will therefore consist of two contributions. Based on this Zhao found the following expressions for gas residence time:

$$t_{\text{res1}} = \frac{\pi(R^{*2} - R_e^2)S}{Q} \quad (3.13)$$

which is the contribution from the flow around the vortex finder. Due to the short-circuit flow only 90 % of Q will continue down the cyclone. Further it is assumed that the interface between the inner and outer vortex is located at R_e

and that the flow rate exchanged between these are linear. By using the average volumetric flow $(0.9Q/2)$ for calculation purposes, the second contribution is:

$$t_{\text{res2}} = \frac{\pi(R^{*2} - R_e^2)l}{(0.9Q)/2} \quad \text{for } l \leq L_c + L_b - S \quad (3.14)$$

or

$$t_{\text{res2}} = \frac{\pi(R^{*2} - R_e^2)(L_c + L_b - S)}{(0.9Q)/2} \quad \text{for } l > L_c + L_b - S \quad (3.15)$$

The total residence time will be the sum of both contributions

$$t_{\text{res}} = t_{\text{res1}} + t_{\text{res2}} \quad (3.16)$$

3.4 Pressure Drop

Even though cyclone pressure drop is not the focus of this paper, it is worth mentioning. The work of Sheperd and Lapple showed that the pressure loss in a cyclone was made up from five contributions:

1. Loss due to the expansion of gas entering the cyclone
2. Kinetic energy lost in the cyclone chamber
3. Loss due to friction losses at the wall
4. Additional friction loss at the exit duct due to turbulence
5. Pressure energy retrieved from kinetically rotational energy

In her dissertation, Wang derived models for each contribution and calculated the total pressure drop as the sum of these. She found that the pressure drop is independent of cyclone diameter, making it a function of both inlet velocity and cyclone height.

The largest contribution comes from kinetic energy lost in the cyclone chamber. The kinetic energy of the outer vortex are lost accordingly to:

$$p + \frac{1}{2}\rho_g v_\theta^2 \quad (3.17)$$

In other words, the kinetic energy dissipation is proportional to v_θ^2 . Factors strengthening the vortex, such as increased wall friction, will therefore contribute to a higher pressure drop. The total pressure has its maximum value at the cyclone wall and decreases slowly to a minimum at the cyclone core. A strong vortex that causes high tangential velocity values, can result in very high velocity pressures such that the static pressure becomes negative relative to the atmosphere. This negative static pressure zone can reach the bottom of the cyclone hopper. This can cause collected dust to swirl back up into the inner vortex and follow the gas out of the cyclone. This is more likely to occur if the hopper is not completely air tight, or if the wrong kind of damper/feeder is used at the dust outlet [4] [20].

When designing a cyclone it is important to evaluate the pressure drop against the cut-off diameter. A bad design will result in low performance and high power consumption, which should be avoided. When evaluating these parameters it is common practice to use non dimensional numbers so that the scale up (or down) is also taken into consideration. The Euler number is used to evaluate pressure drop and the Stokes number for cut-off diameter. They are defined as:

$$\text{Eu} = \frac{\Delta p}{(\rho_g V_c^2 / 2)} \quad (3.18)$$

where Δp is pressure drop over the cyclone and ρ_g is the gas density. And

$$\text{Stk}_{50} = \frac{d_{50}^2 \rho_p V_c}{18 \mu D} \quad (3.19)$$

For a well designed cyclone there is a direct correlation between Eu and Stk_{50} . The general trend can be described by the following approximate empirical correlation [5]:

$$\text{Eu} = \sqrt{\frac{12}{\text{Stk}_{50}}} \quad (3.20)$$

This shows that a smaller cut-off diameter is obtained at the expense of increasing pressure drop. And that increased inlet velocity causes higher pressure drop.

Table 3.2 shows different standard cyclones. The suggested designs aims at minimizing pressure drop with best possible performance. The pressure drop is given as velocity heads, which can be calculated from the following formula:

$$\Delta p = \Delta H_{\text{vh}} \left(\frac{1}{2} \rho_g V_c^2 \right) \quad (3.21)$$

Determining cyclone design based on velocity heads and application is quite similar to Elkem Materials' method (section 5.3). This method however, does not account for gas temperature.

Source	Recommended duty	D	$\frac{H}{D}$	$\frac{W}{D}$	$\frac{D_e}{D}$	$\frac{S}{D}$	$\frac{L_b}{D}$	$\frac{L_c}{D}$	$\frac{D_d}{D}$
Stairmand	High-efficiency	1	0.5	0.2	0.5	0.5	1.5	4.0	0.375
Swift	High-efficiency	1	0.44	0.21	0.4	0.5	1.4	3.9	0.4
Lapple	General-purpose	1	0.5	0.25	0.5	0.625	2.0	4.0	0.25
Swift	General-purpose	1	0.5	0.25	0.5	0.6	1.75	3.75	0.4
Stairmand	High-flow	1	0.75	0.375	0.75	0.875	1.5	4.0	0.375
Swift	High-flow	1	0.8	0.35	0.75	0.85	1.7	3.7	0.4

Source	Recommended duty	ΔH_{vh}	$\frac{Q}{D^2}$ (m/h)
Stairmand	High-efficiency	6.4	5500
Swift	High-efficiency	9.2	4940
Lapple	General-purpose	8.0	6860
Swift	General-purpose	7.6	6680
Stairmand	High-flow	7.2	16500
Swift	High-flow	7.0	12500

Table 3.2: Standard designs for tangential inlet cyclones [19]

The next table shows some of the prediction models discussed in this section.

Model	Equation	Remarks
Lapple [1]	$\eta = \frac{1}{1+(d_{50}/d_p)^2}$ $d_{50} = \frac{9\mu W}{2\pi N V_c (\rho_p - \rho_g)}$ $N = \frac{1}{H} \left(L_b + \frac{L_c}{2} \right)$	
Barth [11]	$\eta = \frac{1}{1+(v_t/v_t^c)}$ $\frac{v_t}{v_t^c} = \frac{\pi L^m \rho_p v_{\theta \max}^2 d_p^2}{9\mu Q}$ $L^m = L - S, D_e \leq D_c$ $\frac{(L-L_b)(D-D_e)}{D-D_c} + (L_b - S), D_e > D_c$ $v_{\theta \max} = V_c \left[\frac{(D_e/2)(D-W)\pi}{2HW\alpha + L^m(D-W)\pi\lambda} \right]$ $\alpha = 1 - 1.2 \frac{W}{D}$	$v_t^c =$ based on cut-size diameter $L^m =$ geometrical parameter $\lambda =$ friction factor Scroll inets $\alpha \approx 1$
Ioza and Leith [13]	$\eta = \frac{1}{1+(d_{50}/d_p)^\beta}$ $d_{50} = \left(\frac{9\mu Q}{\pi \rho_p l V_{\max}^2} \right)^{0.5}$ $\frac{d_c}{D} = 0.47 \left(\frac{HW}{D^2} \right)^{-0.25} \left(\frac{D_e}{D} \right)^{1.4}$ $l = (L_b + L_c - S) - \left[\frac{L_c}{(D/D_c)-1} \right] \left(\frac{d_c}{D_c} - 1 \right), d_c > D_c$ $l = L_b + L_c - S, d_c \leq D_c$ $V_{\max} = 6.1 V_c \left(\frac{HW}{D^2} \right)^{0.61} \left(\frac{D_e}{D} \right)^{-0.74} \left(\frac{L_b+L_c}{D} \right)^{-0.33}$ $\ln(\beta) = 0.62 - 0.87 \ln(d_{50}) + 5.2 \ln \left(\frac{HW}{D^2} \right) + 1.05 \left[\ln \left(\frac{HW}{D^2} \right) \right]^2$	$d_c =$ geometry parameter $\beta =$ cut-size exponent

Table 3.3 cont.

Model	Equation	Remarks
Leith and Licht [2]	$\eta = 1 - \exp \left\{ -2 \left[\frac{G t_{\text{res}} Q}{D^3} (n + 1) \right]^{1/(2n+2)} \right\}$	
	$G = \frac{D_e}{H^2 W^2} \left\{ 2 \left[\pi \left(S - \frac{H}{2} \right) (D^2 - D_e^2) \right] + V_L \right\}$	$G = \text{geometrical parameter}$
	$V_L = \frac{\pi D^2}{4} (L_b - S) + \left(\frac{\pi D^2}{4} \right) \left(\frac{l+S-L_b}{3} \right) \left(1 + \frac{d_c}{D} + \frac{d_c^2}{D^2} \right) - \frac{\pi D_e^2 l}{4}, (L_b + L_c - S) > l$	$V_L = \text{geometrical parameter}$
	$V_L = \frac{\pi D^2}{4} (L_b - S) + \left(\frac{\pi D^2}{4} \right) \left(\frac{L_c}{3} \right) \left(1 + \frac{D_c}{D} + \frac{D_c^2}{D^2} \right) - \frac{\pi D_e^2 (L_b + L_c - S)}{4}, (L_b + L_c - S) > l$	
	$d_c = D - (D - D_c) \left(\frac{S+l+L_b}{L_c} \right)$	
	$l = 2.3 D_e \left(\frac{D^2}{HW} \right)^{1/3}$	
	$n = 1 - (1 - 0.67 D^{0.14}) \left(\frac{T}{283} \right)^{0.3}$	$T = \text{temperature in K}$
	$t_{\text{res}} = \frac{\rho_p d_p^2}{18\mu}$	
Rhodes [5]	$\eta = \frac{(d_p/d_{50})^2}{1+(d_p/d_{50})^2}$	
	$d_{50}^2 = \frac{18\mu R}{(\rho_p - \rho_g)} \frac{v_R}{v_{\theta R}^2}$	
	$v_R = \frac{Q}{2\pi RL}$	
	$v_{\theta R} = V_c$	

Table 3.3: Different cyclone efficiency models

4 Filter South - Elkem Thamshavn

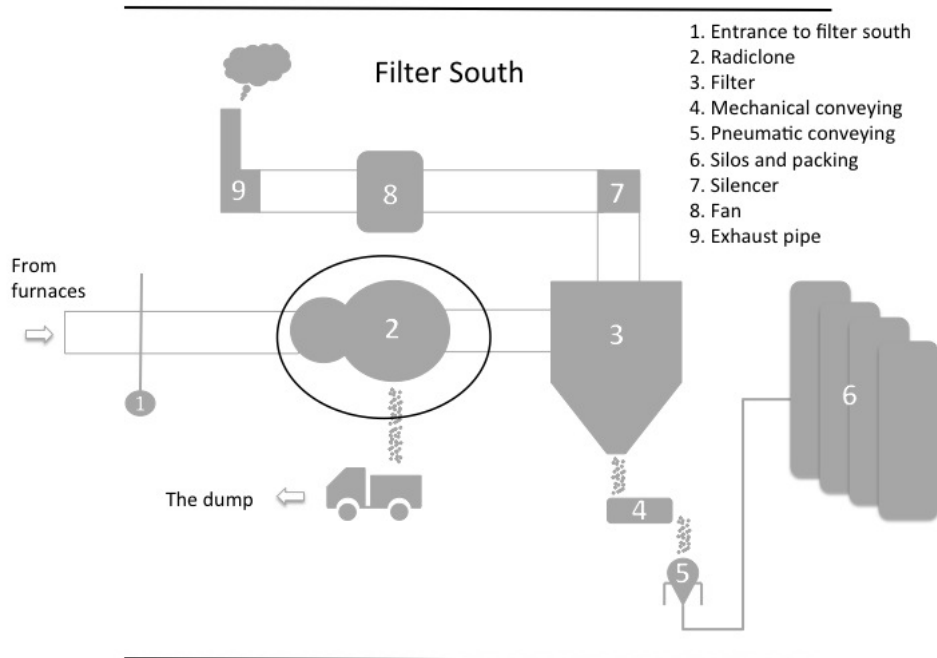
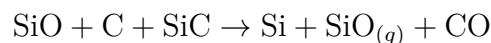


Figure 4.1: Filter south layout

The plant at Thamshavn produces silicon and microsilica. The silicon is extracted from quartz according to this reaction:



The process starts with loading two electrical ovens with carbon and quartz. These are labeled “oven 1” and “oven 2” and provides 46 MW and 25 MW respectively. The reaction above occurs at very high temperatures and the ovens at Thamshavn operates at temperatures exceeding 2000 °C. The carbon needed is provided by coke and coal, and for improved texture, wood chips are added to the mix. As a result of this reaction, large quantities of fumes are produced as by-products. The SiO gas rising from the furnaces is the origin of microsilica. The escaping gas oxidize when it comes in contact with air and microsilica is produced. Typically 10-15% of the quartz ends up as microsilica, and much of it is trapped as it condensates. In addition to microsilica a number of impurities follows. These impurities consists of: Oxides of alkalis, coke residues, silicon carbide, some tar related organics and carbon black [25].

Elkem Thamshavn is the only silicon plant in the world that retrieves energy from its excessive heat [26]. By-products from both ovens are led through a heat exchanger that uses the energy acquired to power a gas turbine. The electricity produced, goes back to the plant. When the gas turbine is active it is capable of providing 180 000 MWh.

One of the most important steps in the microsilica production is to separate the microsilica from the off-gas produced by the ovens. This is done by an industrial filter. At Thamshavn there are two such filters: Filter north and filter south. When operation is normal, filter north is fed from oven 2 and filter south from oven 1.

Filter south is made up by two separation stages. The first separation stage removes all the impurities and big microsilica particles which reduces the product quality. By definition, this is all the particles with a particle diameter above $45 \mu\text{m}$. This operation is performed by a radiclone. This is designed and manufactured by Elkem Materials. The next separation stage removes all the remaining particles from the gas. This is done by a pulse-jet filter, delivered by Alfsen og Gunderson. Such a filter is shown in figure 4.2. Off gas enters the filter and is forced upwards towards the exit. Particles are then separated from the gas and remains on the filter outside. Clean gas exits at the top. When enough dust has accumulated on the outside of the filter bags, the cleaning sequence begins. Pressured air is shot down into each bag which causes the dust to disengage. At filter south there are six such chambers.

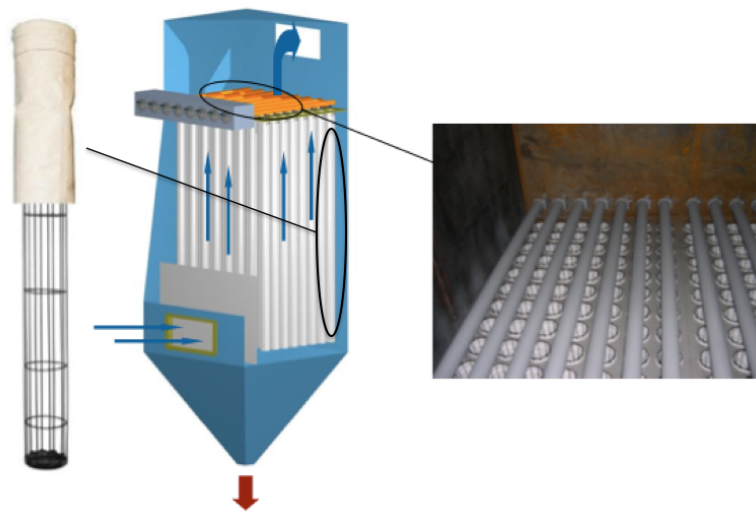


Figure 4.2: Single chamber pulse-jet filter (pictures provided by Alfsen og Gunderson (AG))

Dust separated at the filter is sent to storing silos with pneumatic transport. Microsilica is stored in different silos according to quality. Clean gas from the filter is sent through a silencer to reduce noise. Further, it is passed through the fan and out into the environment through an exhaust pipe.

Dust samples that is gathered for analysis, described in the following sections, are taken from the two locations shown in figure 4.3. The three components shown in this figure are also showed in figure 4.1.

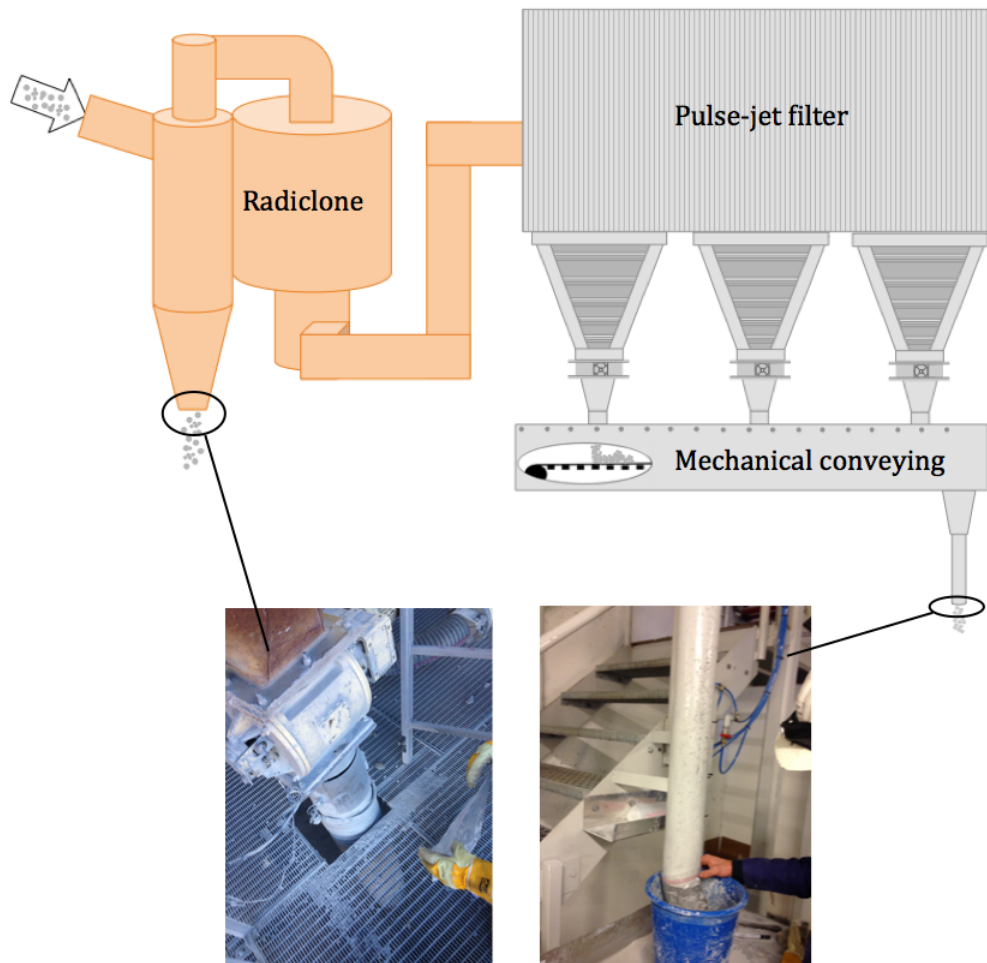


Figure 4.3: Dust sampling locations

5 Radiclone at Filter South

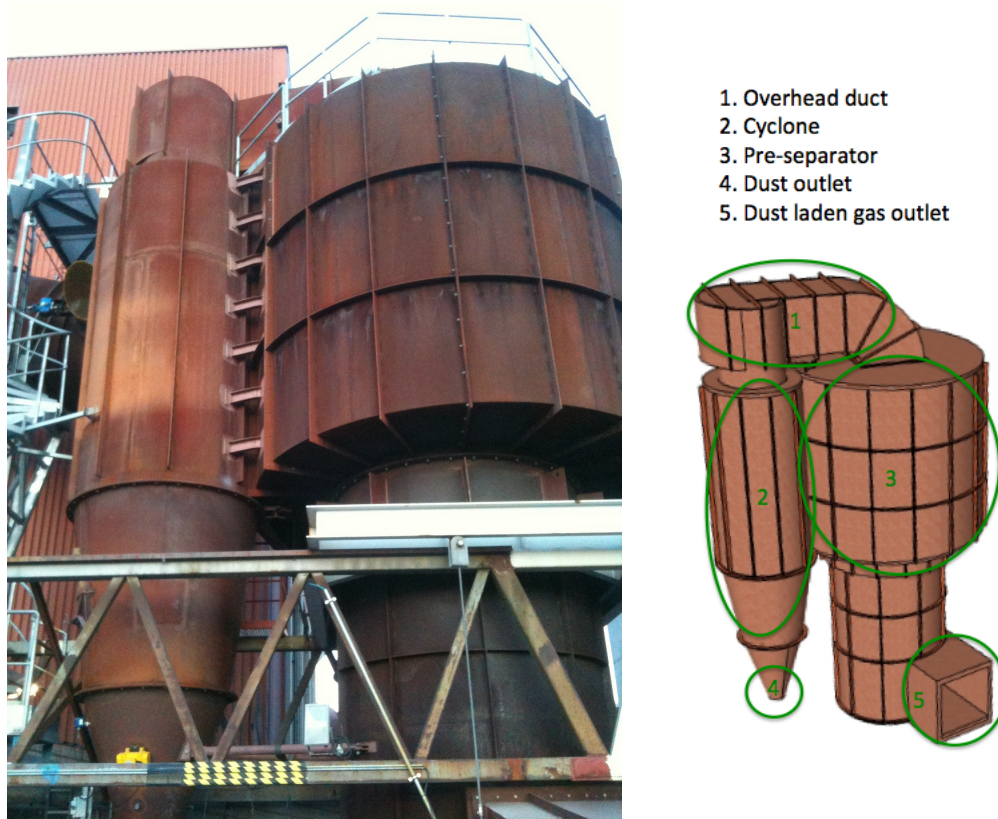


Figure 5.1: Radiclone at filter south

5.1 Functionality

In order to describe the radiclone more accurately, a graphic model was made in Google Sketchup according to the drawings in appendix A.

The radiclone of filter south is made up by two main parts. A cyclone and a pre-separator (shown on figure 5.1). The pre-separator splits a fraction of the gas. This fraction contains the biggest and heaviest particles, and these are led into the cyclone. Here, the particles are removed from the gas and gathered in the bottom of the conical part, also called cyclone hopper. The hopper is constantly emptied by a cell feeder located at the hopper outlet. If the dust starts to pile up in the hopper, a vibrator is mounted on the outside to restore the particle flow. The particles separated by the radiclone are stored in a container and thrown away.

Gas is pulled through the radiclone by a 1400 kW industrial fan. The fan provides required under pressure for the entire filter south.



Figure 5.2: Cell feeder (left) and vibrator (right)

Dust laden gas from the ovens are led into filter south through a $\text{Ø}2000$ mm circular duct. Figure 5.3 shows the radiclone from above and is taken from a technical drawing of filter south.

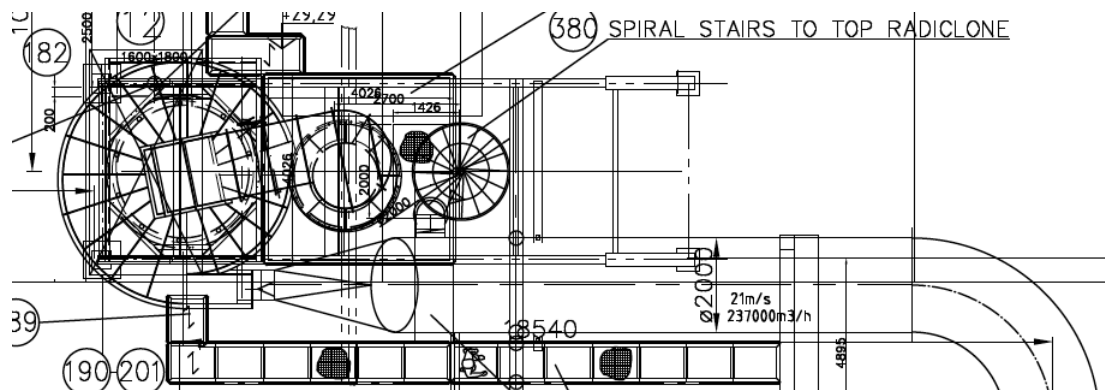


Figure 5.3: Radiclone at filter south from above. Drawing is provided by Alfsen og Gunderson (AG)

The first component of filter south is the radiclone. The gas is transported through the circular duct to a point where the duct changes geometry to a rectangular cross section. This rectangular cross section is the inlet to the pre-separator, and the gas is pulled tangentially in. This is easier understood by looking at the Google Sketchup drawing on the next page.

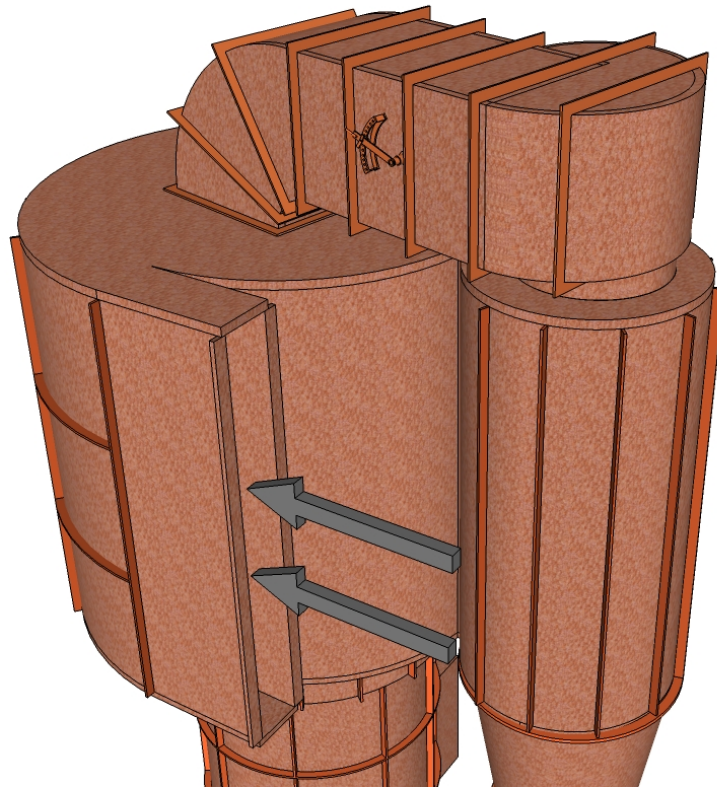


Figure 5.4: Inlet of the radicle cyclone

The part shown in figure 5.5 is connected to the radicle cyclone inlet and transports dust laden gas from the ovens.

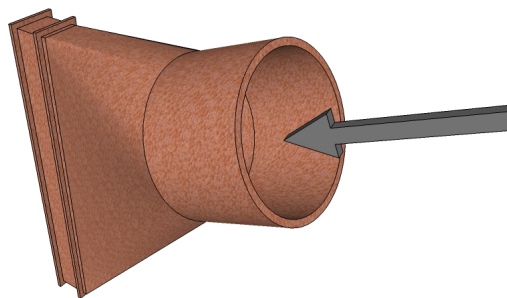


Figure 5.5: Inlet gas transport duct

Removing the radiclone body as done in in figure 5.6, reveals the inside. The top and bottom part are held together and supported by nine pillars. The gas outlet duct has an entry hatch further downstream. This is used for maintenance purposes and a ladder gives access to the pre-separator body.

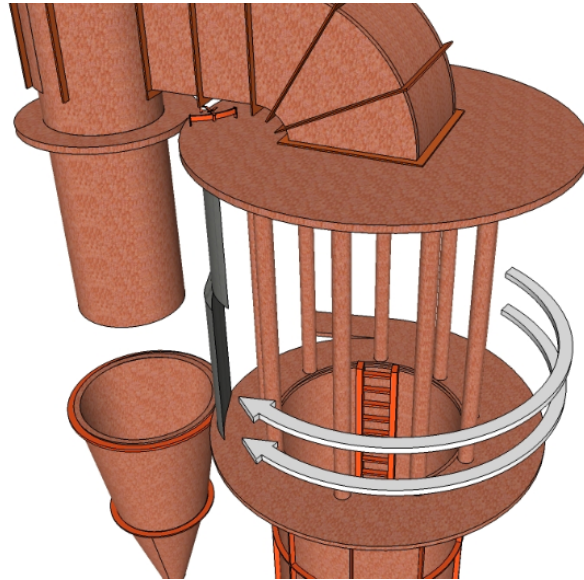


Figure 5.6: Gas path in pre-separator

Due to centrifugal forces the heaviest particles will move closest to the wall as the gas is forced to move around the pre-separator axis. Two knife dampers, located at the cyclone inlet, separate the fraction of gas that moves close to the wall, which contains the heavier particles. In theory, the knife dampers should be set to such positions that all particles over $45 \mu\text{m}$ is led into the cyclone. The gas that is not led into the cyclone will pass the knife dampers and continue its trip around the pre-separator axis. Eventually this gas is pulled down through the pre-separator bottom and through the gas outlet. This gas contains salable microsilica which is recovered at the pulse jet filter.

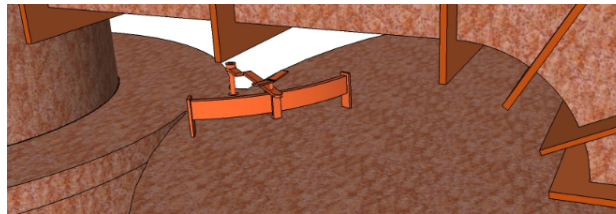


Figure 5.7: Upper knife damper position handle. Located under the overhead gas duct.

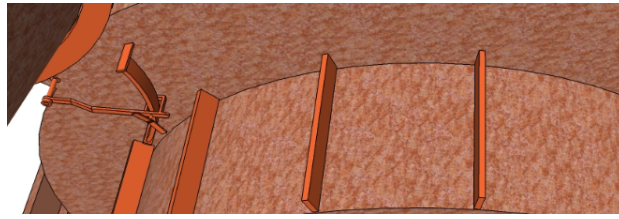


Figure 5.8: Lower knife damper position handle. Located under the pre-separator body.

When calculating performance, the fraction of gas from the pre-separator is assumed to enter the cyclone tangentially. In reality the gas experience a slight change in direction due to the curvature of the knife dampers. But this effect is negligible. The inlet can be seen to reach a long way down in the cyclone, from figure 5.9. The long inlet can cause particles to escape into the inner vortex right after entering the cyclone. To avoid this, the vortex finder length S , is designed to be longer than for conventional cyclones.

Entering gas forms an outer vortex around the vortex finder. As the outer vortex reaches a certain point it will slow down and eventually reverse its direction, creating an inner vortex. This vortex moves upwards and into the overhead duct inlet. The duct transports the gas back into the pre-separator. In theory, this gas continues in axial direction after entering the pre-separator and out of the radiclone gas outlet. It does not interfere with the incoming gas from the ovens.

This cyclone has the same characteristics as the "reverse-flow" cyclone with tangential inlet discussed in section 2.

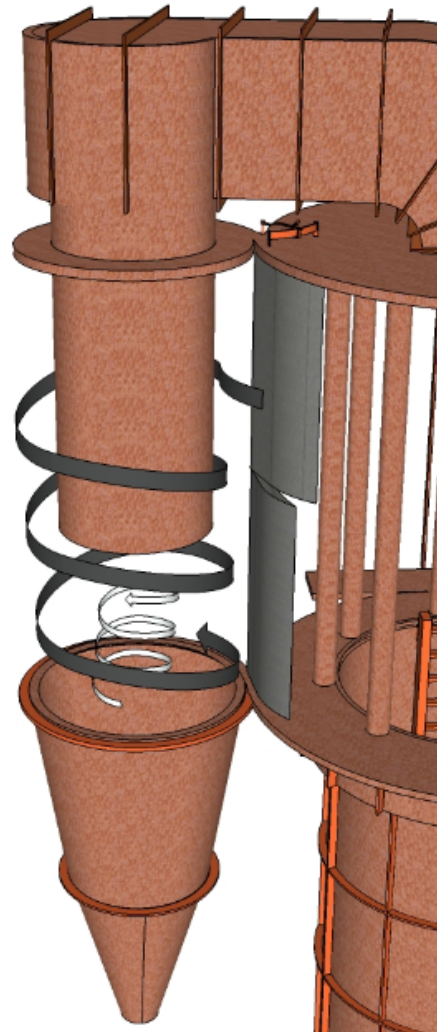


Figure 5.9: Gas path in the cyclone

The volumetric flow through the over head duct is controlled by an over head damper, as shown in figure 5.10. The position of this damper will influence the inner and outer vortex size in the cyclone, hence influencing cyclone performance. The damper has twelve positions.

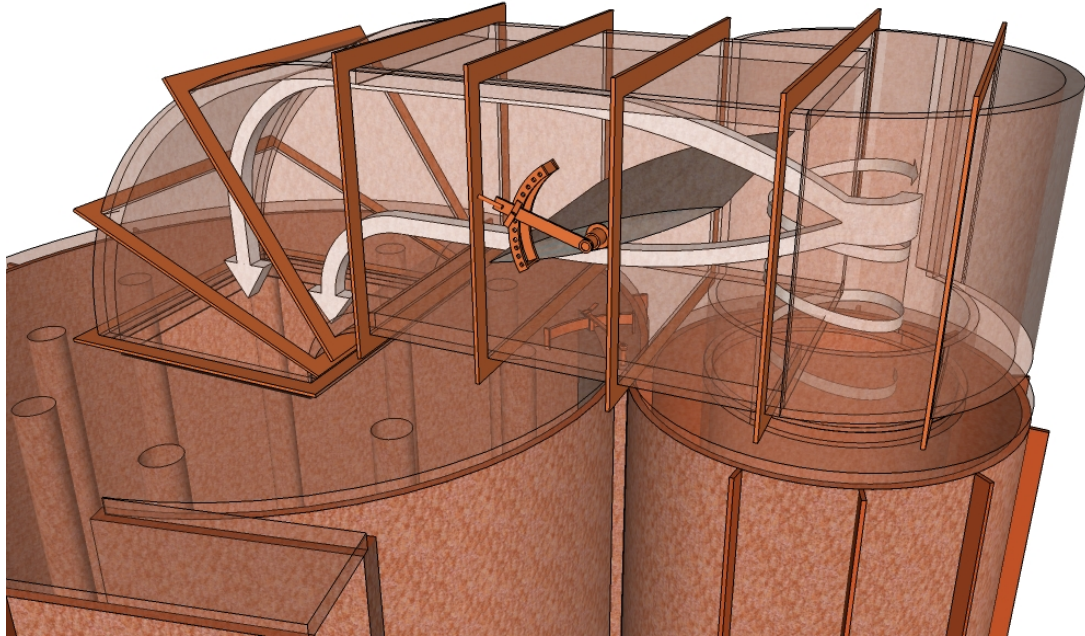


Figure 5.10: Over head duct and the associated damper

Finally the gas exits at the bottom of the radiclone. In theory this gas should now only contain high quality microsilica. This duct leads the pulse-jet filter that separates the remaining particles from the gas.

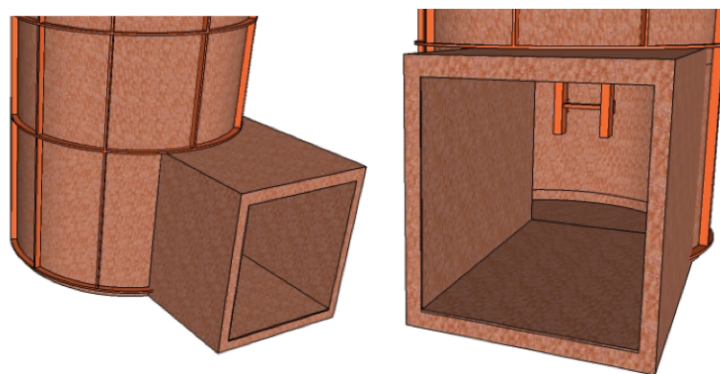


Figure 5.11: Radiclone gas outlet

5.2 Dimensions

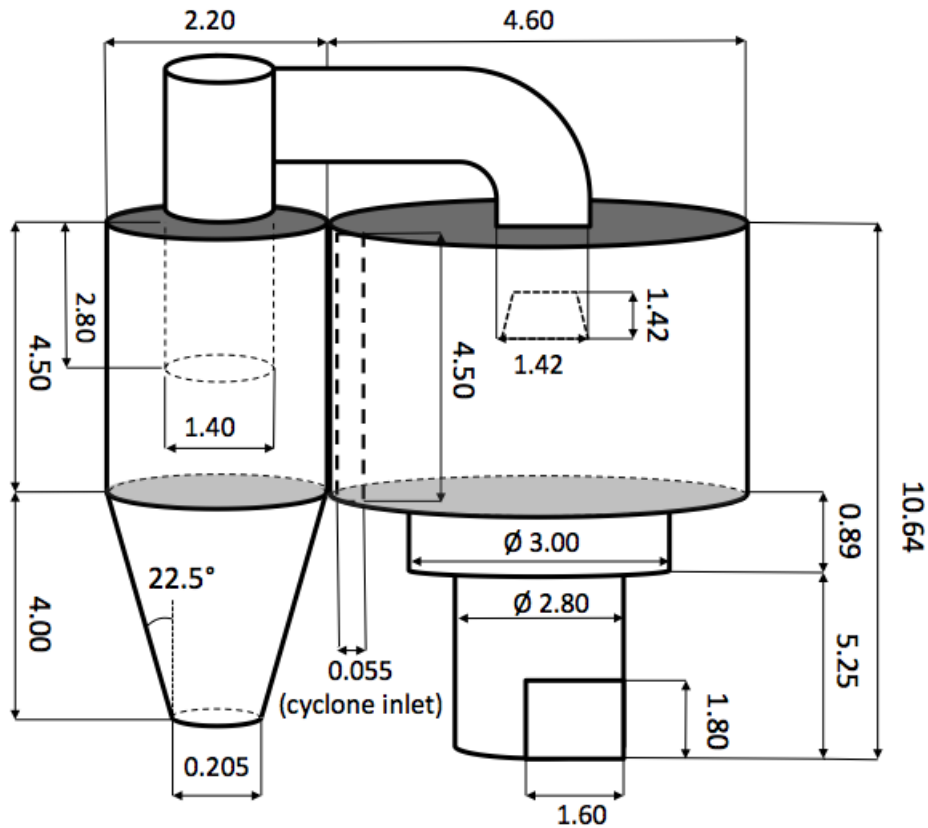


Figure 5.12: Radiclone dimensions. All values are given in meters, except cone angle.

These numbers was found on production drawings provided by Elkem (appendix A). The top and the bottom plate (highlighted with gray on figure 5.12), are showed in figure 5.13.

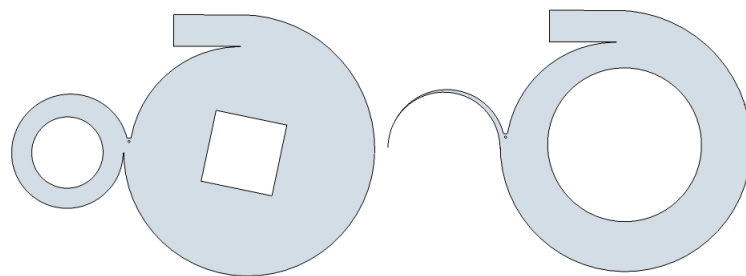


Figure 5.13: Top (left) and bottom (right) radiclone plate

Because of the pre-separator inlet, and the cyclone inlet, both these plates have circles with an increasing radius. When calculating radiclone performance in the next section these shapes are approximated with a circular shape as shown in figure 5.12. The overhead duct dimensions are presented in figure 5.14.

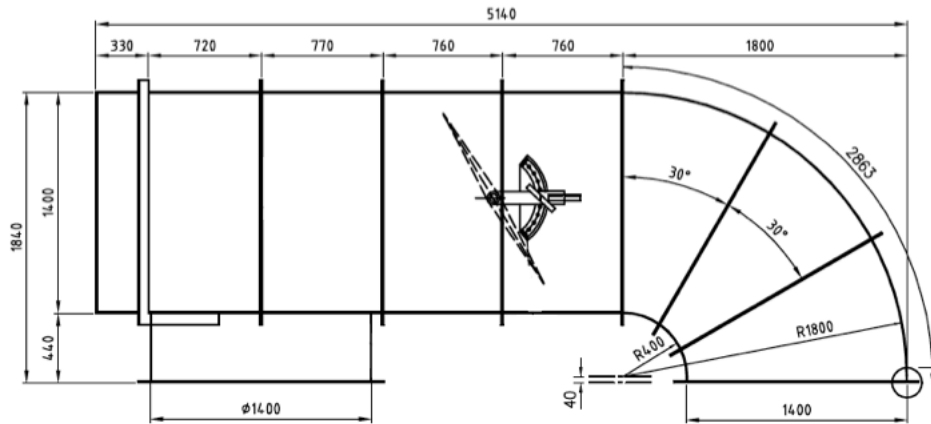


Figure 5.14: Overhead duct dimensions (appendix A)

5.3 Theoretical Basis for Performance

The radiclone at Thamshavn filter south is delivered by Elkem Materials. Elkem Materials has developed a standard design that has been used at several of Elkem's plants. Depending on the process, this design is scaled up or down in order to give the wanted performance. Processes that uses these types of separators are rarely alike, which must be accounted for in the calculations. The process at Thamshavn is one of the simplest cases, where one duct transports the gas to the radiclone and is pulled by a fan.

Scaling of the standard design is done by calculating the "Bøckmans Pressure Factor" K . Knowing this pressure factor allows calculation of the pressure drop according to this equation

$$\Delta p = K \cdot Q^2 \frac{T}{T_0} \quad (5.1)$$

where Δp is the pressure drop over the radiclone. K is given in $\text{Pa}/(\text{Nm}^3/\text{s})^2$, where N stands for normal state (1 atm and 0 °C). K remains constant so that an increasing load Q will result in increased Δp . If this bigger load results in a calculated pressure drop that is unacceptably high, a bigger radiclone is needed.

When scaling the radiclone, a “linear size parameter” D_l is used. If, for instance, a radiclone that is twice as big as the standard one is needed, D_l equals 2. The relationship between K and D_l is [27]:

$$K \sim \frac{1}{D_l^4} \quad (5.2)$$

The radiclone at filter south is a scaled up version of the smallest one at filter north. Given the design values of filter south the K -value can be calculated:

T	Q	Δp
[K]	[Nm ³ /s]	[Pa]
453	41	650

$$K = \frac{650 \text{ Pa}}{(41 \text{ Nm}^3/\text{s})^2} \cdot \frac{273}{453} = 9.55 \frac{\text{Pa}}{(\text{Nm}^3/\text{s})^2} \quad (5.3)$$

Dividing equation 5.2 for two different radiclones gives:

$$D_l = \sqrt[4]{\frac{K_n}{K_s}} \quad (5.4)$$

Where K_n and K_s represents the radiclone at filter north and south respectively. Elkem has documented K_n to be 15.0 [27], which means that (from equation 5.4) $D_l=1.12$. The radiclone at filter south is then 12 % bigger than the smallest one at filter north, which corresponds to the model by Elkem Materials called “Radiclone 1600”. This is much easier done by using a diagram as the one showed in figure 5.15. This diagram shows four different sized cyclones. Such a diagram is based on equations 5.1 and 5.2. Even though Elkem’s radiclones is not represented in this diagram, the principles are the same. Based on the temperature, pressure drop and gas flow, the appropriate radiclone can be selected. Instabilities in such processes are common, and it is therefore important to check the chosen design for increased gas flows and temperatures. If the resulting pressure drop is too high, a slightly bigger model should be chosen to withstand such effects.

Most processes are very different, and problems as limited space and limited accessibility can make it difficult to install a standard design. Calculating the K values, assumes that identical geometries are used, and any exceptions from this geometry will influence the pressure drop. If this assumption is maintained, the K value is a good indication of performance. A well built radiclone should have a

measured K value within 6 % of the calculated one [27]. Any discrepancies from this could indicate a production flaw or that the process is not as expected. Several cases have been reported where large amounts of dust was stuck to the cyclone-part inside. This causes a chain reaction because once dust starts to pile up more will follow. As this happens the pressure drop increases gradually which causes K to increase.

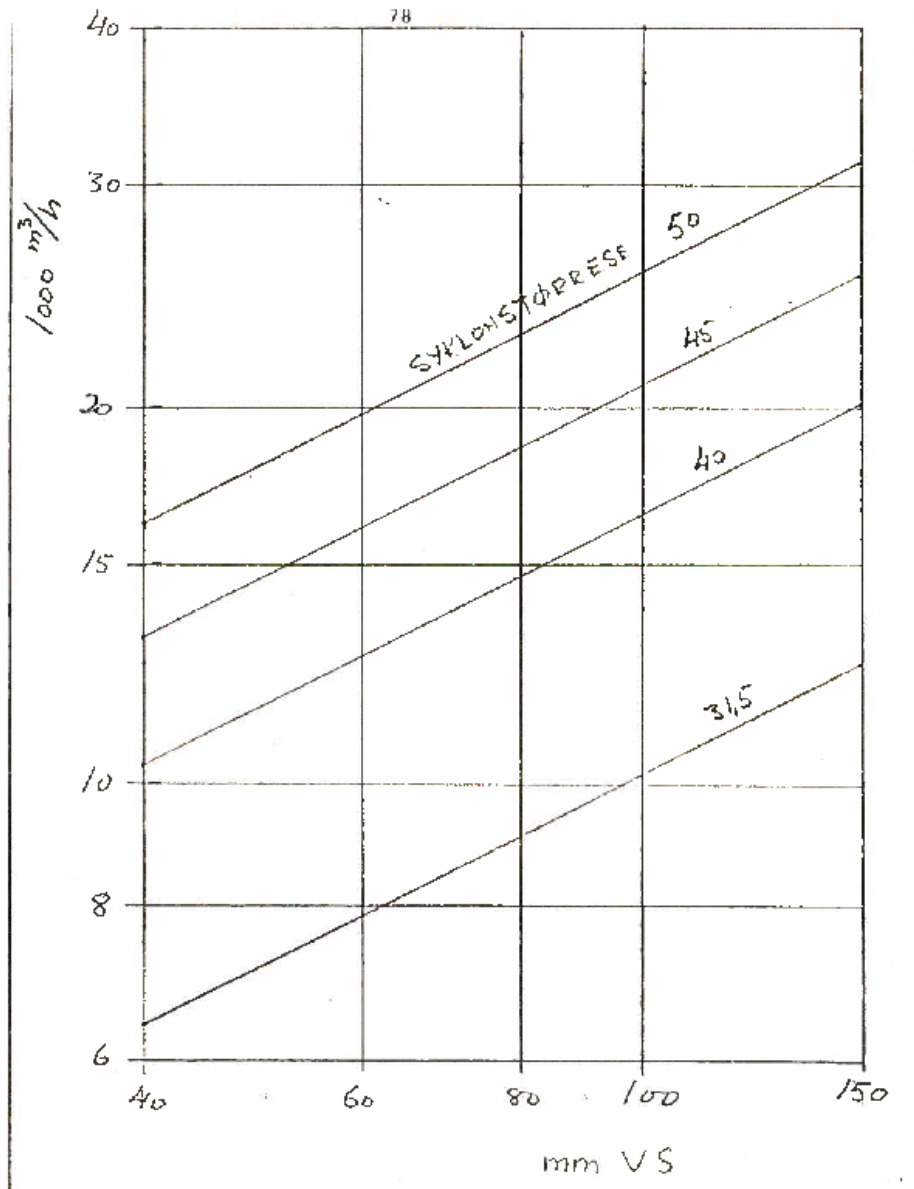


Figure 5.15: Diagram for determining cyclone size [27]

5.4 Current Performance

To determine the current performance of the radiclone, dust samples was gathered from the locations shown in figure 4.3. The samples was gathered 14.05.2013.

To analyze these samples, a Coulter analysis was performed by SINTEF. This produces a particle size distribution as shown in figure 2.3. This distribution shows particle diameter versus a relative frequency such that the sum of all the frequencies equals 1. From the radiclone dust outlet and the pulse-jet filter dust outlet, two such distributions was obtained and are presented in figure 5.16 and 5.17.

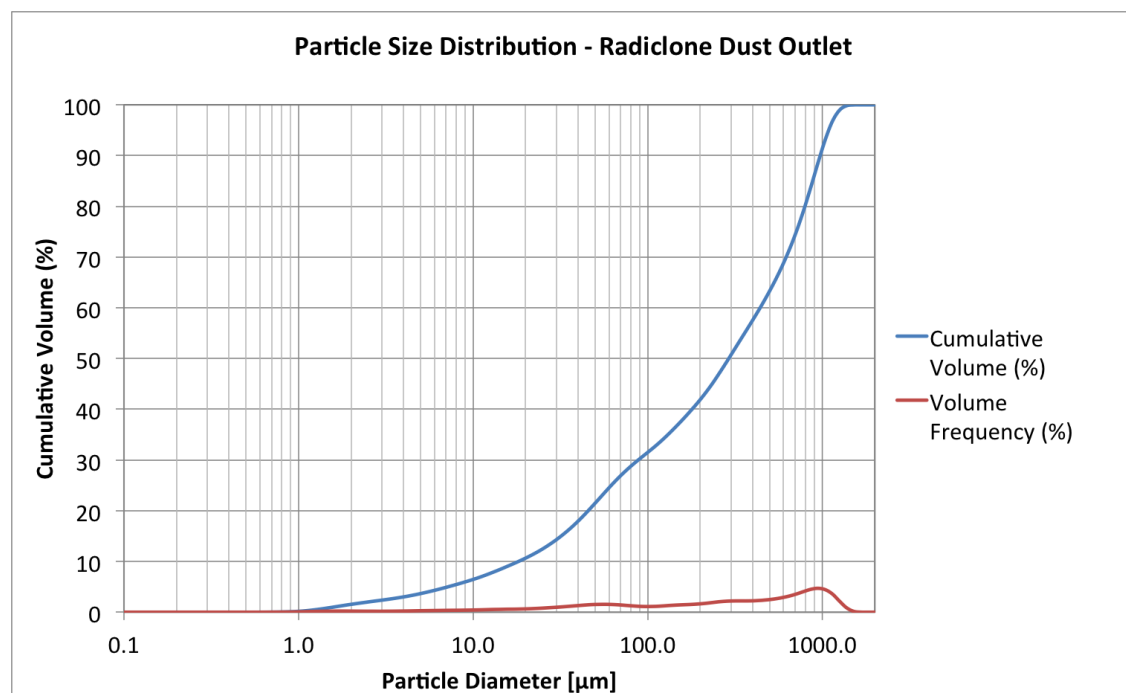


Figure 5.16: Particle size distribution

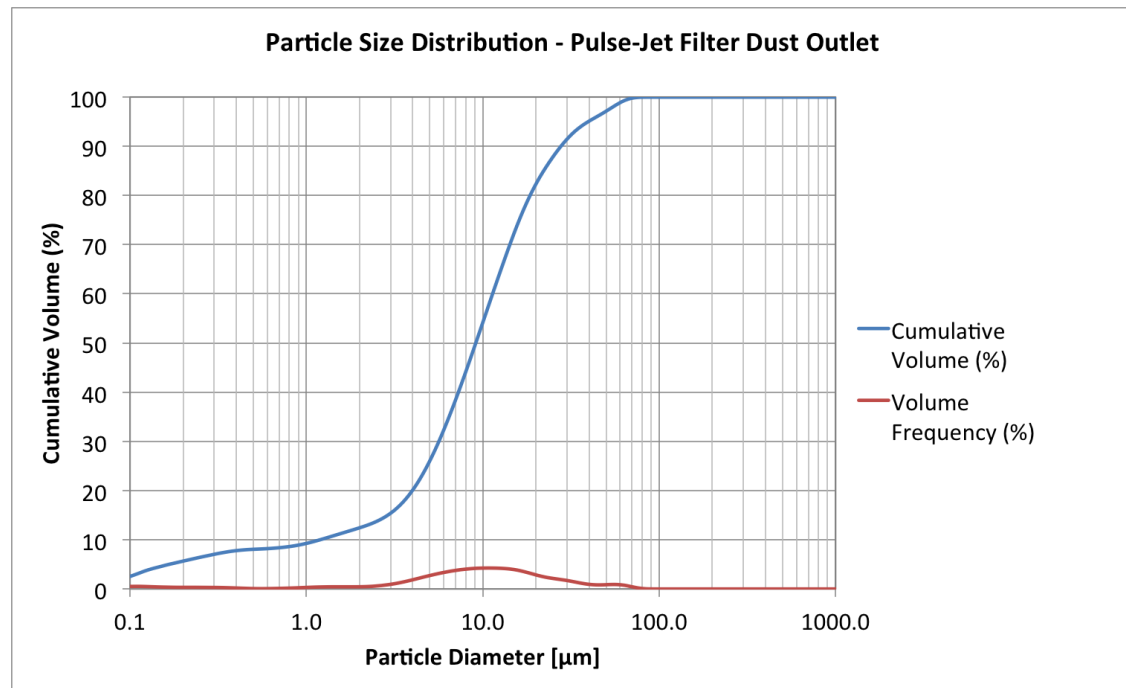


Figure 5.17: Particle size distribution

In order to relate these particle size distributions to the actual operation, all the frequencies was multiplied by the mass flow at the sampling location. By doing this, the resulting distribution shows particle diameter versus mass flow.

Sampling from the radiclone dust outlet was done in a 10 second period and then weighed. The radiclone dust outlet sample had a weight of 0.33 kg after 10 seconds which corresponds to a mass flow of 120.2 kg/h. For the samples at the pulse-jet filter, it was read from the operating screen at filter south that the dust production was 1250 kg/h during sampling.

To obtain the distribution curve for all the dust that entered the radiclone, the frequency from figure 5.16 and 5.17 was multiplied with the corresponding mass flow and the sum was calculated. This is shown in figure 5.18.

A section of the previous mentioned curve is presented in figure 5.19. The total mass flow into the radiclone is compared to the mass flow out of the radiclone dust outlet. The two curves are plotted together, and the radiclone performance can easily be seen from this figure. By inspection, d_{100} is determined to be 90 μm . Applying equation 2.3, the total efficiency η_T is found to be 8.8 %.

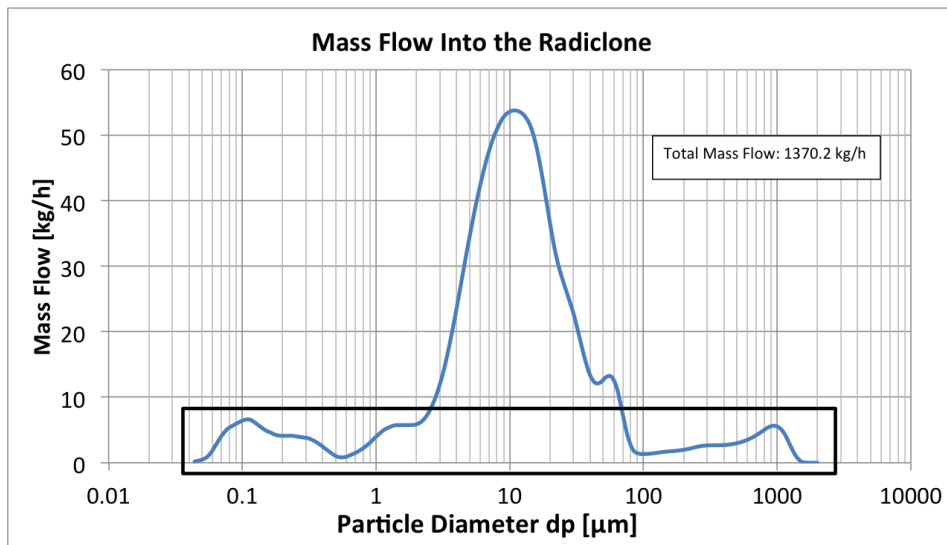


Figure 5.18: Total mass flow into the radiclone versus particle diameter. The part inside the rectangle is shown in the next figure.

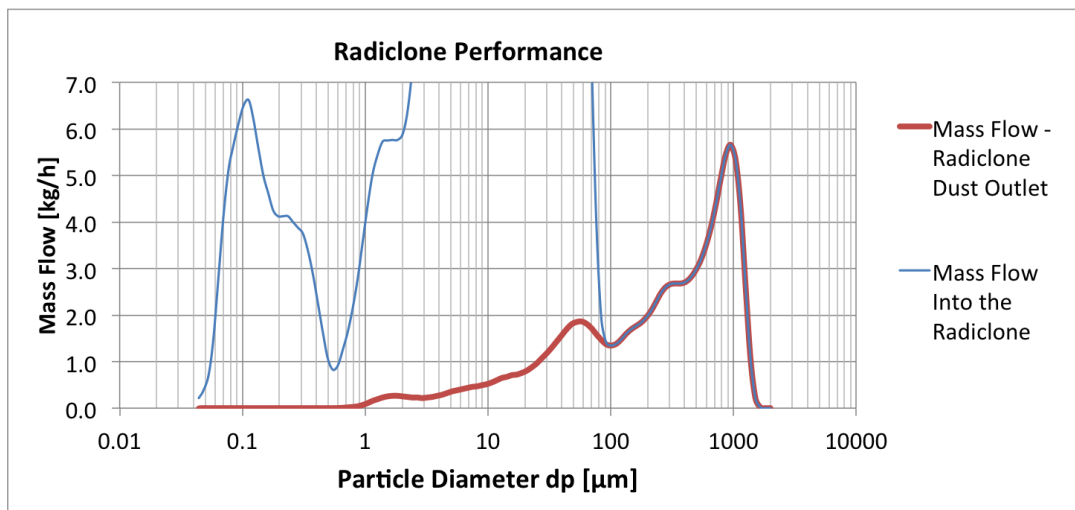


Figure 5.19: Mass flow into the radiclone and mass flow at the radiclone dust outlet versus particle diameter

For each particle diameter, the mass flow from the radiclone dust outlet was divided by the total mass flow into the radiclone. Based on this, a grade efficiency curve was produced, and is shown in figure 5.20. From the typical grade efficiency curves presented in section 3, this is slightly different. The main difference is that the curve behaves with a moderate slope for $d_p < 40 \mu\text{m}$. This can be explained by the pre-separator. The pre-separator prevents the majority of small particles from

entering the cyclone. Because of this the separation efficiency is relatively low for particles under $45 \mu\text{m}$. This is intentionally achieved by Elkem because these particles are collected at the pulse-jet filter. It is also seen that a significant fraction of the separated dust is good quality microsilica. Integrating the red curve in figure 5.19 from 0 to $45 \mu\text{m}$ gives approximately 25 kg/h of good quality microsilica. This is 2 % of the total production that goes to waste. By inspection of figure 5.20, d_{50} is determined to be $79 \mu\text{m}$.

Subtracting the two curves in figure 5.19 and integrating the subtraction from $45 \mu\text{m}$ to $+\infty$ gives approximately 41 kg/h. This is 3 % of the dust production. Appendix B shows the product specification for microsilica 971 quality. It states that the content of particles bigger than $45 \mu\text{m}$ must be less than 0.5 %. These samples show that this requirement is not satisfied.

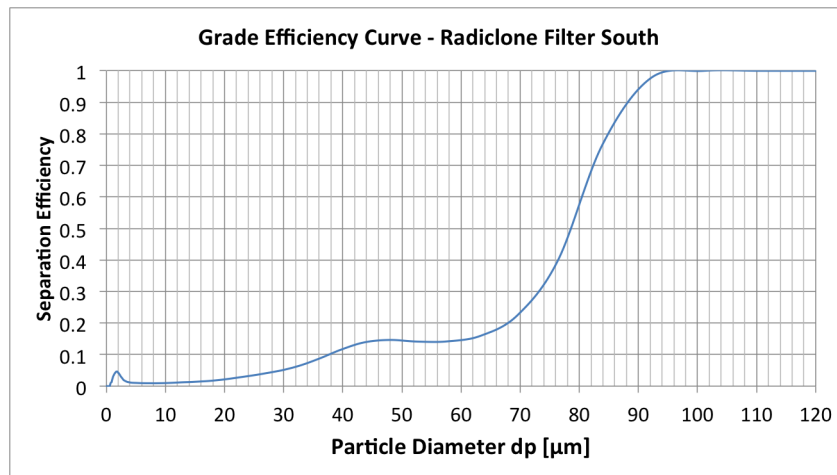


Figure 5.20: Grade efficiency curve

Ideally, this analysis should not be based on two samples. The Coulter analysis is very accurate, but the dust sample analyzed must be very well mixed to be trustworthy. Total randomness is almost impossible to obtain and different results are often observed, even from the same dust sample. This is a factor that must be taken into consideration when interpreting the results. Another factor is agglomeration. The samples were isolated in a container for 2 weeks before they were analyzed. The smaller particles tend to fuse together, creating bigger particles. If the samples were analyzed upon gathering it is likely that less coarse particles in the product, and fewer fine particles wasted had been observed. In other words, particles with $d_p < 45 \mu\text{m}$ at the radiclone dust outlet are expected to be somewhat higher than the results indicate. And particles with $d_p > 45 \mu\text{m}$ at the pulse-jet filter outlet are expected to be lower.

6 An Analytical Model for Predicting Radiclone Efficiency

A model for predicting performance in such a component entails many assumptions. Describing the complex flow field involves differential equations that has not yet been solved analytically. The use of CFD tools are a natural approach to such a problem, and would result in a better physical understanding. However, high anisotropy in the turbulent flow makes this a challenging simulation. Strong instabilities would also demand a transient solving of the problem. Expensive and complicated schemes like LES or DNS would be needed to give satisfactory results. In addition, experimental results would be needed to tune the model correctly. An analytical model would be simple to use in addition to the low costs. It would also give a fair understanding and an indication of how the component would perform, which are in many cases, all that is needed.

An analytical model has been developed for the flow in a tangential inlet cyclone, with a pre-separator, to obtain the collection efficiency. This model is based on the early work of Lapple, Alexander, Leith and Licht. It is also based on the latest work of Zhao and Wang. The model created is a hybrid model based on both static particle theory and timed flight theory.

6.1 Radiclone Velocity Profile

The actual separation occurs in the cyclone. The majority of this model is therefore based on the cyclone. Most of the microsilica are created from condensate droplets when the furnace off-gasses comes in contact with air. This gives each particle a circular shape and it is fair to assume spherical particles. It is also assumed that nearby particles do not influence each others behavior. The tangential velocity component of the particle is assumed to be the same as for the gas stream and is constant. In addition, the radial gas velocity is neglected, and a uniform particle concentration is assumed.

6.1.1 Radial Particle Velocity

As a particle moves out of the outer vortex due to the centrifugal forces, it follows a curvilinear motion.

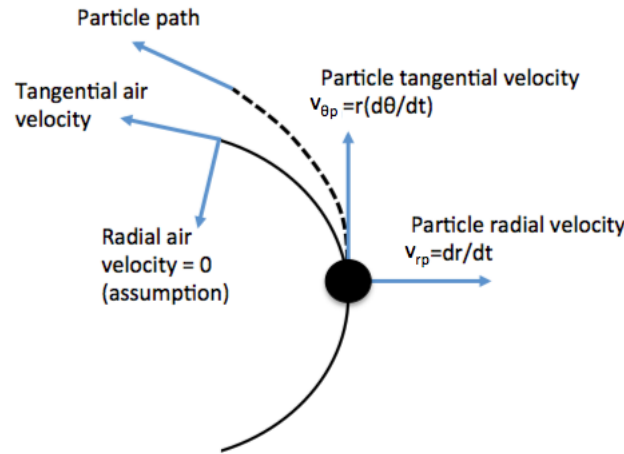


Figure 6.1: Particle path when the centrifugal forces exceeds drag forces

Unity vectors in polar coordinates (r, θ) are given as:

$$\mathbf{u}_r = \cos(\theta)\mathbf{i} + \sin(\theta)\mathbf{j} \quad (6.1)$$

and

$$\mathbf{u}_\theta = -\sin(\theta)\mathbf{i} + \cos(\theta)\mathbf{j} \quad (6.2)$$

where $\mathbf{i} = (1, 0)$ and $\mathbf{j} = (0, 1)$ in cartesian coordinates, and bold faced symbols represents a vector.

From curvilinear theory [28] the particle velocity \mathbf{v}_p is given as:

$$\mathbf{v}_p = \mathbf{v}_{rp} + \mathbf{v}_{\theta p} = \frac{dr}{dt}\mathbf{u}_r + r\frac{d\theta}{dt}\mathbf{u}_\theta \quad (6.3)$$

Taking the derivative of \mathbf{v}_p with respect to time gives the particle acceleration.

$$\mathbf{a}_p = \frac{d\mathbf{v}_p}{dt} = \frac{d^2r}{dt^2}\mathbf{u}_r + \frac{dr}{dt}\frac{d\mathbf{u}_r}{dt} + \frac{dr}{dt}\frac{d\theta}{dt}\mathbf{u}_\theta + \frac{d^2\theta}{dt^2}r\mathbf{u}_\theta + r\frac{d\theta}{dt}\frac{d\mathbf{u}_\theta}{dt} \quad (6.4)$$

From figure 6.2 it is known that

$$\frac{d\mathbf{u}_\theta}{dt} = -\frac{d\theta}{dt}\mathbf{u}_r \quad (6.5)$$

$$\frac{d\mathbf{u}_r}{dt} = \frac{d\theta}{dt}\mathbf{u}_\theta \quad (6.6)$$

Inserting 6.5 and 6.6 into 6.4 gives the following equation for particle acceleration

$$\mathbf{a}_p = \mathbf{a}_{rp} + \mathbf{a}_{\theta p} = \left(\frac{d^2 r}{dt^2} - r \left(\frac{d\theta}{dt} \right)^2 \right) \mathbf{u}_r + \left(2 \frac{dr}{dt} \frac{d\theta}{dt} + \frac{d^2 \theta}{dt^2} r \right) \mathbf{u}_\theta \quad (6.7)$$

Since we assumed that the tangential particle velocity is the same as the gas stream and constant, the tangential acceleration = 0. Therefore the particle acceleration can be written as:

$$a_p = \frac{d^2 r}{dt^2} - r \left(\frac{d\theta}{dt} \right)^2 \quad (6.8)$$

By applying Newton's second law it is possible to determine a particle force balance.

$$m_p \frac{Q}{Q_O} \frac{d\mathbf{v}_p}{dt} = \Sigma \mathbf{F} \quad (6.9)$$

where m_p is the particle mass. Because m_p is the mass of all particles entering the radicle it is multiplied with Q/Q_O to calculate the mass of particles entering the cyclone. This is based on the assumption of a uniform concentration. Assuming spherical particle shape m_p can be expressed as $\frac{4}{3}\pi\rho_p\frac{d_p^3}{8}$. Where d_p is particle diameter and ρ_p is particle density. The forces that influence particle motion is: Gravity, drag force, and centrifugal force.

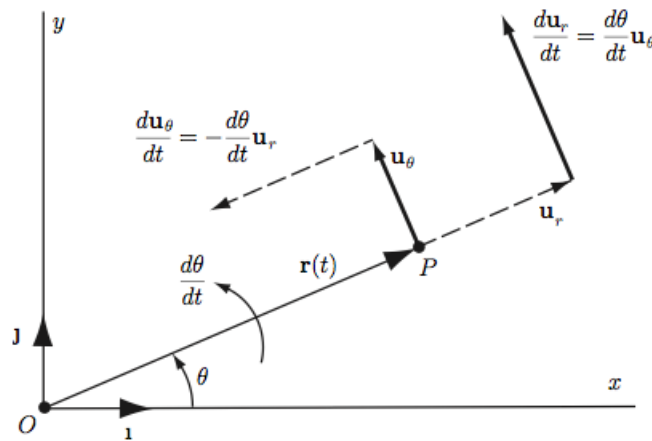


Figure 6.2: Curvilinear motion [28]

Gravity

The contribution from gravity on a particle can be evaluated by looking at the settling velocity. This is the particle velocity when the drag force from the gas equals gravity.

$$F_d = F_g = m_p g \quad (6.10)$$

Due to small particle sizes (in the range 1-50 μm) it is assumed that $Re_p < 2$ (see figure 6.3). This makes the Stokes' law valid so the drag force becomes

$$F_d = 3\pi\mu d_p v_t = m_p g \quad (6.11)$$

where μ is the viscosity of air and v_s is the particle settling velocity.

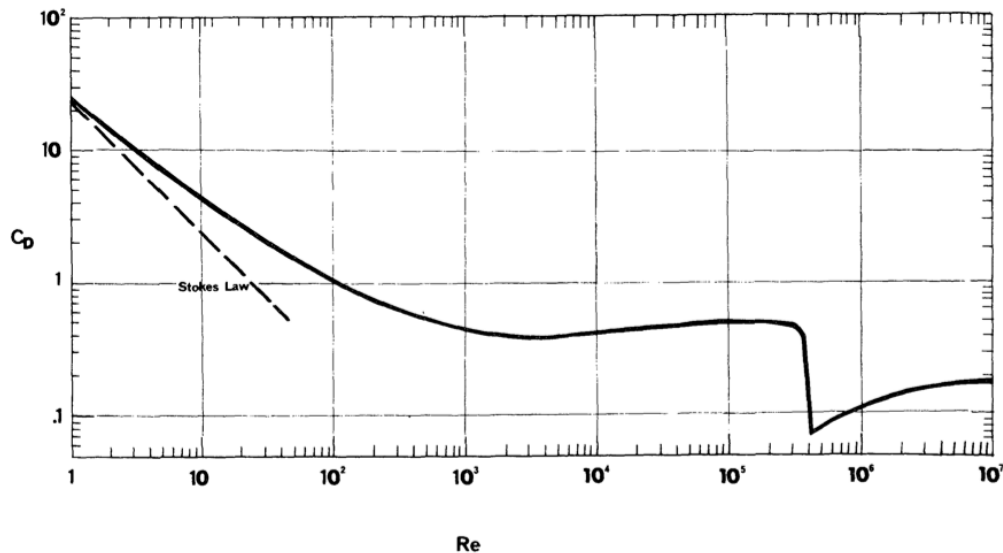


Figure 6.3: Drag coefficient of a spherical particle as a function of Reynolds number. As Re gets smaller, Stokes' law becomes more accurate [29]

The buoyancy force is neglected due to the fact that $\rho_p \gg \rho_{\text{gas}}$. Rearranging equation 6.11 and writing the mass in terms of volume times density, gives an expression for terminal velocity.

$$v_t = \frac{1}{18} \frac{\rho_p g d_p^2}{\mu} \quad (6.12)$$

By using a particle diameter of $10 \cdot 10^{-6}$ m with density 2300 kg/m^3 and a gas viscosity of $25.8 \cdot 10^{-6} \text{ kg/ms}$ the resulting settling velocity becomes $4.9 \cdot 10^{-3} \text{ m/s}$. This is very small compared to radiclone inlet velocity, hence the force contribution from gravity is neglected.

Centrifugal

The centrifugal force is calculated from particle acceleration in the radial direction.

$$F_c = m_p \frac{Q}{Q_O} a_p = \frac{1}{6} \pi d_p^3 \frac{Q}{Q_O} \left[\frac{d^2 r}{dt^2} - r \left(\frac{d\theta}{dt} \right)^2 \right] \quad (6.13)$$

Drag

To verify the use of Stokes' law, the particle Reynolds number based on terminal velocity is calculated:

$$Re_p = \frac{\rho v_t d_p}{\mu} = \frac{1.2 \text{ kg/m}^3 \cdot 4.9 \cdot 10^{-3} \text{ m/s} \cdot 45 \cdot 10^{-6} \text{ m}}{25.8 \cdot 10^{-6} \text{ kg/ms}} = 0.01 \quad (6.14)$$

Using Stokes' law again with the particle velocity relative to the air flow in the radial direction.

$$F_d = 3\pi\mu d_p (v_{rp} - v_r) \quad (6.15)$$

As previously discussed it is assumed that all the air moves in a vortex motion, so the radial air velocity component is neglected. The drag force can then be expressed as:

$$F_d = 3\pi\mu d_p \frac{dr}{dt} \quad (6.16)$$

If the sum of all the forces acting on a particle is zero, there will be a 50% chance for collection. From this logic, $F_c > F_d$ causes a particle to be collected and $F_c < F_d$ causes it to escape with the gas stream. Theoretically, the force balance below causes the particle to be trapped in the vortex.

$$F_d + F_c = 0 \rightarrow 3\pi\mu d_p \frac{dr}{dt} + \frac{1}{6} \pi d_p^3 \frac{Q}{Q_O} \left[\frac{d^2 r}{dt^2} - r \left(\frac{d\theta}{dt} \right)^2 \right] = 0 \quad (6.17)$$

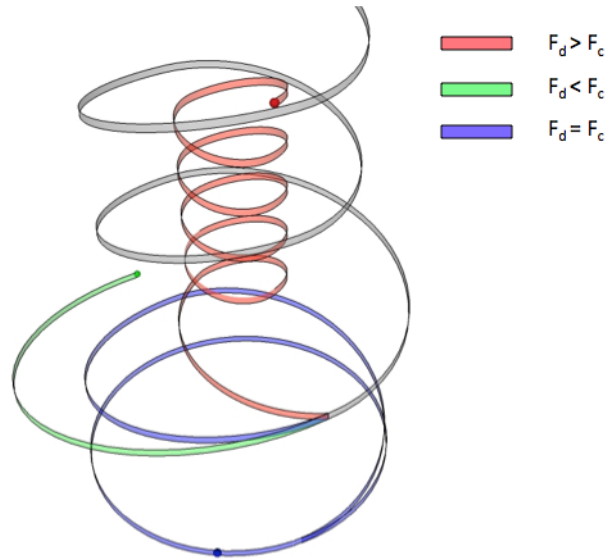


Figure 6.4: Three different scenarios of particle trajectory within the cyclone

Knowing that $\frac{d\theta}{dt} = \frac{1}{r}v_{\theta p}$ equation 6.17 becomes:

$$\frac{d^2r}{dt^2} + \frac{18\mu}{\rho_p d_p^2} \frac{Q_O}{Q} \frac{dr}{dt} - \frac{v_{\theta p}^2}{r} = 0 \quad (6.18)$$

This equation is not ready for solving. An approximate solution can be obtained by neglecting the second derivative. The physical effect of doing this, is assuming that the particle moves outward with a constant radial velocity. From equation 6.18 the radial particle velocity then becomes:

$$v_{rp}(r) = \frac{Q}{Q_O} \frac{\rho_p d_p^2}{18\mu} \frac{v_{\theta p}^2}{r} \quad (6.19)$$

6.1.2 Tangential Particle Velocity

It was assumed that the tangential particle velocity is equal to the tangential gas velocity. The tangential gas velocity is therefore calculated and used in the model. This velocity is influenced by a centrifugal and a pressure force. Wang derived an expression for the centrifugal velocity by evaluating a small control volume within the cyclone [10].

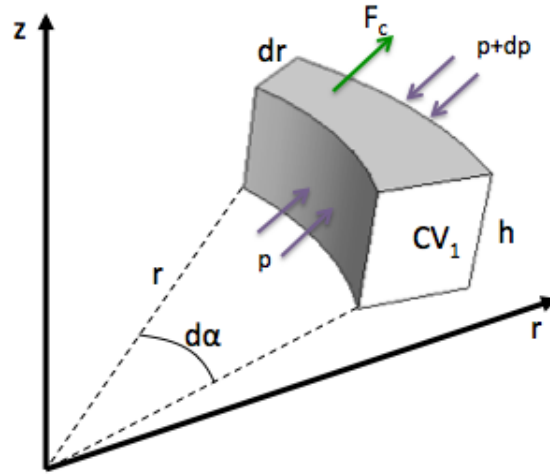


Figure 6.5: Control volume for calculating the tangential gas velocity

Based on the figure above the centrifugal force acting on CV_1 is:

$$F_c = \rho_g \cdot hr \cdot d\alpha \cdot dr \frac{v_\theta^2}{r} \quad (6.20)$$

and the pressure forces are:

$$F_p = p \cdot hr \cdot d\alpha \quad (6.21)$$

$$F_{p+dp} = h \cdot (p + dp)(r + dr)d\alpha \approx hr \cdot (p + dp)d\alpha \quad (6.22)$$

dr is neglected in 6.22 because of the assumption that the gas stream has no radial acceleration, thus no force contribution from radial direction. A force balance for CV 1 gives:

$$F_c + F_p - F_{p+dp} = 0 \quad (6.23)$$

$$\rho_g \cdot hr \cdot d\alpha \cdot dr \frac{v_\theta^2}{r} + p \cdot hr \cdot d\alpha - hr \cdot (p + dp)d\alpha = 0 \quad (6.24)$$

As mentioned earlier the flow in the outer vortex is irrotational. The pressure drop along a streamline can therefore be calculated by using Bernoulli's equation.

$$p + \rho_g \frac{v_\theta^2}{2} = \text{constant} \quad (6.25)$$

Taking the derivative with respect to r gives:

$$\frac{dp}{dr} + \rho_g v_\theta \frac{dv_\theta}{dr} = 0 \quad (6.26)$$

Combining equation 6.24 and 6.26 gives the following expression for the tangential velocity, which is the equation for a free vortex. :

$$\frac{dv_\theta}{v_\theta} + \frac{dr}{r} = 0 \rightarrow \ln(v_\theta) + \ln(r) = \text{constant} \rightarrow v_\theta r = \text{constant} \quad (6.27)$$

The cyclone at filter south has an inlet that covers the whole cyclone body length. It is therefore appropriate to assume that the tangential velocity is constant in this part. From figure 3.7 it is found that a tangential velocity of $0.7V_c$ is a good approximation at R^* , considering free vortex characteristics.

$$v_{\theta(\text{body})} = 0.7V_c \quad (6.28)$$

Using equation 6.27 with $v_{\theta 2} r = V_c R$ the velocity for the cone part becomes:

$$v_{\theta(\text{cone})} = \frac{R}{r} V_c = \frac{R \cdot V_c}{R_e + z \cdot \tan(\phi)} \quad (6.29)$$

6.2 Radiclone Grade Efficiency

The calculation of grade efficiency it is based on Bingtao Zhao's time-of-flight model [9]. By using the equivalent cyclone radius R^* it is assumed that particles that reaches this radius within the cyclone is collected. Looking at CV_2 (figure 6.6) the particle flux reaching R^* can be expressed as $cv_{rp}(R^*)$ where c is the particle concentration. Including the surface area of the cylindrical control volume gives the rate of particles intercepting the equivalent wall as $2\pi R^* cv_{rp}(R^*) dz$. The amount of particles removed from the control volume can be expressed as the rate of change in concentration, which is $d(\pi R^{*2} cdz)/dt$. Combing the two last terms in a particle mass balance yields:

$$\frac{d(\pi R^{*2} cdz)}{dt} = -2\pi R^* cv_{rp}(R^*) dz \quad (6.30)$$

When extracting the constants from the rate of change term and rearranging, the mass balance becomes:

$$\frac{dc}{c} = -2 \frac{v_{rp}(R^*) dt}{R^*} \quad (6.31)$$

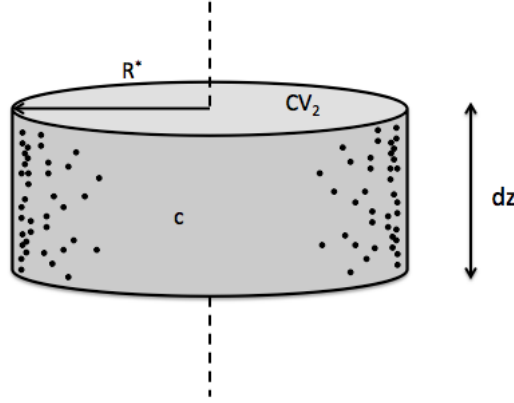


Figure 6.6: Control volume for particle separation model [9]

Integrating the previous equation with the boundary conditions $c = c_0|_{t=0}$ and $t = t_{\text{res}}|_{c=c}$ gives:

$$\frac{c}{c_0} = \exp \left[-\frac{2v_{rp}(R^*)t_{\text{res}}}{R^*} \right] \quad (6.32)$$

Recalling that the grade efficiency can be expressed as in equation 2.8, the separation model becomes:

$$\eta = 1 - \exp \left[-\frac{2v_{rp}(R^*)t_{\text{res}}}{R^*} \right] \quad (6.33)$$

Where t_{res} is given in equation 6.38, 6.39, 6.40 and 6.41. And $v_{rp}(R^*)$ is given from equation 6.19 as

$$v_{rp}(R^*) = \frac{Q}{Q_O} \frac{\rho_p d_p^2}{18\mu} \frac{v_\theta(R^*)}{R^*} \quad (6.34)$$

considering that $v_{\theta p} = v_\theta$. $v_\theta(R^*)$ can be estimated by using the weighted average for the tangential velocity in the cone and body.

$$v_\theta(R^*) = \frac{1}{2} \left[\bar{v}_{\theta(\text{body})} + \frac{L_c}{L_b} \bar{v}_{\theta(\text{cone})} \right] \quad (6.35)$$

Using $v_{\theta(\text{cone})}r = R^*V_c$ (equation 6.27) the average tangential velocity in the cone is

$$\begin{aligned} \bar{v}_{\theta(\text{cone})} &= \frac{1}{L_c} \int_{L_b}^{L_b+L_c} \frac{R^* \cdot V_c}{R_e + z \cdot \tan(\phi)} dz = \\ &= \frac{R^* \cdot V_c}{L_c \cdot \tan(\phi)} [\ln(R_e + (L_b + L_c) \cdot \tan(\phi)) - \ln(R_e + L_b \cdot \tan(\phi))] \end{aligned} \quad (6.36)$$

The final equation for tangential velocity is then:

$$v_{\theta}(R^*) = \frac{V_c}{2} \left[0.7 + \frac{R^*}{L_b \cdot \tan(\phi)} \ln \left(1 + \frac{R_e + L_c \cdot \tan(\phi)}{R_e + L_b \cdot \tan(\phi)} \right) \right] \quad (6.37)$$

The radicle at Thamshavn is different from a standard cyclone in several ways. The high and narrow inlet, the long vortex finder and the pre-separator. The effects of the pre-separator are discussed in 6.3. In a standard cyclone, the outer vortex will have a negative tangential velocity gradient that eventually reverses itself creating the inner vortex. The long inlet at filter south reduces this negative gradient. The outer vortex will conserve its intensity until slowed down when entering the cone part of the cyclone. This gives room for two assumptions. As previously stated the tangential velocity in the cyclone body is equal to the inlet velocity. And due to this reduce in velocity gradient, the residence time is decreased. To derive equation 3.13, 3.14 and 3.15, Zhao assumes that the flow rate exchanged between the outer and inner vortex decreases linearly toward the cyclone bottom. At filter south it is assumed that this exchange remains constant because of the inlet geometry. The short-circuit flow caused by the vortex finder is still taken into consideration. The residence time used in this model is as following:

$$t_{\text{res1}} = \frac{\pi(R^{*2} - R_e^2)S}{Q} \quad (6.38)$$

The natural vortex length exceeds the radicle dimensions ($l > L_c + L_b - S$) so

$$t_{\text{res2}^*} = \frac{\pi(R^{*2} - R_e^2)(L_c + L_b - S)}{0.9Q} \quad (6.39)$$

$$t_{\text{res}} = t_{\text{res1}} + t_{\text{res2}^*} \quad (6.40)$$

Using this residence time assumes that any particle, no matter what height it enters the cyclone, has the same probability of being collected. This is clearly not the case since the inlet has a height of 4.5 m. Because of this, the two extreme situations is calculated. Using equation 6.40 gives the highest residence time, thus best performance. As this is the most optimistic result it will be labeled $t_{\text{res (max)}}$ from now on. Worst case scenario would then be that all particles are collected with the same probability as the ones entering at the bottom inlet. Using the modified cyclone volume, the minimum residence time would be:

$$t_{\text{res (min)}} = \frac{\pi(R^{*2} - R_e^2)L_c}{0.9Q} \quad (6.41)$$

The true grade efficiency curve is located somewhere between these two extremes.

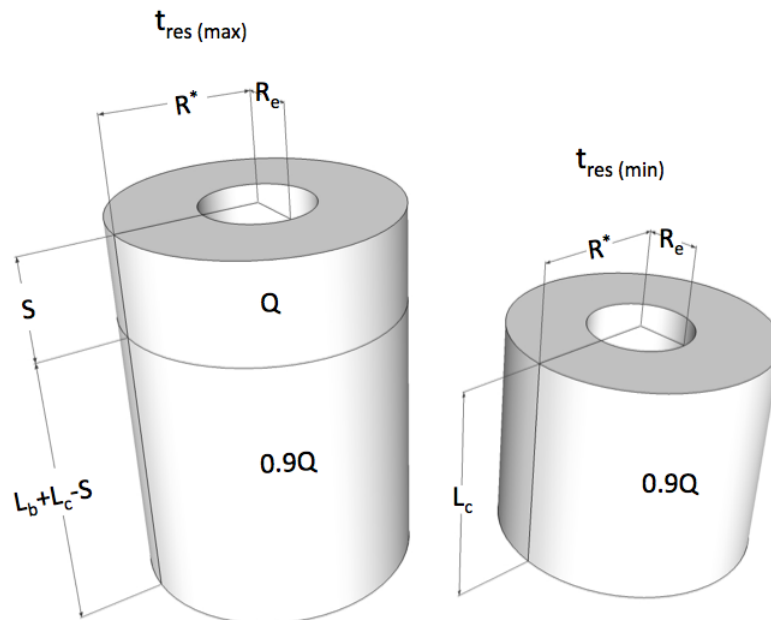


Figure 6.7: Volumes used for calculating t_{res}

Radiclone model summary		
Value	Equation	Assumptions
R^*	$\left[\frac{V_{cs}}{\pi(L_b+L_c)} \right]^{1/2}$ $V_{cs} = \frac{\pi D^2 L_b}{4} + \frac{\pi D^2 L_c}{4} \frac{1}{3} \left[1 + \frac{D_e}{D} + \left(\frac{D_e}{D} \right)^2 \right]$	<ul style="list-style-type: none"> - Uniform radial concentration - Cyclone geometry is transformed into a cylinder by using conservation of effective volume
$v_{rp}(R^*)$	$\frac{Q}{Q_0} \frac{\rho_p d_p^2 v_{\theta p}}{18\mu R^*}$	<ul style="list-style-type: none"> - Curvilinear motion - Spherical particle shape - Zero acceleration in tangential direction - No buoyancy force - Negligible gas density compared to particle density - Stokes law is valid - Particles moves towards the wall with constant radial velocity ($d^2r/dt^2 = 0$)
$v_{\theta}(R^*)$	$\frac{V_c}{2} \left[0.7 + \frac{R^*}{L_b \cdot \tan(\phi)} \ln \left(1 + \frac{R_e + L_c \cdot \tan(\phi)}{R_e + L_b \cdot \tan(\phi)} \right) \right]$	<ul style="list-style-type: none"> - Tangential particle velocity equals tangential gas velocity - The gas stream has no radial acceleration - Irrotational flow - Tangential velocity in cyclone body is equal to inlet velocity
t_{res}	$\frac{\pi(R^{*2} - R_c^2)S}{Q} + \frac{\pi(R^{*2} - R_c^2)(L_c + L_b - S)}{0.9Q}$	<ul style="list-style-type: none"> - 10 % of Q goes straight into the inner vortex after passing the vortex finder - The long inlet prevents any further loss to the inner vortex
η	$1 - \exp \left[-\frac{2v_{rp}(R^*)t_{res}}{R^*} \right]$	<ul style="list-style-type: none"> - Particle collection probability is independent of entrance height

Table 6.1: A mathematical model to predict grade efficiency for filter south at Thamshavn

6.3 Model Parameters

In the model, d_p is the variable and η is the response. The remaining values, the parameters, are constants that needs to be determined.

The total volumetric flow that enters the pre-separator is the sum of the volumetric flow from the oven (Q_O) and the volumetric flow from the over head duct (Q). No gas escapes through the cyclone dust outlet so Q must also be the volumetric flow entering the cyclone. The cyclone inlet velocity is then calculated from the volumetric flow divided by cyclone inlet:

$$V_c = \frac{Q}{HW} \quad (6.42)$$

As Q is unknown this had to be determined by taking pitot samples at the overhead duct. Ideally, such samples should be taken at a location where there is no disturbances in the flow caused by bends. This was not possible for the overhead duct, and some error had to be expected.



Figure 6.8: Location for taking pitot samples at the overhead duct

Formulas for calculating velocity from pitot measurements is given in appendix E. Sampling was taken at four different locations inside the duct, shown in figure 6.8.

From table 6.2, the average dynamic pressure was calculated to be 2.5 mmWC, which corresponds to a gas velocity of 7.8 m/s (used $\rho_g = 0.8$ for a gas temperature of 170°C). Using the duct dimensions from figure 5.12:

$$Q = 7.8 \text{ m/s} \cdot 1.42 \text{ m} \cdot 1.42 \text{ m} = 15.7 \text{ m}^3/\text{s} \quad (6.43)$$

$p_{\text{dyn}} = p_{\text{tot}} - p_{\text{static}}$ [mmWC]			
Location 1	Location 2	Location 3	Location 4
1.4	0.2	3.1	3.6
0.7	5.9	4.5	1.5
0.3	4.3	3.9	1.3
1.6	2.1	1.7	1.0
3.4	1.3	2.4	4.2
1.2	3.8	3.0	3.5

Table 6.2: Pitot measurements in overhead duct

This is approximately 24 % of Q_O (table 6.3). Using equation 6.42 gives $V_c = 24.9$ m/s. Because of the inlet direction this is a tangential velocity.

Table 6.3 shows the model parameters. Geometrical values are found in figure 5.12, gas properties at wikipedia.com and particle properties from Elkem.

Model Parameters								
Geometrical								
H	W	ϕ	D	D_c	D_e	L_b	L_c	S
[m]	[m]	[$^\circ$]	[m]	[m]	[m]	[m]	[m]	[m]
4.50	0.14	22.5	2.20	0.55	1.40	4.50	4.00	2.80
Gas and Particle Properties								
T	μ	ρ_g	ρ_p					
[K]	[kg/ms]	[kg/m 3]	[kg/m 3]					
443	$2.46 \cdot 10^{-5}$	0.8	2300					
Velocity								
Q	Q_O	V_c						
[m 3 /s]	[m 3 /s]	[m/s]						
15.7	65.0	24.9						

Table 6.3: Radiclone parameters

6.4 Result - Radiclone Model

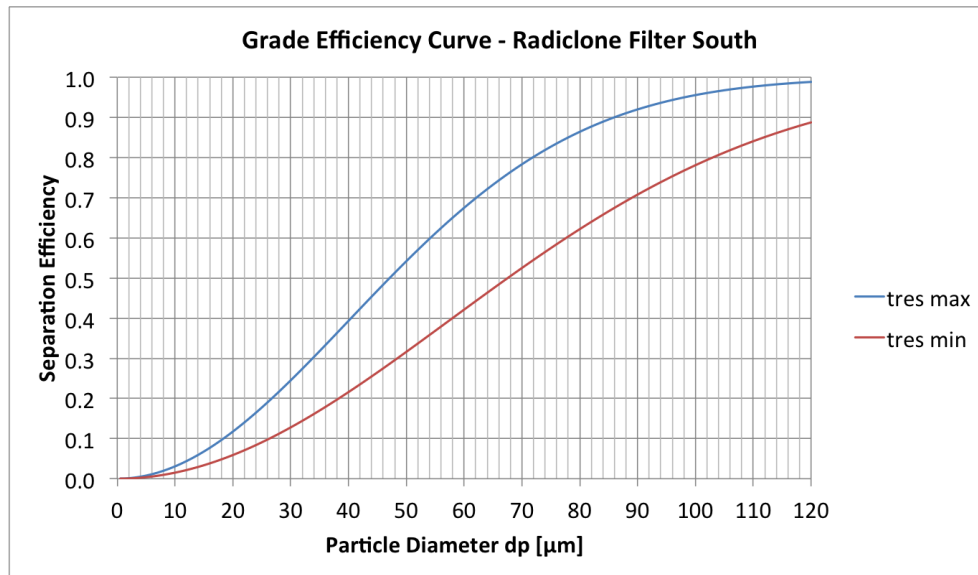


Figure 6.9: Grade efficiency curve, radiclone filter south

6.5 Verification and Validation

This model assumes that there are relatively few particles in the flow, such that they do not affect each others movement. At Thamshavn this is not the case. Particle content in the off-gas is maximized to get most microsilica as possible. Because of this, particles will move together in particle clouds and behave accordingly. Hence, the model is best suited for flows with dilute phases.

Turbulent flow will behave differently for different length scales. This phenomena is called dispersion. The behavior of particles close to the wall in a turbulent flow is known as resuspension. Whether the particle will stick to the wall or how it will move away from it, is controlled by many complex factors such as adhesion forces and friction. Both dispersion and resuspension affect the particle concentration in the radiclone. Because these turbulent features are very challenging to calculate, this model assumes a uniform particle concentration in the radial direction. As it was pointed out in the theoretical study (section 3), a concentration gradient in the radial direction has been observed for cyclones [17] [10]. To calculate the effect of this gradient, several models propose the use of a “turbulent dispersion coefficient” [9] [4]. Smaller particles are more easily affected by turbulence, which leads to a

more uniform concentration. Bigger particles will then cause bigger concentration gradients, and this model is best suited for flows with small particles.

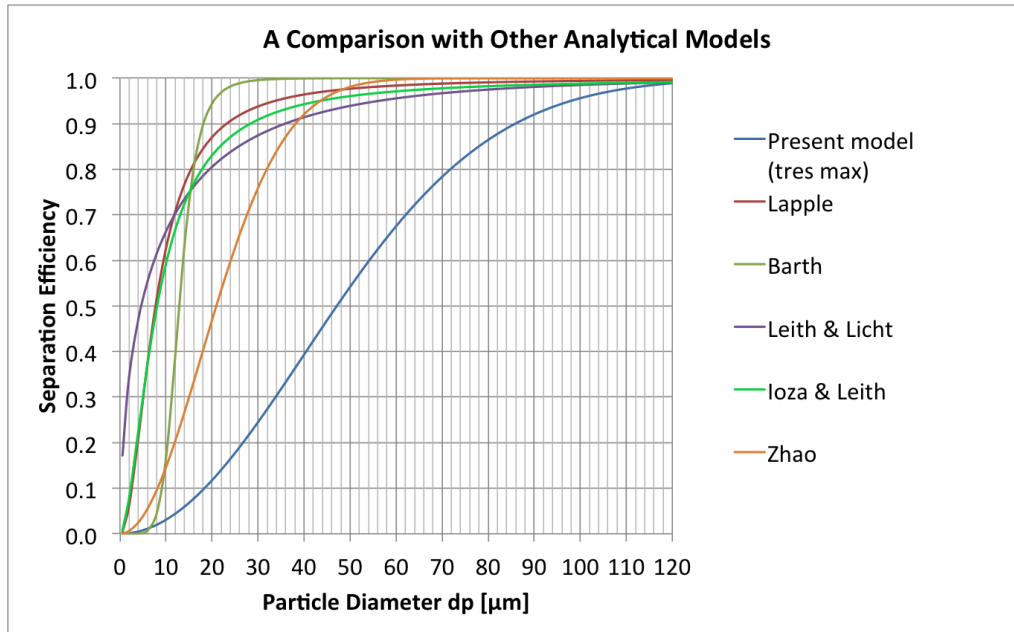


Figure 6.10: Present model compared to the models of Lapple [1], Barth [19], Leith & Licht [2], Izoa & Leith [13] and Zhao [9]

Figure 6.10 compares the present model to a selection of other analytical prediction models. It can be seen that the majority of these calculates a better efficiency than the present model. This can be explained by the long and narrow inlet ($W = 0.14$ m). Many prediction models are sensitive to small numbers which leads to very optimistic results. Calculating an equivalent cylindrical cyclone volume based on the natural vortex length, eliminates the effect of the long inlet. This is because the inlet parameters are only used to determine l . For this particular cyclone geometry, l exceeds the cyclone height which eliminates l from the calculation. The same procedure was used in Zhao's model which is also shifted slightly to the right in figure 6.10. Zhao's model however, does not account for the long vortex finder (S) that also characterize the cyclone at Thamshavn. This estimates a residence time that is too low. Nor does the model from Zhao include the effect on tangential velocity from the long inlet. Because gas is provided from the whole cyclone body height, the average tangential velocity is higher than in a conventional cyclone. The equivalent cylindrical cyclone volume was also used by Leith and Licht, but the inlet parameters are also included at several other locations in the calculation.

Figure 6.11 shows a comparison between the present model and experimental values

from figure 5.20. It can be seen that the predicted efficiency differs significantly from the experimental values. It appears that a bigger fraction of the fine particles do not enter the cyclone as predicted. This indicates that the pre-separator is more efficient than assumed. In the model, m_p was multiplied by Q/Q_O to account for the amount of mass that did not enter the cyclone. This should obviously be taken into account in a different way, and the majority of particles up to the size of $40\ \mu\text{m}$ remains in the pre-separator. This observation should be given most focus when developing the model further.

By playing with the model parameters, it was seen that a closer fit is obtained when reducing either Q or t_{res} . Q was determined at a difficult and inaccurate position with a pitot tube. This produced a significant source of error, and a better estimate of the flow rate into the cyclone would improve the model. t_{res} was based on an effective volume divided by an effective volumetric flow. This is a very rough estimate, but calculating the residence time has been shown to be tricky (section 3.3). More knowledge of how the unique inlet affects the velocity profile, is needed to predict the residence time more accurately. Reading Saruchera dissertation [22] on residence time carefully, could provide further information on how to determine this. Experimental testing is also an option.

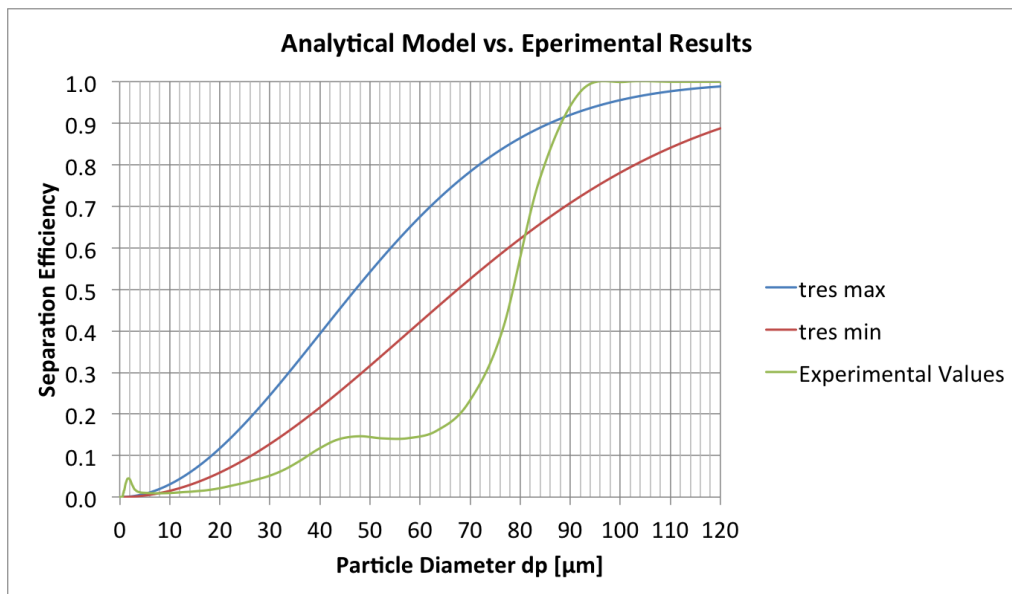


Figure 6.11: Comparing model to experimental results

The experimental values was obtained two months after the model was created. Any further adjustments to the model was therefore not done because of the limited time resources. Suggestions for developing this model further is however summarized in section 10.

7 Optimizing the Radiclone Performance

Microsilica used for creating refractory material, also known as 971, is very challenging to produce. This causes high market demand, and good profits for those with a successful production. Among other criteria, the 971 must contain a maximum of 0.5 % particles bigger than $45 \mu\text{m}$ and maximum 0.7 % carbon as mass percentage. This is just the upper limits, and Elkem aims to get these as low as possible. The carbon and large particle content are both factors that are greatly influenced by the radiclone. It is therefore a vital component in the microsilica production and improving its performance will result in a higher quality product.

7.1 Method

In order to determine the best operating conditions for the radiclone, a factorial analysis was performed. Evaluating the measured values was done using Minitab.

The radiclone performance can easily be manipulated by adjusting fan power, overhead duct gas flow, and the knife damper position. In this experiment the fan power remained at normal operation; giving a 1.8 mbar pressure drop across the filter.



Figure 7.1: Radiclone dampers

The knife and overhead duct dampers were adjusted to wanted positions during normal operation. Dust samples was gathered from the conveyor belt (see figure

4.3), located after the pulse-filter, every 15 minutes during the experiment. After a given period of time, one damper was adjusted to another position, and the process repeated. In figure 7.1, the return duct damper is set to position 7 and both knife dampers is set to 5.5 inches. Even though the knife damper is made up by two individual controllable parts, they were treated as one part. Hence both positions were the same.

The dust samples was analyzed to find amount of carbon and coarse particles. Carbon content was found using a CS-2000 Carbon/Sulfur Determinator.

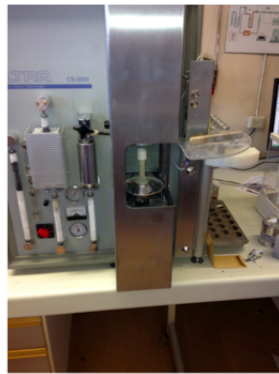


Figure 7.2: CS-2000 Carbon/Sulfur Determinator

The amount of coarse particles was determined using a sieve with $45\ \mu\text{m}$ mesh size. 10 g of dust was used for each sample as showed in figure 7.3. All the particles under $45\ \mu\text{m}$ was forced through the sieve by applying water for two minutes. The sample was then dried at $105\ ^\circ\text{C}$ in six minutes before weighing.



Figure 7.3: Sieving with $45\ \mu\text{m}$ mesh size

7.2 Radiclone Damper Experiment

Dust samples was gathered over a 25 hour period. Staring the experiment at 11:00 14.02.13 the following procedure was conducted.

Date	Time	Knife Damper	Overhead Damper
14.02	11:00	5.5	7
14.02	15:00	4.0	7
14.02	19:00	4.0	9
14.02	23:00	2.5	9
15.02	03:00	2.5	7
15.02	11:00	2.5	9

Table 7.1: Damper positions

To analyze the samples, a 2x2 factorial design was used. Using such a design, tests all the combinations in addition to evaluate them with respect to each other. If a level 2x3 design was to be used, one additional sampling series would have been required with overhead position 9 and knife position 5.5. With limited time and resources this was not possible. The 2x2 design was therefore conducted and then compared with the values obtained for overhead position 7 and knife position 5.5. The design setup is given in the tables below.

Damper	Low Level (-)	High Level (+)
Overhead	7	9
Knife	2.5	4.0

	Knife	Overhead
1	+	+
2	+	-
3	-	+
4	-	-

Table 7.2: 2x2 factorial design setup

This design account for one sample per damper combination. The design is then repeated for any additional samples, and the mean results are presented.

7.2.1 Results

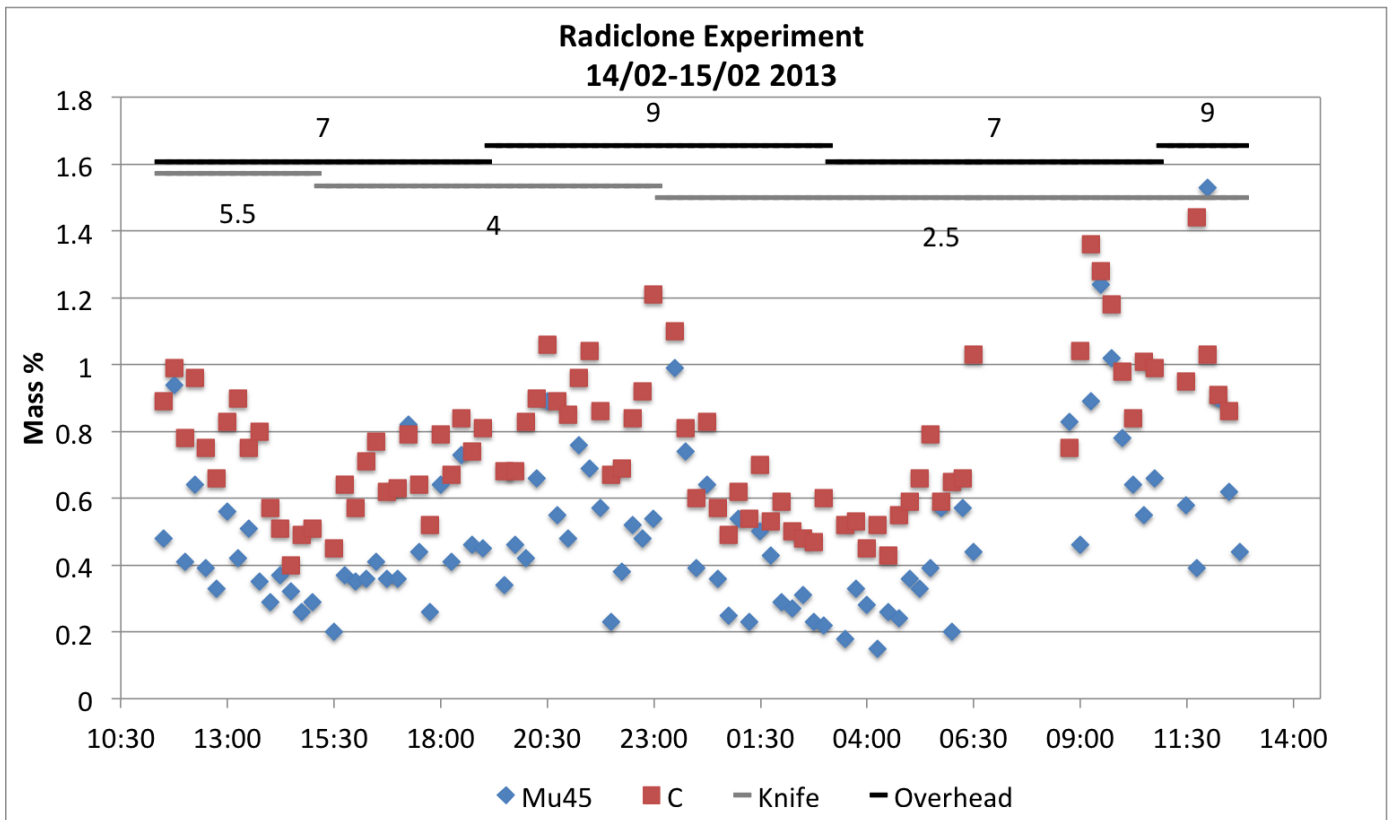


Figure 7.4: Radiclone experiment 14/02-15/02

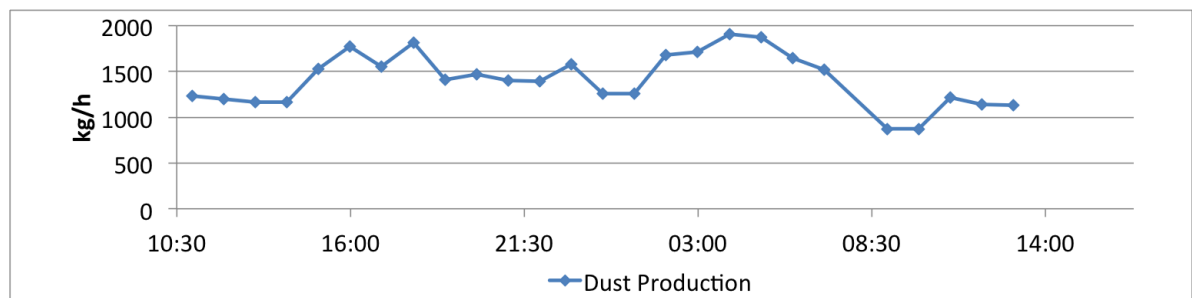


Figure 7.5: Dust production

Figure 7.4 shows overhead and knife damper positions along with the mu45 and C content as mass percentage versus time. Mu45 is the relative weight of particles with a particle diameter $\geq 45 \mu\text{m}$. C is the relative weight of carbon.

7.2.2 Evaluating Data

The results in figure 7.4 shows that there are two different minima points for both carbon and mu45. The first one is obtained for overhead position 7 and knife position 5.5. The second minima is found to be for both overhead potions 7 and 9, when the knife has its narrowest position, 2.5. Figure 7.5 indicates that the highest dust production for this experiment corresponds with overhead position 7. At 06:30 there was a stop in sample gathering. When sampling continued, the new recored values did not correspond very well with the previous ones. There are many factors that determine the microsilica production. Raw materials used in the furnace, occasional stirring of this to prevent clogging and amount of off-gas obtained are just a few factors that influences production. Due to this fact, most attention will be given to those recorded values that shows continuous development. Hence, the samples after 09:00 will be treated with extra skepticism.

Figure 7.6 clearly shows that there is a strong correlation between mu45 and carbon content. This is expected because the larger particles in the off-gas is in fact carbon that comes from the coke and coal used in the furnaces. Reduction of carbon will therefore directly affect the mu45 content in an advantageous way. Further, figure 7.7 and 7.8 shows no correlation to pressure drop over the radiclone. This shows that the mu45 and carbon content can be influenced without adding to the operational costs. Finding good damper combinations would therefore result in higher quality product with no additional costs. It was also observed that the temperature in the radiclone was unaffected by damper openings. This remained at approximately 170°C during the whole experiment.

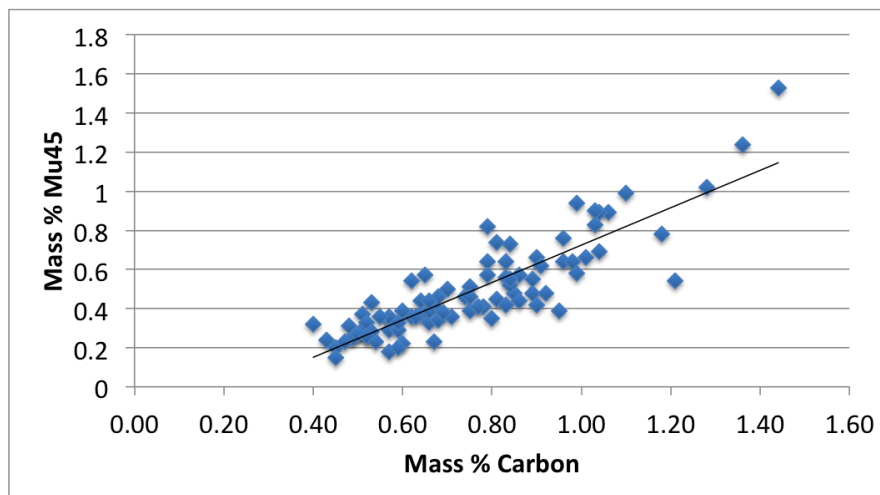


Figure 7.6: Correlation between mu45 and C

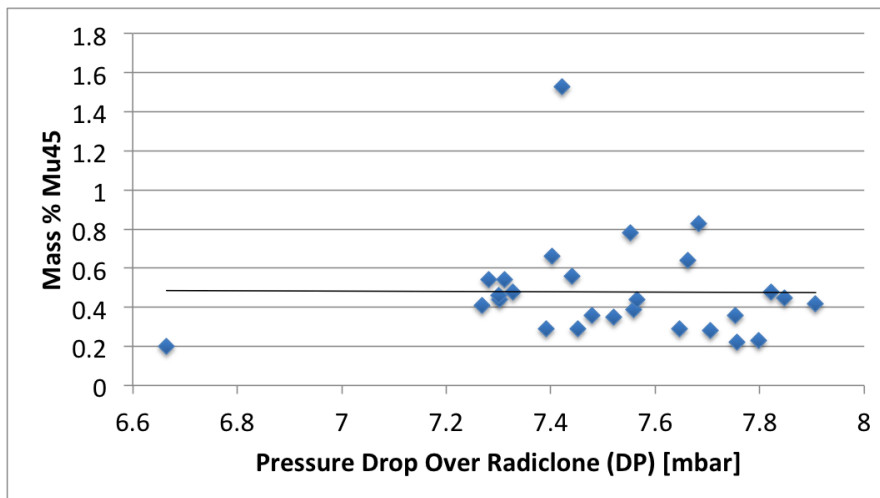


Figure 7.7: Correlation between mu45 and DP

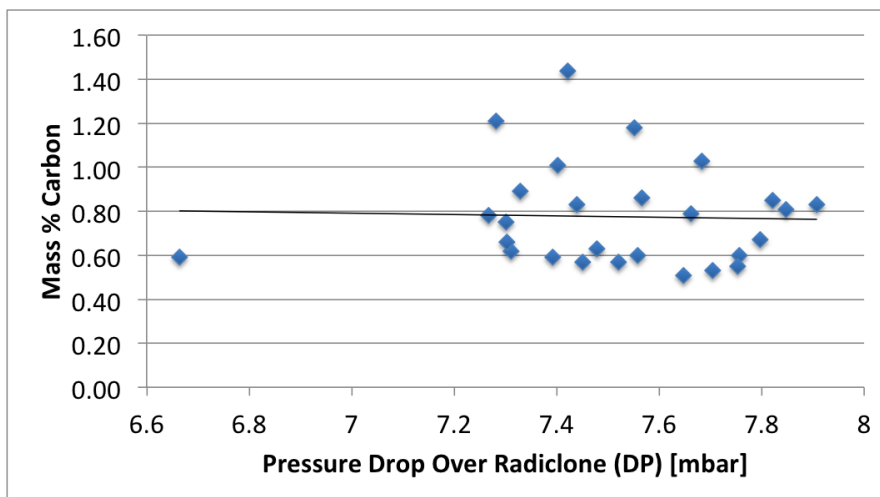


Figure 7.8: Correlation between C and DP

The analysis from Minitab is presented in figure 7.9. The interaction and cube plots show that decreasing overhead and knife position reduces carbon and mu45 content. The residuals show that a large variation in these means are present. The majority of these however, is below zero and represent an even bigger reduction in mu45 and carbon content. This fact contributes to strengthen the above statement of reducing overhead and knife positions.

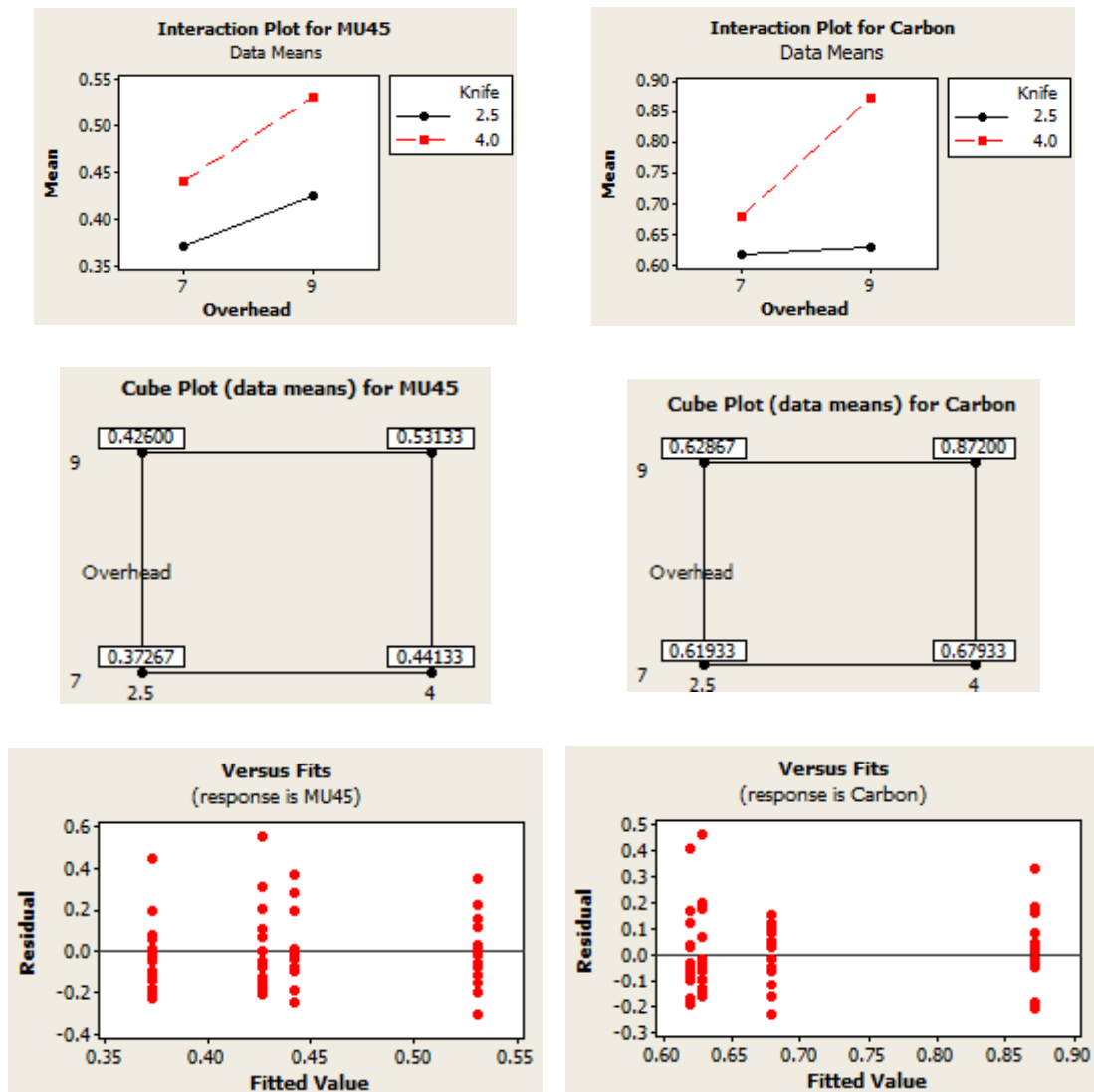


Figure 7.9: 2x2 factorial analysis performed in Minitab

Minitab also provided the following regression fit:

$$\text{mu45} = 0.285 - 0.040 * \text{knife} - 0.004 * \text{overhead} + 0.012 * \text{knife} * \text{overhead} \quad (7.1)$$

With R-Sq = 0.0915, which means that 9.15 % of the samples are explained by the model.

$$C = 1.556 - 0.388 * \text{knife} - 0.148 * \text{overhead} + 0.061 * \text{knife} * \text{overhead} \quad (7.2)$$

With R-Sq = 0.3334, which means that 33.34 % of the samples are explained by the model.

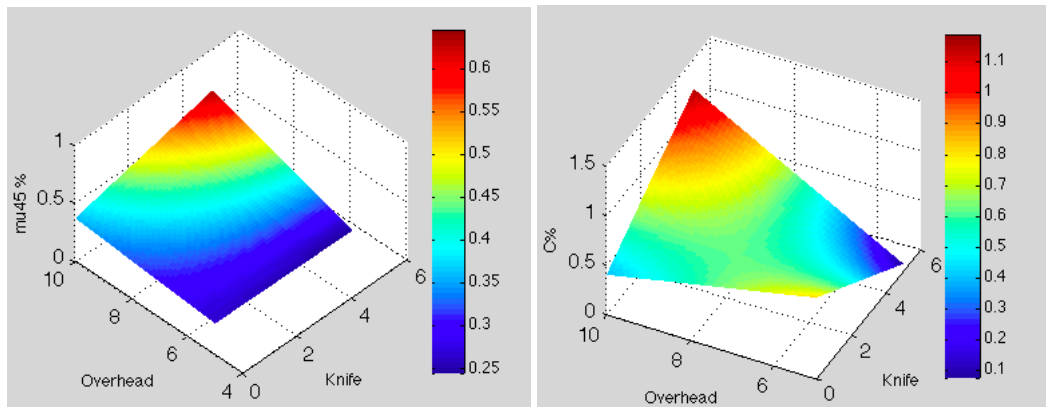


Figure 7.10: Regression fit for mu45 and C

The carbon content model has best fit, and must therefore be given most weight. However, such regression fits must be treated with caution. The samples follow a vague pattern as seen in figure 7.4, and to extrapolate the few samples into a model is most likely to give high errors. The best fit of the two is only 33%, so unfortunately these models are not very trustworthy. Both models suggests that an overhead position close to 6 combined with a knife position of 6.0 gives the the least amount of carbon and mu45. This does not correspond very well with the interaction plot, also produced by minitab (figure 7.10). Weighting the carbon model most, it states that of all the tested damper arrangements, the initial is best suited. From figure 7.4 it can be seen that it is possible to lower both carbon and mu45 content with different arrangements. Based on these observations, the regression models is given less weight when determining what damper positions that should be used.

7.2.3 Recommended Measures

Generally it has been observed that the radiclone performance increases when decreasing the damper positions. How far decreasing dampers can sustain the increasing performance is currently unknown. This is why another experiment should be conducted based on the results of this one. The new experiment should test overhead position 5 and 6 together with knife position 2.0 and 3.0. From the results it is clear that there are still potential improvements to be obtained. And it is also known what range of damper positions that should be used.

Until new experiments has been conducted the overhead damper should be set to 7 to maximize dust production as discussed earlier. And knife position should be 2.5.

7.3 Radiclone Damper Post Experiment

In order to document the effects of changed damper positions, new dust samples was gathered. This was done the same way as described in section 7.1. Unfortunately oven 2 had to be shut down shortly after the damper experiment. Because of this, the load from oven 1 was given to filter north and filter south was inactive for a long time. Because of this, samples could only be gathered from 12.03-18.03 and 11.05-14.05. Gathering of samples in March began one day after filter south was started again. After a stop, it can take up to two weeks before operation is stable again [26], which must be taken into consideration. During both sampling sessions, the dampers had positions: Knife: 2.5, overhead: 7

7.3.1 Results

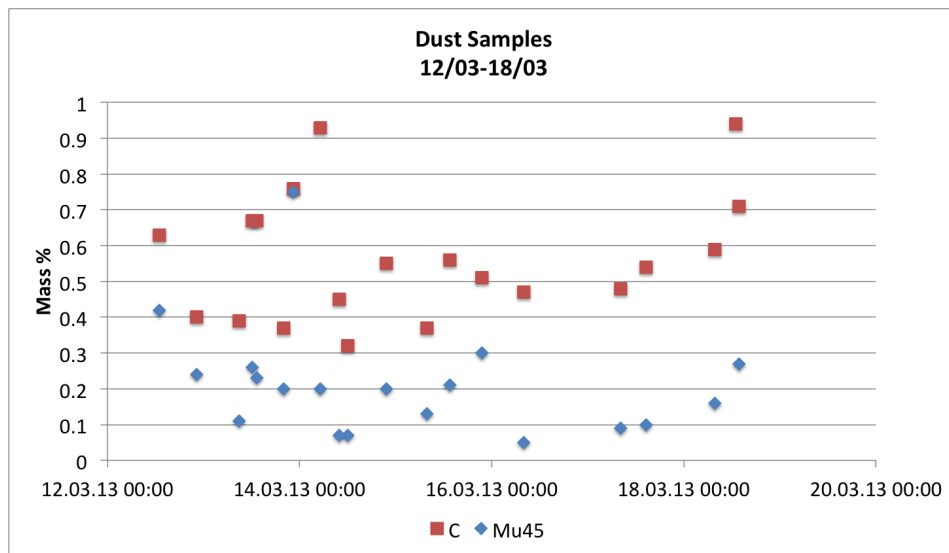


Figure 7.11: Dust samples taken from filter south

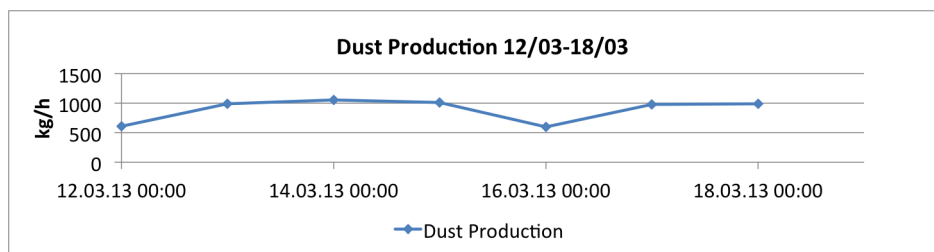


Figure 7.12: Dust production over time

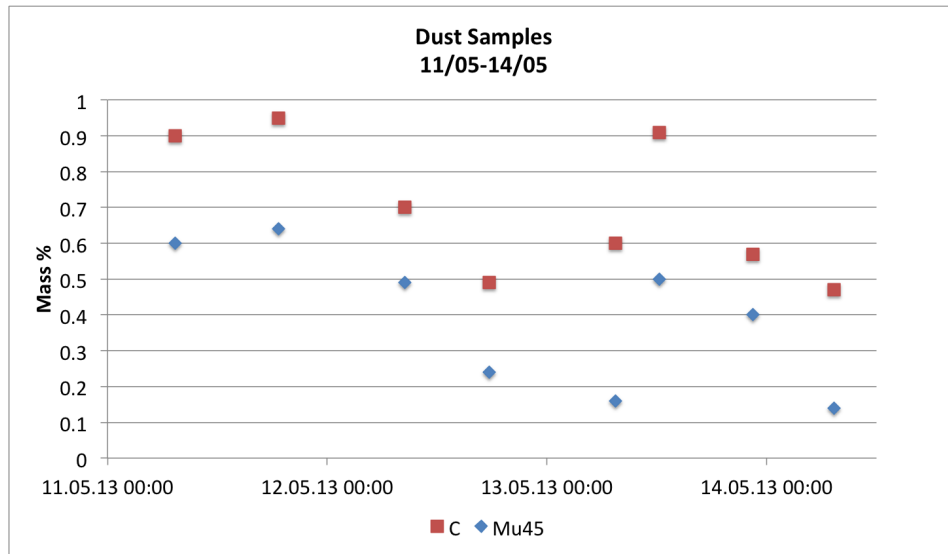


Figure 7.13: Dust samples taken from filter south

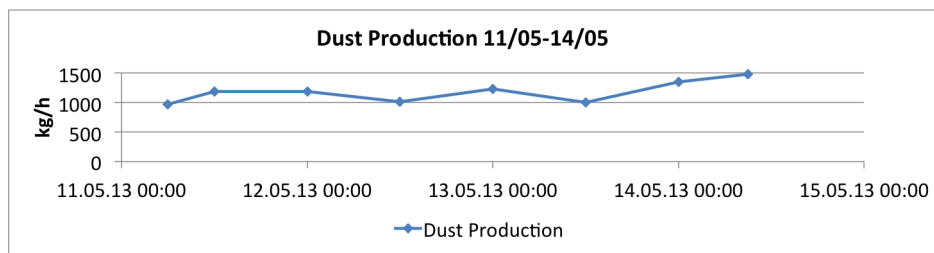


Figure 7.14: Dust samples taken from filter south

7.3.2 Evaluating Post Experiment Data

To document the effect of changing damper positions, the samples from March and May was compared to the first samples taken in February. These samples were taken with damper positions: Knife: 5.5, overhead: 7. This was the former standard positions which makes these samples representative for a stable production before dampers was changed.

The dust production for March and May is more stable than in the first experiment. This suggests that production uses some time to stabilize after damper positions has been changed. For new experiments one should therefore consider more time between damper changing.

From sampling in February and May it can be seen that decreasing dust production

tends to cause both high μ_{45} and C content. The opposite is shown for the samples taken in March. This could be explained by the production stop, one day before the samples was taken. The pressure obtained when operation is normal, makes a thin layer of dust inside the radicle. This layer develops over time, and would not be present after a stop. The surface forces generated by such a layer will push many particles out of the knife dampers reach. In other words, more dust will enter the cyclone, be separated from the gas and dumped after a stop. This causes low dust production, but also a better product.

From the results it is obvious the the process still has big fluctuations in μ_{45} and C content. Table 7.3 shows statistical data for the three sampling sessions. The standard deviations are close to constant which indicates that the spread in quality variations remains the same. The samples taken in February and May is, due to the discussion in the previous paragraph, most representative for a stable operation. It is shown that the mean content of both μ_{45} and C is lowered since February.

Looking at the standard deviation for all samples taken in February from table 7.3, it can be seen that this is slightly higher than the ones taken in March and May. This could indicate that the overall process was affected by the damper positions. It is however possible that this is caused by the nature of the microsilica production which is influenced by many factors. Due to this "random" nature there is not yet enough evidence to claim that the damper positions is the cause of the reduction in μ_{45} and C content.

Damper positions	Date	Mu45 content		Carbon content	
		Sample mean	Standard deviation	Sample mean	Standard deviation
Knife: 5.5 Overhead: 7	14/02-15/02	0.44	0.18	0.72	0.19
Knife: 2.5 Overhead: 7	12/03-18/03	0.21	0.16	0.57	0.18
Knife: 2.5 Overhead: 7	11/05-14/05	0.40	0.20	0.70	0.20
All samples from figure 7.4	14/02-15/02		0.25		0.24

Table 7.3: Statistical data for the three different sampling sessions

8 Additional Separation Stage at Filter South - Cyclone With Air Injection

As mentioned earlier, all of the coarse particles removed in the radiclone is dumped. From the mathematical model, and the experimental results, it is shown that among these coarse particles there are a significantly fraction of salable microsilica particles. The object of the additional separation stage is to recover this fraction of microsilica and transport them back into the process. This is done by using a smaller cyclone that is fed from the radiclone outlet. The coarse particles are dropped from this outlet down into a gas stream of clean air. The particles mix with the air and is led into the cyclone. Due to quality demands, it is required that only the particles with a particle diameter $< 45 \mu\text{m}$ is returned back to the process. The main challenge of the new cyclone would then be to set the cut-off diameter such that the bigger particles are collected, and the ones under $45 \mu\text{m}$ is brought back to the process.

8.1 A Theoretical Study of Cyclones With Additional Streams

In most processes using a cyclone, the goal is to remove as many particles as possible. However, in some cases, there are a certain range of particle sizes that is needed for further applications. Considering the many advantages of a cyclone, it would be beneficial to extend its practical horizon. Many research hours have been spent on this idea, and it has been found that one way of controlling the cut-off diameter is to introduce an additional stream into the cyclone. This stream usually consist of clean air, and the cut-off can be manipulated by varying the volumetric flow.

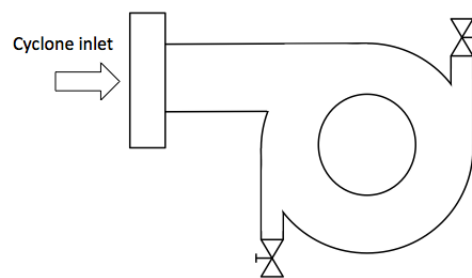


Figure 8.1: Test cyclone, seen from above with two clean air inlets

The origin of this idea came from the work of Unal et al. [30]. A cyclone was used to recover unburned particles from a combustor for re-usage. The idea was to introduce clean air into the cyclone to enhance the unburned particles combustion properties.

The purpose of this research was to determine if the air stream could be applied without affecting cyclone performance. In figure 8.2 the y-axis indicates the centrifugal to drag force ratio (F_c / F_d). As long as this ratio increases the particles will move towards the wall. In order to not disturb F_c / F_d Unal found that the air stream had to be brought tangentially in to the cyclone. Any stream that disrupted the naturally generated vortexes, would give a negative contribution to efficiency. In addition the air stream velocity must equal the the tangential velocity in the cyclone. As seen to the right on figure 8.2, this velocity changes vertically which must also taken into consideration. Unal tested these results further using different air stream inlets at different heights.

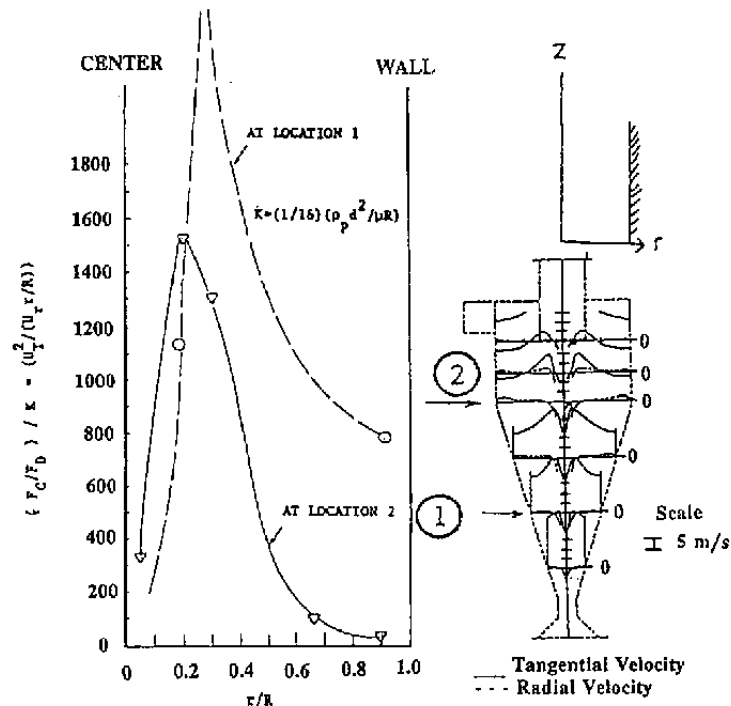


Figure 8.2: Showing F_c / F_d versus radial distance. Also showing velocity profile in a cyclone

The results of this research showed that the cyclone performance would not change significantly until the volumetric flow of the air stream was equal to the primary inlet velocity. For large particles the there was almost none change at all. The small

particles was much more influenced by the air, and for high air stream velocities the overall efficiency improved.

Extending this line of thought, Lim et al. [31] suggested to supply the clean air parallel to the primary dust laden gas. The two streams were separated by a metal plate as showed in figure 8.3. The theory was that the air would push the particles towards the wall when applied next to the primary stream. The experiment was compared with another cyclone without the double inlet, but with same dimensions. It turned out that the double inlet cyclone had a 5 - 15% better performance. Increasing the air flow rate also enchanted the performance further. In addition to push the particles towards the wall, Lim suspected that the air caused them to swirl in the close wall region giving them a better chance of being collected. This is due to the reduced inertia needed when the particles are already moving away from the primary gas stream.

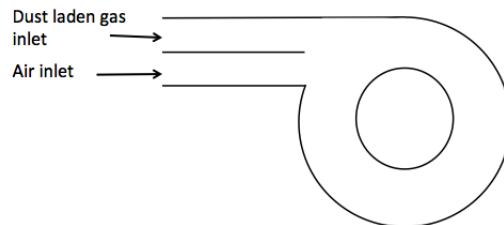


Figure 8.3: Double inlet cyclone. Seen from above

Yoshida et al. [32] suggested to place the air stream inlet in the opposite direction of the primary inlet. Then investigate the effect on performance when shifting axial position of the air stream inlet as shown in figure 8.4. The results showed that using the inlet closest to the top plate produced the smallest cut-off diameter. The hypothesis was that the friction from the top plate slowed the particles down. Because of this, more particles were caught in the inner vortex and therefore escaped with the outgoing gas. By increasing the tangential velocity at this location the majority of particles remained in the outer vortex. There were also performed experiments with increased air flow in which the top air inlet still gave the best cyclone performance. The overall performance also improved with increasing air flow for all the three cases. This is expected because of the increasing centrifugal force that follows higher velocity.

Building further on these discoveries, Fuki et al. [33] investigated the effects of injecting air through the entire cyclone body. A cyclone was made with $2 \mu\text{m}$ pores covering the entire body. Clean air was constantly applied through the pores during

each experiment. Reduced friction at the cyclone wall caused by the air injection resulted in an increased tangential velocity. This is the same effect seen on air hockey tables. The increased tangential velocity gave better cyclone performance with a limited range of air flow rates. When flow rate exceeded a certain level it also influenced the particles and pushed them away from the wall.

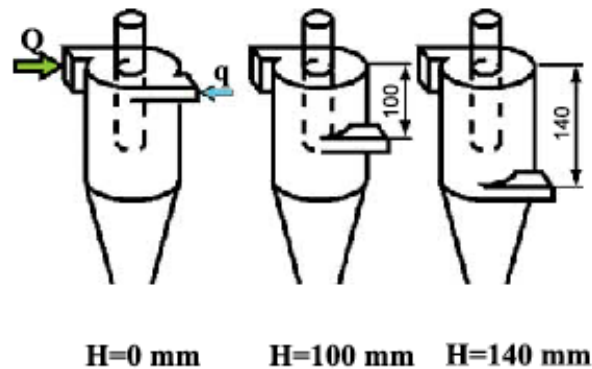


Figure 8.4: Experimental cyclones used by Yoshida et al. Q is dust laden gas flow and q is air flow.

All the previous results indicate that it is possible to influence the cut-off diameter of an existing cyclone by applying additional volumetric flow. For increased performance, this additional volumetric flow should be supplied tangentially into the cyclone at the same height as the primary inlet. As more matter is subjected into the cyclone the pressure drop will increase. This increased performance will not be cost free of course. Usually gas is pulled through the cyclone by a fan. Increased pressure drop must be compensated by increased fan power. The extra supply of pressured air is also added to the operating cost.

8.2 New Cyclone Description



Figure 8.5: The new cyclone

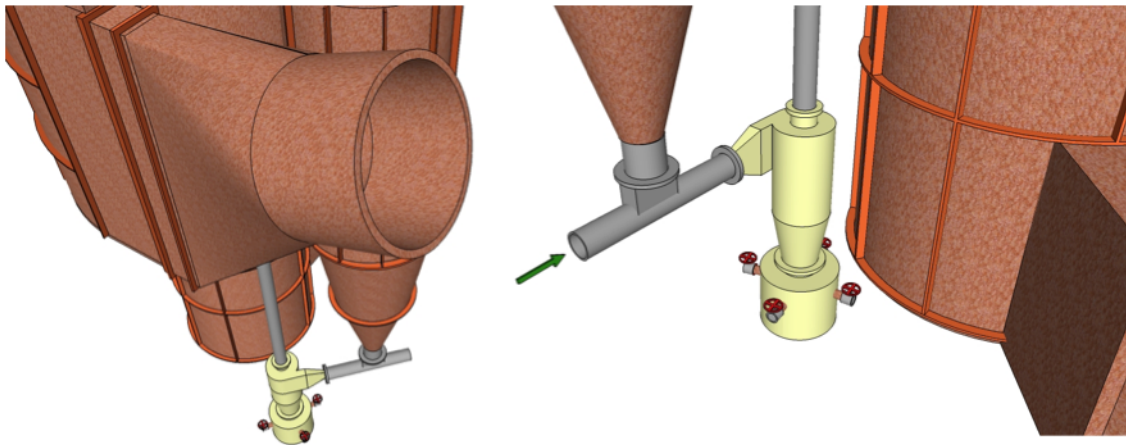


Figure 8.6: The new cyclone. The green arrow indicates where the pressured air is supplied.

The additional cyclone at Thamshavn (C2) is required to collect all the particles above $45\ \mu\text{m}$. This requirement can vary due to quality demand from the customers,

or because Elkem wants to produce microsilica for different purposes. C2 is therefore equipped with four pressured air inlets, and each one is controlled by a valve. As shown in figure 8.5, these pressured air inlets have not yet been connected.

C2 is located between the current cyclone outlet and the radiclone bottom. Dust from the current cyclone outlet is continuously fed down to a tube that leads to C2. This tube is supplied by an air stream that mixes with the dust from the radiclone. This creates a dust laden gas that is sent into C2, and the particles that are not separated are sent back into the radiclone inlet (see figure 8.6). These particles will go through the whole radiclone process again, and hopefully stay with the gas until it is collected by the filter.

8.3 Calculating Optimal Volumetric Flow Into the New Cyclone

There are five possible flows into C2. One primary that carries the dust, and four secondary air injections that is used to control the cut-off diameter. All the flows are controlled by valves that is connected to the pressure system of the plant. The major challenge when integrating this into the separation process, is to obtain the appropriate cut-off diameter. A cut-off too small will send large particles back into the process which will decrease product quality. A cut-off too big will be without purpose, and will give the same result as not having an additional cyclone. Currently filter south is supposed to deliver microsilica with max 0.5 % particles bigger than 45 μm . When calculating the necessary volumetric flow to obtain this, it is convenient to look at the critical diameter (d_{100}), which gives 100 percent collection. As discussed earlier, d_{100} has been derived in many different ways. The one used for this problem involves the residence time, and is from table 3.1:

$$d_{100} = \left[\frac{9\mu D^2 \left(1 - \frac{2r_i}{D}\right)^{2n+2}}{4(n+1)V_c^2 \rho_p t_{\text{res}}} \right]^{1/2} \quad (8.1)$$

It should be noted that Elkem could not provide the dimensions of C2. The values used in this calculation are therefore based on physical measurements done with measuring tape. The values used, are given in table 8.1. The following calculations assumes that all the valves are shut, and the total flow into the cyclone comes from the primary inlet.

Model Parameters						
Geometrical						
H	W	D	D_e	L_b	L_c	S
[m]	[m]	[m]	[m]	[m]	[m]	[m]
0.50	0.10	0.60	0.35	1.70	1.30	0.80
Gas and Particle Properties						
T	μ	ρ_p	d_{100}			
[K]	[kg/ms]	[kg/m ³]	[m]			
283	$1.81 \cdot 10^{-5}$	2300	$45 \cdot 10^{-6}$			

Table 8.1: Radiclone parameters

Rearranging the previous equation and using $Q = V_c HW$, gives

$$Q = HW \left[\frac{9\mu D^2 \left(1 - \frac{2r_i}{D}\right)^{2n+2}}{4(n+1)d_{100}^2 \rho_p t_{\text{res}}} \right]^{1/2} \quad (8.2)$$

where r_i is defined as:

$$r_i = \frac{D}{2} - W \quad (8.3)$$

The vortex exponent n is given from the empirically obtained equation:

$$n = 0.67D^{0.14} \quad (8.4)$$

This is valid for 283 K. As pressured air is used for C2, the gas temperature is equal to the ambient temperature. It is assumed that the average temperature at Thamshavn is about 10 °C.

Remembering that the residence time derived by Zhao was dependent on the length of the natural vortex length l , it is necessary to calculate this from equation 3.6:

$$l = 2.3 \cdot 0.4 \text{ m} \cdot \left(\frac{0.85^2 \text{ m}^2}{0.7 \text{ m} \cdot 0.1 \text{ m}} \right)^{1/3} = 2.0 \text{ m} \quad (8.5)$$

This shows that $l > L_c + L_b - S$ so t_{res} is given by equations 3.13 and 3.15:

$$t_{\text{res}} = t_{\text{res1}} + t_{\text{res2}} = \frac{\pi(R^{*2} - R_e^2)(2L_c + 2L_b - 1.1S)}{0.9Q} \quad (8.6)$$

Inserting this into equation 8.2 gives the final expressions for optimum volumetric flow.

$$Q = \left\{ HW \left[\frac{81}{40} \frac{\mu D^2 \left(1 - \frac{2r_i}{D}\right)^{2n+2}}{(n+1)d_{100}^2 \rho_p \pi (R^{*2} - R_e^2)(2L_c + 2L_b - 1.1S)} \right]^{1/2} \right\}^{1/2} \quad (8.7)$$

By inserting all the values, Q is determined to be $0.25 \text{ m}^3/\text{s}$.

8.4 Discussion

Four valves is used for controlling the amount of pressured air that is let into C2. Based on the theoretical study in section 8.1, higher air load will reduce efficiency. This is because the pressured air is introduced in the opposite direction relative to the outer vortex. Higher air load will therefore cause more particles to be sent back to the radiclone. It will also increase the particle size of those particles returned.

From the calculations, $Q = 0.25 \text{ m}^3/\text{s}$. To validate this result, it is compared with experimental results given by Zhao [9], cyclone IV. Cyclone IV is quite similar in dimensions, but smaller. The test-particles are also close in density compared to microsilica. Experimental values for cyclone IV shows the limit d_{100} very close to $45 \text{ }\mu\text{m}$ with $Q_{IV} = 0.61 \text{ m}^3/\text{s}$. From this it is obvious that the calculated Q is too low. It is 41% lower than the experimental value, when it should be slightly bigger because C2 is larger. The model used for calculating d_{100} assumes that the particle has no radial acceleration, the same assumption that was used in section 6. It was also assumed that the radial velocity is equal to zero. This makes d_{100} dependent on the residence time only, and opens for many errors since the radial position will in fact influence the residence time. Further, the calculations for residence time assumes that all particles enters C2 at the same position, and that they all have

the same probability for collection. This is not true and particles that enters at the bottom of the inlet will have a shorter residence time, thus higher Q is needed to collect these. This is one of the factors that causes the calculated Q to be small. The turbulent features will also cause some error. As discussed earlier, these features are hard to implement in an analytical model and has been neglected.

For this simple model, the best approximation for additional air into C2 must be based on Q . One way of doing this would be to divide a fraction of Q equally on the four different inlets. One would then obtain a very rough estimate for operation criteria for C2. However, introducing such extra flow will completely change the flow pattern and the model will be even less accurate. Improvements could be made to the model, but the physical problem is too complicated to produce any good results from such a method.

8.5 Recommended Measures

It was calculated that a volumetric flow of $0.25 \text{ m}^3/\text{s}$ is needed for C2 to separate all particles above $45 \mu\text{m}$.

Calculating cyclone performance analytically is a difficult task, and introducing additional air streams makes it even more complicated. Q was calculated by assuming that this amount entered the primary inlet. Making this assumption shows that it is theoretically possible to achieve $d_{100} = 45 \mu\text{m}$ without using any of the four air supplies. However, such a process is much easier to control by using additional air streams. It is also highly unlikely that the calculated Q will cause the exact wanted performance. Implementing C2 into the process should therefore be done experimentally and the calculated Q must only be used as a guideline. The experimental method would be a “trial and error” procedure. Using the same kind of experimental set up as in section 7, along with good preparations, would be an efficient way of determining good operation conditions. Rough testing by Elkem Materials indicates that the four valves should have an opening of 10-50% [34].

9 Conclusion

In this master thesis, a theoretical study of cyclone models has been performed. Basic theory has been presented, followed by a discussion of analytical approaches to determine velocity profile and efficiency. From this discussion, the theory best suited to describe the radiclone at Thamshavn filter south, was used to build an efficiency model. This model has been used to create a grade efficiency curve for the radiclone. It was found that this model is best suited for dilute flows containing small particles.

The current performance of the radiclone has been documented by gathering and analyzing dust samples. These samples were taken at the radiclone outlet and the pulse-jet filter outlet. From the obtained samples it was found that 2 % of the separated dust are profitable microsilica. And that 3 % of the produced microsilica contains particles bigger than 45 μm .

Comparing the predicted grade efficiency curve to the experimental, it was found a slightly mismatch. Based on the experimental grade efficiency curve, several measures have been suggested to improve the model further. Determining the fraction of microsilica removed in the pre-separator showed to be the most significant deviation. Experimental values indicated that particles with a diameter $<65 \mu\text{m}$ had less than 20 % collection efficiency. The present model however, predicts an efficiency of 50-75 % for this particle size.

In order to improve the radiclone performance, a factorial analysis has been performed. The analysis has shown that improvements are obtainable by changing the radiclone damper configurations. It was also found that further investigations are necessary. Running more of these experiments are a minor economical liability, and it was shown that there is a significant potential for further improvements. With the current knowledge, a knife damper position of 2.5 and an overhead position of 7 gives satisfactory production.

An attempt of calculating the amount of gas flow needed for the new cyclone at filter south has been made, with modest successes. The calculated value was determined to be too low by comparing it with similar experimental values presented by Zhao [9]. Introducing additional flows into the cyclone outlet causes complicated flow patterns. It was shown that this complexity was very hard to describe analytically, and that the calculated value should be used with caution. It can however, be used as an initial value for experimental testing.

10 Further Research

Analytical Model

- Create a new prediction model to calculate the fraction of particles that is removed by the pre-separator. The documented particle size distribution would be an important tool in doing this. The current parameter Q/Q_O used for this purpose was unable to give satisfactory results.
- Increase model accuracy by eliminating assumptions. Factors like buoyancy force, particle shape and axial velocity can be incorporated fairly easy and will contribute to a better approximation of the physical problem. Another factor that should be incorporated is the concentration distribution. This is a more complex challenge, but it is discussed thoroughly in different literature and involves the calculation of a turbulent dispersion coefficient [9] [4].
- Determining the current model parameters with less error. Volumetric flow into the cyclone Q are included at various calculations in the model. The present method of using a pitot tube showed limited accuracy. Improving the estimate of residence time t_{res} will also give an significant better accuracy.

Radiclone Optimization

- Further experimenting with the damper positions should be conducted. Based on the current results, knife position 2 and 3 should be tested along with overhead position 5 and 6. A longer sampling period with each damper position is recommended to stabilize production.
- Analyzing dust samples should be done upon gathering. This is to eliminate the effect of agglomeration that causes a higher fraction of bigger particles. Taking dust samples with an impactor is one option.

Cyclone with Air Injection

- Experimental testing on the new cyclone to determine efficient operation criteria. Further attempts of calculating this analytical is not recommended.

References

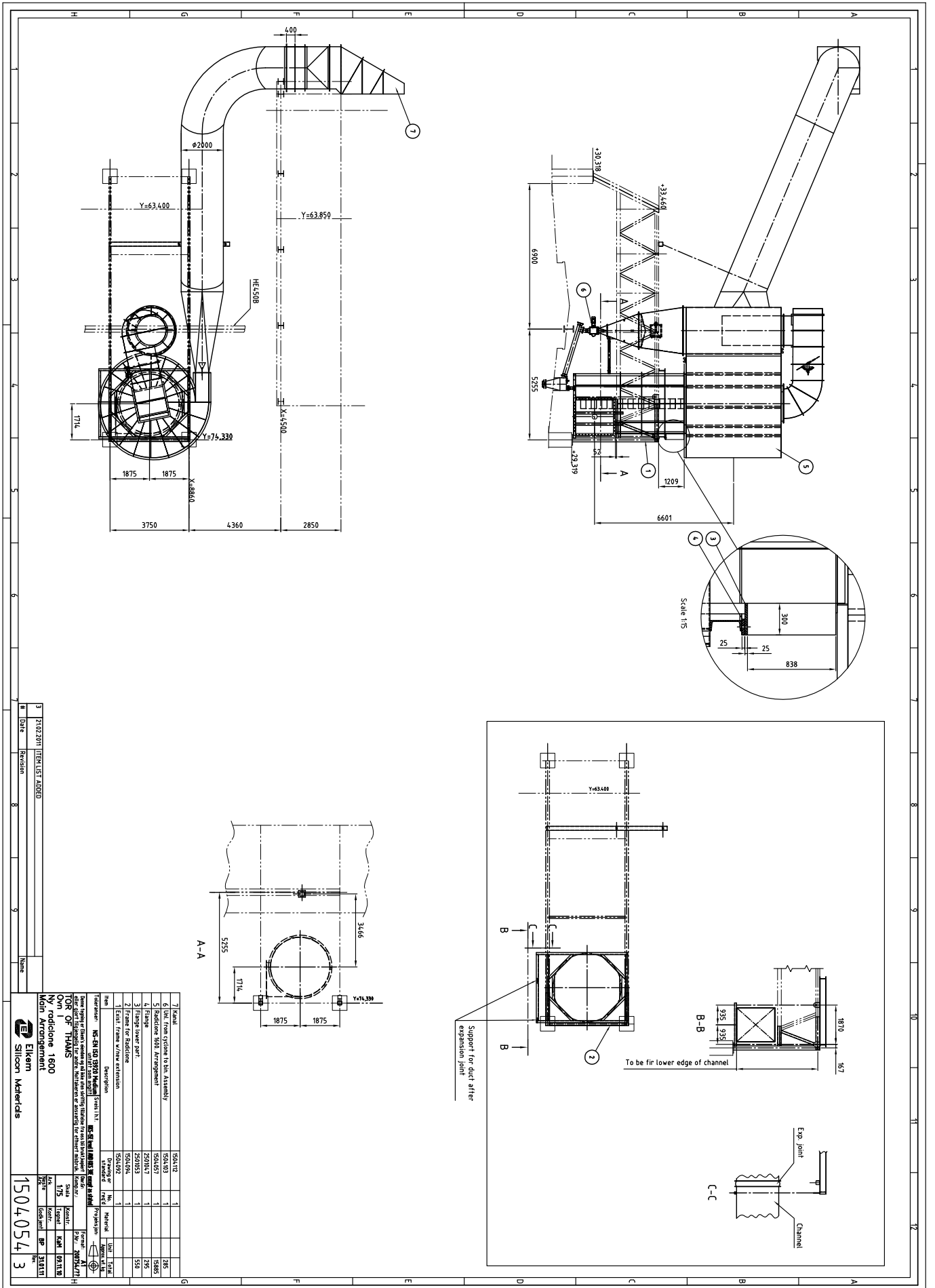
- [1] C.E. Lapple. Processes use many collector types. *Chemical Engineering*, 58:144–151, 1951.
- [2] W. Licht D. Leith. The collection efficiency of cyclone type particle collectors: a new theoretical approach, in: airpollution and its controll'. *AIChE Symp.*, 68:196–206, 1972.
- [3] 02.2013. <http://www.farrapc.com/products/cyclone/how-cyclone-works>.
- [4] A. Gil C. Cortes. Modeling the gas and particle flow inside cyclone separators. *Progress in energy and combustion science*, 33:409–452, 2007.
- [5] Martin Rhodes. *Introduction to Particle Technology*. Wiley, 1998.
- [6] 04.2013. www.frbiz.com.
- [7] 04.2013. <http://www.skepune.net>.
- [8] 05.2013. <http://www.dyson.com/vacuums.aspx>.
- [9] B. Zhao. Prediction og gas-particle separation efficiency for cyclones: A time-of-flight model. *Separation and Purification Technology*, 85:171–177, 2011.
- [10] L. Wang. *Theoretical study of cyclone design*. PhD thesis, Texas A and M University, 2004.
- [11] M.A Goula N.D. Charisiou, G.J. Tsevrenis. Software development for the design of control equipment for particulate pollutants. *In Proc. 12th International Conference on Enviromental Science and Technology*, pages 295–302, 2011.
- [12] W. Barth. Design and layout of the cyclone separator on the basis of new investigations. *Brennstoff-Warme-Kraft*, 8:1–9, 1956.
- [13] D. Leith D.L. Iozza. The logistic function and cyclone fractional efficiency. *Aerosol Science Technology*, 12(3):598–606, 1990.
- [14] C.B. Parnell. Cyclone design for air pollution abatement associated with agricultural operations. *In Proc. 1996 Beltwide Cotton Production Conference*, 1996.
- [15] R. M. Alexander. Fundamentals of cyclone samplers. *Aerosol Science*, pages 152–153, 1949.
- [16] I. Karagoz A. Avci. Effects of flow and geometrical paameters on the collection efficiency in cyclone separators. *Aerosol Science*, 34(7):937–955, 2003.

-
- [17] B. Zhao. Development of a new method for evaluating cyclone efficiency. *Chemical Engineering and Processing*, 44(4):447–451, 2005.
- [18] J. W. Lee C.H. Kim. A new collection efficiency model for small cyclones considering the boundary-layer effect. *Aerosol Science*, 32:251–269, 2001.
- [19] L. Otten M. E. Fayed. *Handbook of powder science and technology*. Springer, 2 edition, 1997.
- [20] C.B. Shepherd and C.E. Lapple. Flow pattern and pressure drop in cyclone dust collectors. *Chemical Engineering*, 32:972–984, 1940.
- [21] F. Löffler H. Mothes. A model for particle separation in cyclones. *Chemical Engineering and Processing: Process Intensification*, 18(6):323–331, 1984.
- [22] T. Saruchera. *Measurement and modelling of particle residence time in a return-flow cyclone*. PhD thesis, University of Canterbury, 1999.
- [23] B. Antoine J. Villiermaux J. Lede, F. Verzaro. Flash pyrolysis of wood in a cyclone reactor. *Chemical Engineering and Processing: Process Intensification*, 20(6):309–317, 1986.
- [24] S.D. Kim S.K. Kang, T.W. Kwon. Hydrodynamic characteristics of cyclone reactors. *Powder Technology*, 58(3):211–220, 1989.
- [25] Martin B. Midthun. Compacting of filter dust at elkem thamshavn. 2012.
- [26] Jørund Vangskåsen. *Elkem Engineering Trainee*, Personal communication.
- [27] Elkem Materials. Trykktap i foruskillere.
- [28] R. C. Hibbeler. *Engineering Mechanics: Statics and Dynamics*. Prentice Hall, 13 edition, 2012.
- [29] M. E. Weber R. Cift, J. R. Grace. *Bubbles, Drops and Particles*. Academic Press, 1978.
- [30] C. Soong J. Chen C. Unal, K. Tzula. Experimental study of a cyclone with tangential secondary air injection. *Powder Technology*, 74:79–87, 1993.
- [31] K.W Lee K.S. Lim, S.B. Kwon. Characteristics of the collection efficiency for a double inlet cyclone with clean air. *Aerosol Science*, 34:1085–1095, 2003.
- [32] K. Fukui H. Yoshida, K. Ono. The effect of a new method to fluid flow control on submicron particle classification in gas-cyclones. *Powder Technology*, 149:139–147, 2005.

- [33] K. Jikihara T. Yamamoto K. Fukui, H. Yoshida. Effects of clean-air injection on particle-separation performance of novel cyclone with sintered metal cone. *Separation and Purification Technology*, 80:356–363, 2011.
- [34] Svein Arild Nyrnes. *Project Engineer Elkem Materials*, Personal communication.

Appendix

Appendix A - Technical Drawings of the Radiclone

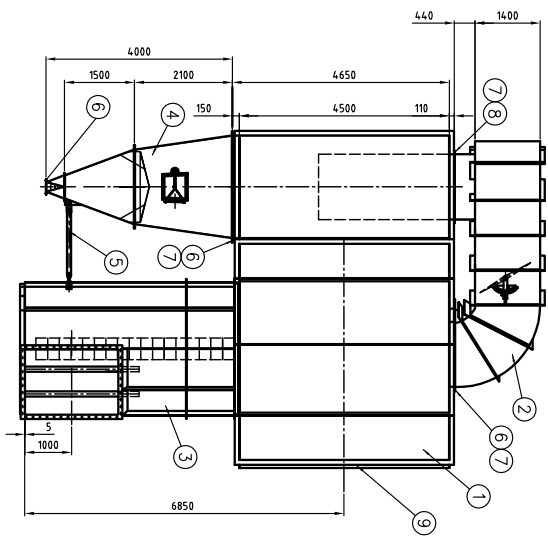
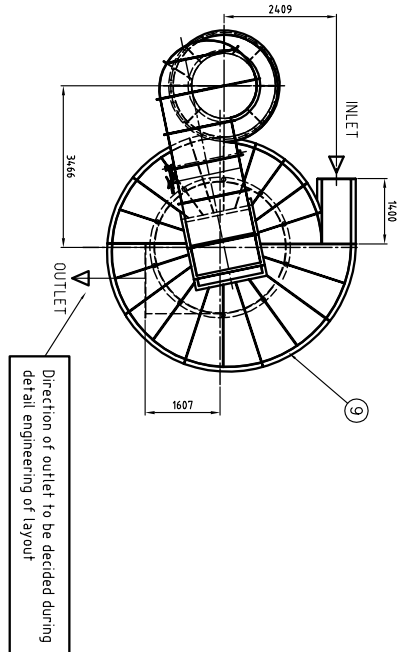


3	21/02/2011	ITEM LIST ADDED	8	None
M	Date	Revision		Notes

Item	Description	Quantity	Material	Unit	Notes
7	Keel	1504054	1	1	
6	Duct from cyclone to bin Assembly	1504053	1	285	
5	Radicle 600 Arrangement	1504057	1	1585	
4	Flange lower Part	2500047	1	295	
3	Flange lower Part	2500053	1	550	
2	Frame for Radicle	1504056	1		
1	Expt Frame with extension	1504052	1		

Material: HE-450B
Reference: HE-450 B (2010) Radicle System (1)
Scale: 1:75
Drawn by: [Signature]
Checked by: [Signature]
Approved by: [Signature]

Item 1504054
Material: HE-450B
Quantity: 1
Unit: 1



* TEMP. MIN. 250 DEGREES

Qty	Description	Unit	Material	Weight	Remarks
46	STRENER 100X2	9	SA.37-2	1305	
24	BOLT M8X30 W/ NUT AND WASHER	8	SA.8.8	9.6	
20	PACKING ROPE AND	7	Konrad	-	
66	BOLT M8X30 W/ NUT AND WASHER	6	SA.8.8	28.7	
1	SAVY TUBE	5	150A070	80	
1	HOPPER	4	150A087	306.3	
1	LOWER PART	3	150A084	2980	
1	CONNECTING BOLT	2	150A082	2177.8	
1	UPPER PART	1	150A059	1895	

NET WEIGHT: ~1485. KG

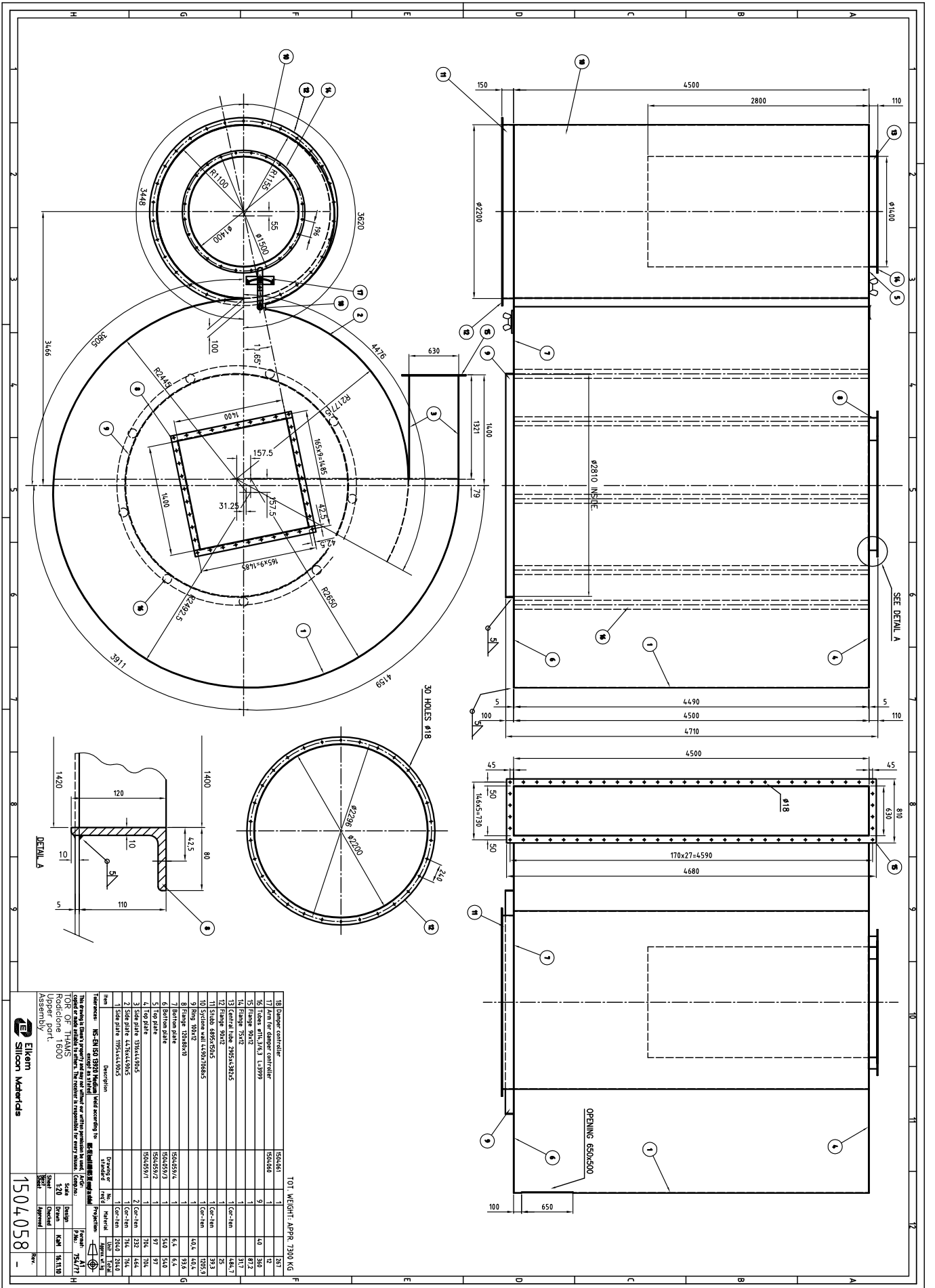
References: MS-EN 10338 Technical sheet according to the manufacturer's data sheet.

This drawing is the property of Elkem and shall not be used or reproduced without the written permission of Elkem. It is the responsibility of the user to ensure that the information is up-to-date and correct.

FOR OF THAVAS
Redicione 1600
Arrangement

Elkem Materials

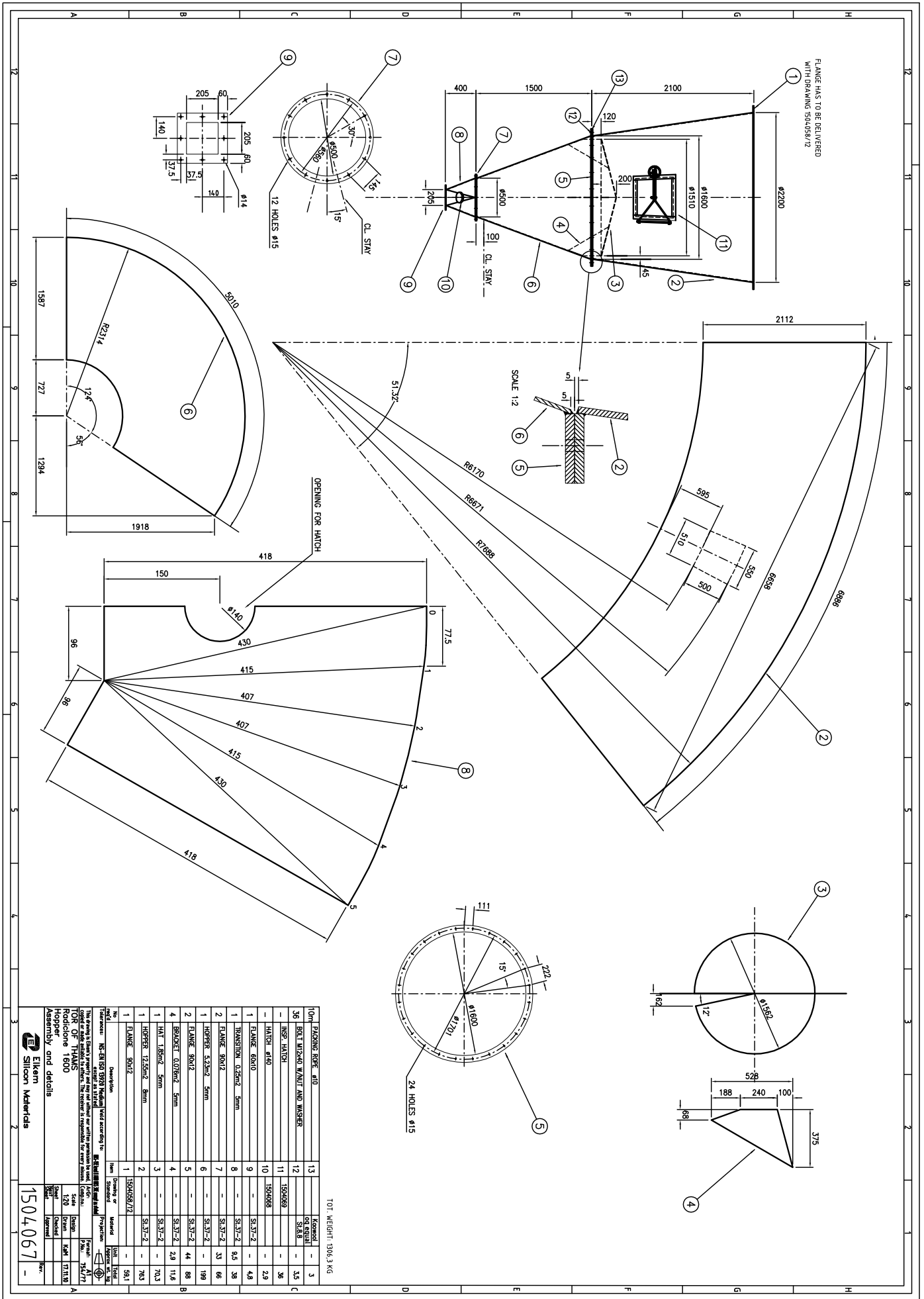
1504057 -



10T WEIGHT: APPROX 390 KG

Item	Description	Material	Quantity	Weight (kg)
18	Upper cover	SA5083	1	287
19	Lower cover	SA5083	1	287
20	Inner shell	SA5083	1	140
21	Outer shell	SA5083	1	140
22	Flange 1502	SA5083	1	812
23	Flange 1502	SA5083	1	812
24	Flange 1502	SA5083	1	812
25	Flange 1502	SA5083	1	812
26	Flange 1502	SA5083	1	812
27	Flange 1502	SA5083	1	812
28	Flange 1502	SA5083	1	812
29	Flange 1502	SA5083	1	812
30	Flange 1502	SA5083	1	812
31	Flange 1502	SA5083	1	812
32	Flange 1502	SA5083	1	812
33	Flange 1502	SA5083	1	812
34	Flange 1502	SA5083	1	812
35	Flange 1502	SA5083	1	812
36	Flange 1502	SA5083	1	812
37	Flange 1502	SA5083	1	812
38	Flange 1502	SA5083	1	812
39	Flange 1502	SA5083	1	812
40	Flange 1502	SA5083	1	812
41	Flange 1502	SA5083	1	812
42	Flange 1502	SA5083	1	812
43	Flange 1502	SA5083	1	812
44	Flange 1502	SA5083	1	812
45	Flange 1502	SA5083	1	812
46	Flange 1502	SA5083	1	812
47	Flange 1502	SA5083	1	812
48	Flange 1502	SA5083	1	812
49	Flange 1502	SA5083	1	812
50	Flange 1502	SA5083	1	812
51	Flange 1502	SA5083	1	812
52	Flange 1502	SA5083	1	812
53	Flange 1502	SA5083	1	812
54	Flange 1502	SA5083	1	812
55	Flange 1502	SA5083	1	812
56	Flange 1502	SA5083	1	812
57	Flange 1502	SA5083	1	812
58	Flange 1502	SA5083	1	812
59	Flange 1502	SA5083	1	812
60	Flange 1502	SA5083	1	812
61	Flange 1502	SA5083	1	812
62	Flange 1502	SA5083	1	812
63	Flange 1502	SA5083	1	812
64	Flange 1502	SA5083	1	812
65	Flange 1502	SA5083	1	812
66	Flange 1502	SA5083	1	812
67	Flange 1502	SA5083	1	812
68	Flange 1502	SA5083	1	812
69	Flange 1502	SA5083	1	812
70	Flange 1502	SA5083	1	812
71	Flange 1502	SA5083	1	812
72	Flange 1502	SA5083	1	812
73	Flange 1502	SA5083	1	812
74	Flange 1502	SA5083	1	812
75	Flange 1502	SA5083	1	812
76	Flange 1502	SA5083	1	812
77	Flange 1502	SA5083	1	812
78	Flange 1502	SA5083	1	812
79	Flange 1502	SA5083	1	812
80	Flange 1502	SA5083	1	812
81	Flange 1502	SA5083	1	812
82	Flange 1502	SA5083	1	812
83	Flange 1502	SA5083	1	812
84	Flange 1502	SA5083	1	812
85	Flange 1502	SA5083	1	812
86	Flange 1502	SA5083	1	812
87	Flange 1502	SA5083	1	812
88	Flange 1502	SA5083	1	812
89	Flange 1502	SA5083	1	812
90	Flange 1502	SA5083	1	812

1504058 -



FLANGE HAS TO BE DELIVERED WITH DRAWING 1504067/2

TOT. WEIGHT: 1906,3 KG

QTY	DESCRIPTION	REVISION	DATE
13	FLANGE FOR 410	1	15/04/07
36	BOLT M12x40 W/ NUT AND WASHER	1	15/04/07
11	INSP. HATCH	1	15/04/07
10	HATCH Ø140	1	15/04/07
9	FLANGE Ø600	1	15/04/07
8	TRANSITION Ø250x2 5mm	1	15/04/07
7	FLANGE Ø600	1	15/04/07
6	HOPPER 5,230x2 5mm	1	15/04/07
5	FLANGE Ø600	1	15/04/07
4	BRACKET Ø300x2 5mm	1	15/04/07
3	HAT 1,350x2 5mm	1	15/04/07
2	HOPPER 12,550x2 5mm	1	15/04/07
1	FLANGE Ø600	1	15/04/07

1504067

Appendix B - Microsilica Grade 971



Elkem AS
Silicon Materials
Hoffsveien 65B
P.O. Box 5211 Majorstuen
NO-0303 OSLO
Tel: +47 22 45 01 00
Fax: +47 22 45 01 52
www.siliconmaterials.elkem.com

Product Data Sheet Elkem Microsilica[®] Grade 971

1. Description

Elkem Microsilica[®] is a key ingredient in advanced low, ultra-low castables and gel-bonding systems. It is highly reactive during sintering, which leads to improved ceramic bonding at reduced firing temperatures. Elkem Microsilica[®] is also utilised in mortars, gunning mixes and other shaped and unshaped materials.

2. Chemical Analysis (weight%)

Element			Spec*	Typical**
SiO ₂	%	min.	98	98.4
C	%	max.	0.7	0.50
Fe ₂ O ₃	%	max.	0.1	0.01
Al ₂ O ₃	%	max.	0.3	0.20
CaO	%	max.	0.3	0.20
MgO	%	max.	0.2	0.10
K ₂ O	%	max.	0.3	0.20
Na ₂ O	%	max.	0.2	0.15
P ₂ O ₅	%	max.	0.10	0.03
SO ₃	%	max.	0.3	0.10
Cl	%	max.	0.10	0.01
H ₂ O ***	%	max.	0.5	0.20

*Test methods are available upon request to refractories.materials@elkem.no.

**Typical values (annual moving average) are for guidance only.

*** When packed

3. Physical Data

Properties		Spec*	Typical**
Loss on Ignition	% max.	0.8	0.50
Coarse Particles >45µm	% max.	0.5	0.20
pH-value		5.5 - 7.5	6.8

Undensified 971U

Bulk density *** kg/m³ 250 - 350 300

Densified 971D

Bulk density *** kg/m³ 450 - 550 500

*Test methods are available upon request to refractories.materials@elkem.no.

**Typical values are for guidance only.

*** When packed

Elkem Microsilica[®] is a registered trademark of Elkem AS.

This product data sheet is property of Elkem AS and may not without its written permission be used, copied or made available to others. The receiver is responsible for every misuse

Revised April 2013 © Copyright Elkem AS

4. Packing

The product is available in 25 kg small bags and various sizes big bags. Please contact our sales representative for more details.

5. Customer benefits

- Improved flow
- More dense castables
- Gel in water
- Hot-strength properties

6. Local Elkem representative

For further information please contact our sales representative. Our specialists will help you to solve any individual problems.

7. Health, Safety and Environment

Please look at Microsilica Safety Data Sheet/Product Safety information on Elkem Website: www.elkem.com/en/Silicon-materials

8. Brochure

See Elkem brochures: "Let's make a castable" No.59 and "Let's make a mullite matrix" No.61.

See technical papers on our website:

<http://www.elkem.com/en/Silicon-materials/Support/Refractories/Technical-papers/>

All data listed are reference values subject to production-related tolerances. Although reasonable care has been taken in the preparation of the information contained herein, it still remains the duty of the user to prove the suitability of this material for his applications.

Appendix C - MatLab Codes for Cyclone Performance

```

***** Lapple, Theodore and DePaola *****

% mu = viscosity
% Ne = number of effective turns
% rho_p = particle density
% rho_g = gas density
% W = inlet width
% V_i = inlet velocity
% d_50 = cut point diameter
% H = inlet height
% Lc= cone length
% Lb = body length
% Cyclone diameter
% n_i = efficiency
% D = cyclone diameter

clear all

Q=15.7;
Q_0=65;

D=2.2;
H=4.5;
W=0.14;
Lc=4;
Lb=4.5;
mu=24.6*10^(-6); %at 170 celsius
rho_g=0.8; %at 170 celsius
rho_p=2300;

V_i=Q/(H*W);

Ne=(1/H)*(Lb+0.5*Lc);

d_pc=((9*mu*W)/(2*pi*Ne*V_i*(rho_p-rho_g)))^(1/2);

n=120;

d=10^(-6)*(0:2:n)';

d(1,1)=10^(-6)*0.5;

n_i=zeros((n/2)+1,1);

for i=1:(n/2)+1
    n_i(i,1)=1/(1+(d_pc/d(i,1))^2);
end

***** Barth *****

% V_0 = gas velocity at cyclone exit (calculated)
% V_max = maximum tangential velocity (calculated)
% D_d = dust exit diameter
% D_e = gas exit diameter
% Q = volumeflow (V_i * duct cross area (2000 mm diameter))
% S = part of exit duct inside the cyclone
% lambda = friction factor (used 0.02 as suggested from Wang)

S=2.8;
D_d=0.55;
D_e=1.4;
lambda=0.02;

alpha=1-1.2*(W/D);

V_0=(4*Q)/(pi*D_e^2);

Lm=(Lc*(D-D_e))/(D-D_d)+(Lb-S);

V_max=V_0*(0.5*D_e*(D-W)*pi)/(2*H*W*alpha+Lm*(D-W)*pi*lambda);

x=zeros((n/2)+1,1);
n2_i=zeros((n/2)+1,1);

for i=1:(n/2)+1

    x(i,1)=(pi*Lm*rho_p*(V_max^2)*d(i,1)^2)/(9*mu*Q);
    n2_i(i,1)=1/(1+x(i,1)^(-3.2));

end

```

```

##### Leith and Licht #####
% T = gas temperature
% d_c = critical particle diameter (calculated)
T=473;
en=1-(1-0.67*(D^(0.14)))*(T/283)^0.3;
Z_c=2.3*D_e*((D^2)/(H*W))^(1/3);
d_c=D-(D-D_d)*((S+Z_c-Lb)/(Lc));
if (Lc+Lb-S)>Z_c
    V_L=0.25*(pi*D^2)*(Lb-S)+(0.25*pi*D^2)*(Z_c+S-Lb)*(1/3)*(1+(d_c/D) ...
        +(d_c^2)/(D^2))-0.25*(pi*Z_c*D_e^2);
else
    V_L=(0.25*pi*D^2)*(Lb-S)+(0.25*pi*D^2)*(Lc/3)*(1+(D_d/D)+ ...
        ((D_d^2)/(D^2))-0.25*pi*(Lb+Lc-S)*(D_e^2);
end
G=(D_e/((H^2)*(W^2)))*(2*(pi*(S-0.5*H)*((D^2)-(D_e^2))+4*V_L);
t_i=zeros((n/2)+1,1);
n3_i=zeros((n/2)+1,1);
for i=1:(n/2)+1
    t_i(i,1)=(rho_p*(d(i,1)^2))/(18*mu);
    n3_i(i,1)=1-exp(-2*((G*t_i(i,1)*Q*(en+1))/(D^3))^(1/(2*en+2)));
end

##### Ioza and Leith #####
% V_max2 = maximum tangential velocity (calculated)
% d_c2 critical particle diameter (calculated)
V_max2=6.1*V_i*((H*W)/D^2)^0.61*((D_e/D)^(-0.74))*((Lb+Lc)/D)^(-0.33);
d_c2=D*0.47*((H*W)/D^2)^(-0.25)*((D_e/D)^1.4);
if d_c2<D_d
    Z_c2=Lc+Lb-S;
else
    Z_c2=(Lc+Lb-S)-(Lc/((D/D_d)-1))*((d_c2/D_d)-1);
end
d_pc2=((9*Q*mu)/(pi*rho_p*Z_c2*V_max2^2))^0.5;
beta=exp(0.62-0.87*log(d_pc2*100)+5.21*log((H*W)/(D^2))+1.05 ...
    *((log((H*W)/(D^2)))^2));
n4_i=zeros((n/2)+1,1);
for i=1:(n/2)+1
    n4_i(i,1)=1/(1+((d_pc2/d(i,1))^beta));
end

```

```

##### Zhao 2011 #####

% l = natural vortex length (calculated from Alexander 1949)
% P= angular momentum parameter given by mothes and löffler

l=2.3*D_e*((D^2)/(H*W))^(1/3);
R_w=D/2;
R_e=D_e/2;

hs_z=(H/R_w)*((2*pi-acos((W/R_w)-1)-1)/(2*pi)-1)+Lb/R_w;%mothes and löffer
v_d=Q/(pi*R_w^2);%mothes and löffer
betas=-0.204*(W/R_w)+0.889;%mothes and löffer
vs_phi=(v_d*R_w^2)/(H*W*betas);%mothes and löffer
zz_e=0.0070;%mothes and löffer
zz_K=0.0070;%mothes and löffer
zz_D=0.0070;%mothes and löffer
v_phi=(v_d/(zz_e*hs_z))*((0.25+zz_e*hs_z* ...
(vs_phi/v_d)^(1/2)-0.5);%mothes and löffer

epsilon=atan((D-D_d)/Lc);

P=(v_phi/v_d)*(zz_D+(zz_K/sin(epsilon)));%mothes and löffer

if l<=Lb+Lc-S
    D_c=D-((D-D_d)*(S+l-Lb))/(Lc);
    V_cs=0.25*(pi*Lb*D^2)+(0.25*pi*D^2)*((1/3)*(S+l-Lb))* ...
        (1+(D_c/D)+(D_c/D)^2);
    Rs_w=(V_cs/(pi*(S+l)))^(1/2);
else
    V_cs=0.25*(pi*Lb*D^2)+(0.25*pi*D^2)*((1/3)*Lc)* ...
        (1+(D_d/D)+(D_d/D)^2);
    Rs_w=(V_cs/(pi*(Lc+Lb)))^(1/2);
end

t_res1=(pi*(Rs_w^2)-R_e^2)*S/Q;
if l<=Lc+Lb-S
    t_res2=(pi*(Rs_w^2)-R_e^2)*1/((0.9*Q)/2);
else
    t_res2=(pi*(Rs_w^2)-R_e^2)*(Lc+Lb-S)/((0.9*Q)/2);
end

t_res=t_res1+t_res2;

v_theta=v_phi/((Rs_w/R_w)*(1+P*(1-(Rs_w/R_w))));

% Cunningham correction factor Davien (1945) and Allen & Raabe (1982)
C_c=1.02;

v_rp=zeros((n/2)+1,1);
n5_i=zeros((n/2)+1,1);

for i=1:(n/2)+1
    v_rp(i,1)=(C_c*rho_p*(d(i,1)^2)*(v_theta^2))/(18*mu*Rs_w);
    n5_i(i,1)=1-exp(-(2*v_rp(i,1)*t_res)/(Rs_w));
end

```

```

***** Midthun *****
t_res3=t_res1+t_res2/2;
V_th1=0.7*v_i;

V_th2=(Rs_w*v_i)/(Lc*tan(epsilon))*(log((D_d/2)+tan(epsilon)* ...
(Lb+Lc))-log((D_d)/2+tan(epsilon)*Lb));
V_th3=(Lc/Lb)*V_th2+V_th1)/2;

n6_i=zeros((n/2)+1,1);
n7_i=zeros((n/2)+1,1);
V_rp2=zeros((n/2)+1,1);

t_resmin=(pi*(Rs_w^2-R_e^2)*Lc)/(0.9*Q);
for i=1:(n/2)+1
    V_rp2(i,1)=(rho_p*(d(i,1)^2)*(V_th3^2))/(18*mu*Rs_w);
    n6_i(i,1)=1-exp(-(Q/Q_0)*(2*V_rp2(i,1)*t_res3)/Rs_w);
    n7_i(i,1)=1-exp(-(Q/Q_0)*(2*V_rp2(i,1)*t_resmin)/Rs_w);
end

%plot(d,n_i,d,n2_i,d,n3_i,d,n4_i,d,n5_i,d,n6_i)
%legend('Lapple','Barth','Leith & Licht','Ioza & Leith', ...
%      'Zhao','Present model',4)

plot(d,n6_i,d,n7_i)
legend('tres max','tres min',4)

```


Pollution Control, Air . . .

materials (glass fibers, animal hair, wood shavings, fiber board, split wire, metal wool or screening, etc.) coated with dust collecting adhesives. Dry air filters may be true filters, but must be of such great porosity (to provide air-conditioning rates of flow) that they have, as Lapple puts it, "negligibly low efficiencies in separating particles below 1 micron in size, and efficiencies of around 85 percent for sizes over 10 microns. They are not, therefore, significant in the problem of pollution and public nuisance."

Some of the newer ultra-filtration media may someday prove important in public nuisance control where bacteria or very fine radioactive dusts are involved.

Starford and Smith describe special asbestos-containing papers which will remove particles in the 0.1 to 1.0 micron size range with efficiencies of 99.9 percent or better. Such media are already in use in Atomic Energy Commission operating areas. They pass air at about 5 dm-per sq-ft. at a pressure drop of around 1 in. of water column; and deliver nearly sterile air such as to suggest use in biological and pharmaceutical work as well as in the filtering of radioactive dusts. Though highly promising, their applications are still specialized, and tend only to low aerosol concentrations.

Goetz, Gooding and Goetz describe paper-like materials in the form of gel structures of cellulose ester polymers for ultra-filtration. Such filters utilize the electrostatic charges developed by air passage through the material to increase effectiveness, even with an unfavorable relationship between pore and particle size. Capacities up to 11.5 cm-per sq-ft. at 1 in. water column pressure differential have been reported.

Other filters making use of electrostatic properties have also been reported. For example, one of the rubber companies has recently announced a "self-charging electrostatic air filter" which takes advantage of the dielectric properties of polyethylene and other plastic materials. High efficiencies with smokes of sub-micron size are claimed. The filter can be cleaned and fully regenerated by immersion in water containing a detergent, and replaced immediately without deteriorating effect.

REFERENCES

A. I. Goetz, A. Gooding, R. A. and Goetz, S. S., A.C.S. Symposium on Dispersion in Gases, Baltimore, Dec. 29, 1950. In Perry's "Chemical Engineers' Handbook," 2nd Edition, McGraw-Hill Book Co., New York, N.Y., 1950, 103-105.

R. Starford, R. D. Smith, and W. J. A.C.S. Symposium on Air Pollution in Gases, Baltimore, Dec. 29, 1950. In Perry's "Chemical Engineers' Handbook," 2nd Edition, McGraw-Hill Book Co., New York, N.Y., 1950, 103-105.

Processes Use Many Collector Types
Settling chambers, impingement and inertial separators,
packed beds and scrubbers are vital in the control of pollution.

C. E. LAPPLE, Department of Chemical Engineering, The Ohio State University, Columbus Ohio.

There are a number of forces or mechanisms which are active in the functioning of dust or mist collection equipment. These may be classified as: (1) gravitational, (2) inertial, (3) filtration or barrier, (4) electrostatic, (5) physicochemical, (6) thermal or diffusional and (7) sonic. Since many units utilize more than one of these forces, it is not convenient to classify available collection equipment according to the underlying operating principle. The tabulation on page 145 gives a classification of dust collection equipment which is based on structural and application similarities. The present paper summarizes the factors that enter into the design and operation of gravity settling chambers, inertial separators, packed beds, and scrubbers. The other classes of collectors listed in the table are covered in other sections of the symposium. For further details the reader is referred to Ref. (6) which presents a fairly comprehensive treatment of 113 references covering the more important work in the field. Details of more current work in the field will be found in Refs. (1), (2), (3), (4), (7) and (8). It should also be noted that, except for scrubbers, the equipment described in this paper is applicable only to the

collection of particulate pollutants, such as dust or mists, and not for the collection of gaseous pollutants.

The gravity settling chamber is probably the simplest and earliest type of dust collector, consisting essentially of an open compartment into which the dust-laden stream passes at one end and leaves at the other. Gas velocity in the chamber is reduced to permit the dust particles to settle out by the action of gravity. Referring to Fig. 1, a particle will be completely removed if it can settle from point (1) to point (2), a height of H_f in the time it takes the stream gas to pass from one end of the chamber to the other. Expressing this mathematically, it will be found that air particle with a terminal settling velocity v_s equal to or greater than $(q/B.L.)$ should be completely settled out. Some smaller particles that are initially close to the bottom of the chamber will also settle out.

It should be noted that the velocity $(q/B.L.)$ is the same as that of the fluid if it passed vertically through the area $B.L.$. Thus the dependence of a gravity settling chamber depends primarily on its horizontal projected area and is practically independent of its height. The height need be made only large enough

modification known as a Howard dust chamber (Fig. 2). Gravity settling chambers are not built as standard commercial units. They are designed for the specific application. The simplicity of such a unit makes it suitable for almost any type of construction. Practically, however, the industrial utility of the simple settling chamber is limited to removing particles larger than 325 mesh (43 microns diameter) since the required chamber size for removing smaller particles is generally excessive. The most frequent application is on natural draft

so that the gas velocity V , in the chamber is not great enough to cause re-entrainment of settled dust. For this reason, V , should not exceed about 10 f.p.s.

Lateral gas distribution at the gas inlet end of a gravity settling chamber is very important for the proper operation of the unit, since this determines the portion of the horizontal projected area of the chamber which is effectively used. Vertical partitions or baffle plates serve little useful purpose, but closely spaced horizontal shelves can be utilized to secure a marked improvement in collection, as in a

General Types and Characteristics of Dust and Mist Collection Equipment

This table gives relative cost and performance data for the main types of units used for removing particulate pollutants. The values given must not be taken too literally, but should serve as a guide in selecting units for given applications.

Equipment Type	Purchase Cost, \$/Cfm*	Particle Diameter, Microns	Removal Throughput, In. Water	Power Consumption**, Kw/1000 Cfm.	Applications, Remarks
A. Gravity settling chamber					
1. Simple		40	0.1-0.5	0.1	Simple, large, low pressure drop; preliminary natural draft exhaust.
2. Howard	0.10-0.30	10	0.1-0.5	0.1	Difficult to obtain, widespread problem.
B. Inertial separator					
1. Inertial separator	0.04-0.08	2	1-5	0.2-1.0	Applicable to existing flues.
2. Cyclone separator	0.10-0.30	10	1-5	0.2-1.0	Requires seal and maintenance.
3. Mechanical centrifugal separator		5	1.2	0.2-2.0	Simple, inexpensive, most widely used.
4. Miscellaneous inertial separator					Comparative ventilation booths.
C. Packed beds	2.00-5.00†	<1	1.10	0.2-2.0	May be adaptable to existing flues.
1. Fine					Removed of radioactive aerosols; sulphuric acid mist removal.
2. Granular (<4 mesh)					
3. Fibrous (<0.005 in.)		5	0.2-2	0.1-0.5	Reattachment elimination.
4. Fibrous (>4 mesh)					
D. Scrubbers					
1. Chamber type	0.15-1.50	0.5	0.1-50	0.1-10.0	Dust is wetted; sludge disposal and corrosion problems.
2. Cyclone type	0.80-1.00				
3. Inertial type	0.80-1.00				
4. Mechanical type	1.00				
5. Spray type					
6. Film type					
7. Miscellaneous					
E. Cloth collectors					
1. Baghouse	0.50-2.50	<0.1	2-6	0.5-1.5	High collection efficiency; temperature and moisture limitations.
2. Tube filter	0.15-1.50				Simple, large.
3. Mechanical filter	0.10-0.70				For high capacity.
4. Automatic filter	0.60-2.00				For high dust concentration (>20 grains/cu. ft.).
F. Biological precipitators					
1. Single-stage	0.30-1.50	<0.1	0.1-0.5	0.2-0.6	For spores, gases, heavy duty, expensive start cost and operation.
2. Two-stage	0.10-0.30		0.1-0.3	0.1	Small compact, air conditioning applications.
3. Alternating current			0.1-0.5	0.1	High capacity, low resistance; for low dust concentrations, air conditioning applications.
G. Air filters					
1. Vycor	0.005-0.080	5			For odor removal.
2. Dry	0.005-0.060	2			Only recently of industrial importance.
3. Automatic	0.05-0.10				Not recommended for industrial applications; used for sampling.
4. Wetted walls					
5. Electrostatic (see F 2 above)					
6. Repulsive					
7. Attractive					
H. Miscellaneous					
1. Small	1.00	<0.5	0.2-6	1-5	
2. Thermal					

*For mild construction based on prices for period 1945-1946. **Gross total power, including electrical energy, water pumping power, pressure drop through separator, and power for necessary auxiliary equipment. † For deep-bed types only.

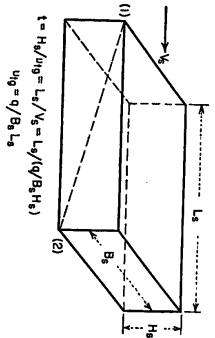


Fig. 1—Operation of gravity settling chambers.

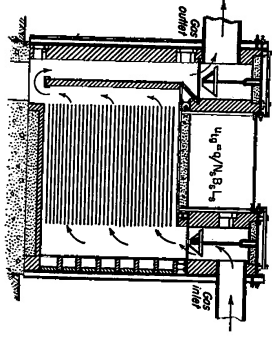


Fig. 2—Forward type settling chamber.

Little exhausts from bins and furnaces, owing to its pressure low pressure drop consists entirely of entrance and exit losses. A Howard type of unit can be used to remove particles as small as 10 microns diam. Its chief disadvantages are the difficulty of cleaning owing to the close shelf spacing, and warpage at elevated temperatures.

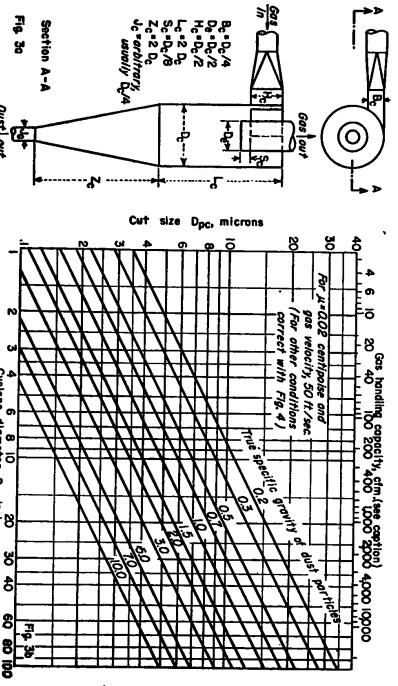


Fig. 3—(a) Proportions for typical cyclone design. (b) Cut size in microns for cyclones of Fig. 3a. For other gas velocities and velocities multiply cut size by correction factors from Fig. 4 (but cut size must be determined from diameter scale at bottom of Fig. 3b, and not from capacity scale at top). Capacity scale gives air handling capacity at inlet temperature and pressure and 50 fps. for cyclones of diameter vertically below.

It should have very definite application for liquid impingement separator.

An impingement separator is a device in which the dust- or mist-laden gas stream is caused to pass around or through fixed elements interposed in the gas stream. The greater inertia of the suspended particles will result in a tendency for the particles to deposit on the collecting element, rather than to follow the gas around the element. Thus a certain fraction of the particles in the gas volume "sweep" by the collecting body will impinge on the body. The efficiency of collection is a function of the dimensionless group $v_p V_g / g D_c$. There is at present considerable disagreement in the literature regarding the quantitative nature of the relationship. As a general rule, it may be stated that if the value of the group is greater than 1, the efficiency of impaction will be large (over 50 percent); whereas, if its value is less than 0.1, the efficiency of impaction will be negligible. Thus, high velocity and small collection elements are conducive to more effective separation. High over-all collection efficiencies can be obtained by using large numbers of collecting elements in series.

As a whole, impingement separators are designed for pressure drops in the range of 0.1 to 1.5 in. water, depending on the type and the application. They are limited to removing dusts that are predominantly larger than 10 to 20 microns diam. The chief advantage of such units lies in their ready adaptability to existing lines and ducts.

The Calder-Fox "scrubber" is a British development in this class, intended primarily for the collection of sulphuric acid mist. It consists essentially of one or more pairs of closely spaced plates in series, where each pair of plates contains orifices staggered with respect to the adjacent pair.

to each other. This unit is reported to be effective in collecting mist particles as small as 2 microns diam. The cascade impactor is a recent development in the field of particle size analysis which is essentially an impingement separator.

One of the least expensive and most widely used types of dust collectors is the cyclone separator.

It consists essentially of a conical or cylindrical chamber (Fig. 5), with the gas entering tangentially at one or more points. Gas leaves axially at the other end, the dust discharging into a receiver at the other end. The action is similar to that of a gravity settling chamber where gravitational acceleration of the dust particles is replaced by centrifugal acceleration, which causes the dust particles to move outward toward the separator wall.

Cyclones are generally applicable for removing solid or liquid pollutants from gases when the particles are larger than 5 microns diam. Unless very small diameter cyclones are used the efficiency of collection will be low if much of the suspended matter in the gas is finer than 5 microns. Cyclones may be used for collecting particles larger than 200 microns but in that case gravity settling chambers will usually be more satisfactory, having a lower pressure drop and being less subject to abrasion wear. In certain cases, collection efficiencies of over 98 percent have been realized with cyclone collectors on dusts having an ultimate size of 0.1 to 2.0 microns, but here the suspended particles were highly flocculated. Extensive flocculation may be expected when dealing with dust concentrations greater than 100 grains per cu ft., although it may be present at much lower concentrations.

The friction loss through a cyclone may be conveniently expressed in the terms of the velocity head based on the immediate cyclone inlet area. This inlet velocity head, expressed in inches of water, may be calculated as follows:

$$h_w = 0.00800 \rho V^2$$

The friction loss through cyclones encountered in practice may range from 1 to 20 inlet velocity heads, depending on the geometric proportions. For a cyclone of the proportions shown in Fig. 3 (Ref. 6), the friction loss is approximately 8 inlet velocity heads.

The performance of a cyclone can be specified in terms of a cut size D_p , which is the size of dust or mist particle which the cyclone will collect to the extent of 50 percent. The cut size of a cyclone depends on the dust properties, the gas properties, the cyclone size, and the operating conditions and may be calculated from

$$D_p = \sqrt{\frac{9 B_s}{2 N_s V_g (g_p - g)}}$$

The term N_s , defined as the effective number

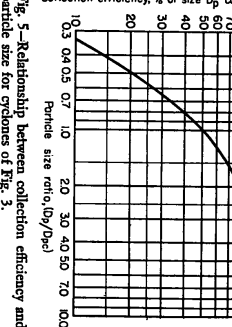


Fig. 4—Viscosity and velocity correction factors for cut size of cyclones in Fig. 3.



Fig. 5—Relationship between collection efficiency and particle size for cyclones of Fig. 3.

of turns made by the gas stream in the cyclone, is actually an empirical quantity which must be determined experimentally. It should, however, be a constant for any size of cyclone of the same geometric proportions. For a cyclone of the proportions shown in Fig. 3a, N, has been found to be about 5. Figs. 3b and 4 present charts which may be used to estimate the cut size of a cyclone of the proportions shown in Fig. 3a, for various cyclone diameters, particle densities, and operating conditions.

Particles larger than the cut size D_p will be collected to an extent greater than 50 percent, while smaller particles will be collected to a lesser extent. This may be represented qualitatively by a curve as shown in Fig. 5, which is essentially a generalized form of the "traction" efficiency plot frequently found in commercial literature. The specific values given in Fig. 5 apply for any cyclone of the proportions shown in Fig. 3.

Cyclones are generally designed to meet specified pressure drop limitations. These set the normal operating range corresponding to an inlet velocity of 20 to 70 fps., usually about 50 fps. A large variety of makes and configurations are commercially available. Typical units are shown in Fig. 6. While the simplest arrangement for a specific application is to use a single cyclone suitably sized for the capacity involved, it is often desirable, when dealing with large air handling capacities, to use an arrangement of multiple small cyclones in parallel in order to attain higher collection efficiencies and reduce headroom requirements. Cyclones in series are generally not justified except (1) where the dust is very fine and

has a relatively uniform particle size distribution, and (2) where the dust is present in a highly flocculated state. Where flocculation is pronounced, estimates of cyclone collection efficiency based on the particle size analysis of the dust will be highly conservative. Also, while collection efficiency is normally increased by increasing the gas throughput in such cases the reverse may be the case due to the deflocculating effect of the higher velocities.

In the removal of dusts, the collection efficiency can be changed to only a minor extent by variations in operating conditions. The primary design factor that can be utilized to control collection efficiency is the cyclone diameter. A smaller diameter unit operating at a fixed pressure drop has a higher collection efficiency but requires a multiple of units in parallel for a specified gas handling capacity. A cyclone will operate equally well on the suction or pressure side of a fan if the dust receiver is airtight. Probably the greatest single cause for poor cyclone performance, however, is the leakage of air into the dust outlet of the cyclone. A slight air leak at this point can result in a tremendous drop in collection efficiency, particularly with fine dusts. For continuous withdrawal of collected dust, a rotary star valve, a double-door valve, or a screw conveyor may be used. Devices, such as cone and disk blades, guide vanes, straightening vanes, and etc. placed inside of a cyclone have in general been found to be of dubious value or actually detrimental.

Cyclones may be used effectively for the removal of liquid droplets from gases, as in the discharge from absorption columns and evaporators. For such applications, however, special

Effect of droplets

Collects liquids also

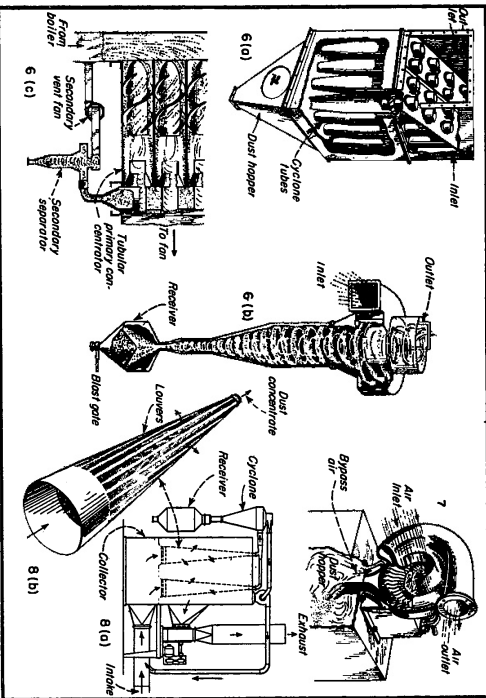


Fig. 6—(a) Multistage (Western Precipitation Corp.); (b) Sirocco Type D cyclone (American Blower Corp.); (c) Sirocco Type D cyclone (American Blower Corp.); (d) Sirocco Type D cyclone (American Blower Corp.).
Fig. 7—Type D Rotadone (American Air Filter Co.).
Fig. 8—(a) Sirocco cyclone; (b) detail of Sirocco tube (Aerodyne Development Corp.).

provisions must be made to prevent the collected liquid from being carried out again as a film by the exit gases. These are discussed in more detail in Ref. (6), p. 1028.

Centrifugal separators

In mechanical centrifugal separators the centrifugal field is developed by a driven rotor rather than by the curvilinear flow of the gas. They are essentially fans into which are incorporated provisions for removing the dust or mist which is thrown outward by the action of the centrifugal field. A typical unit is shown in Fig. 7. Although no comparative data are available, the collection efficiency of units of this type is probably comparable to that of a single-unit, high-pressure-drop cyclone installation. The chief advantages of these units lies in their compactness which may be an important consideration for large installations or plants requiring a large number of individual collectors. Caution must be exercised when attempting to apply this type of unit to a dust that shows a marked tendency to build up on solid surfaces, because of possible high maintenance costs due to rotor unbalancing.

There are several commercially available collectors of the inertial type that do not fall specifically into any of the previous categories. These range in nature from a simple high-velocity gas reversal chamber to a rotary unit containing closely spaced parallel sinusoidal plates. Most steam or compressed air entrainment separators are of the inertial type and are intended for the removal of droplets larger than 20 microns diam.

A recent development in this class is the Aerodyne collector (Fig. 8) in which the dust-laden gases enter at high velocity—100 fps—at the base of a long cone. The sides of the cone are slotted, with the openings pointed in the reverse direction. Most of the gas leaves through these slots while the dust, by virtue of its greater inertia, tends to remain in the cone. Finally it is concentrated in a small fraction of the original gas which carries it out of the apex of the cone to a small cyclone collector. The gas from the cyclone collector is then recycled to the inlet of the cone. The manufacturer's performance curves would indicate that this unit has a collection efficiency comparable to that of a medium-sized single cyclone collector. The chief indicated advantages of the unit are that performance is presumably independent of size, that it is reasonably compact, and that it may lend itself readily to installation in some instances.

Particulate pollutants can be removed from bed gas streams by passing the gases through a bed or layer of packing which may consist of granular materials, such as sand, coke, or kassing rings, or of fibrous materials, such as glass or steel wool. The depth of the bed may vary from a fraction of an inch to several feet, depending on the application and the type of packing. The deposition of the particles on the packing may result from one or more of the following mechanisms depending on the nature and size of the dust or mist particles, the nature and size of the packing material, and the operating conditions: (1) interception, (2) impingement, (3) Brownian

diffusion, (4) gravity settling, and (5) electrostatic attraction. With the coarsest packing materials, impingement is usually controlling while interception, diffusion and gravity settling are predominant in beds of finer packing materials, with electrostatic effects as a possibility.

The general principles of collection by gravity settling and impingement have been previously discussed. The effectiveness of collection by interception is a function of the ratio D_p/D_v while that of Brownian diffusion depends on the group $D_p/\sqrt{V D_p}$. The larger the value of the group or ratio in each case, the greater the collection efficiency. The diffusion coefficient of an aerosol D_p may be calculated from

$$D_p = \frac{6.6 E T k}{3 \pi \mu N D_p}$$

The value of k_m will differ significantly from unity for particles smaller than 1 micron. The value of D_p for a 1 micron particle is on the order of 3×10^{-6} sq. ft. per sec. The principles involved in possible electrostatic phenomena have not yet been adequately developed. For further details see Perry, Johnson and Roberts' and Redehash.

Range of use

Beds of coarse packing are usually used at relatively high capacity—1 to 15 fps. superficial gas velocity—for removing coarse dust or mist particles (larger than 5 microns diam.). Beds of fine packing are used at relatively low capacity—1 to 50 fps. superficial gas velocity—for removing very small particles (smaller than 5 microns). The question of bed life is an important one and is determined by dust concentration and particle size. For this reason, packed beds are limited to the handling of relatively low dust concentration, unless a moving bed is involved. This can be done, as in the Lynch granular filter⁶ by periodically or continuously withdrawing the packing for cleaning as by screening or by using a hundred bed. In the case of mist and sprays, packed beds are generally self-draining, although life may still be a consideration owing to the additional presence of small amounts of dust. Fibrous beds have two basic advantages over granular beds: (1) They are considerably lighter in weight and hence require less structural support, and (2) they have a higher dust capacity. As a whole, packed beds are not produced as commercial units but are engineered specifically for each application. Chambers packed with sized coals have been successfully used for the collection of sulphuric acid mist. Sand filters and glass wool filters have been successfully applied for removing small amounts of radioactive contaminants from very large volumes of gaseous wastes with very high collection efficiencies.

In the category of scrubbers are included all devices which utilize a liquid, usually water, to assist in the removal of a dust, mist, or vapor from a gas stream. There is a very large variety of equipment available in this class. Some units are simply modifications of one of the dry types of separators to permit the addition of liquid, while others are specifically designed for wet operation and cannot be used without liquid addition. The following functions or

mechanisms may be responsible, individually or severally, for the manner in which collection is achieved in a scrubber: (1) impingement and interception, (2) diffusion, (3) humidification, (4) condensation, (5) wetting (6) gas partition, (7) dust disposal and (8) electrostatic precipitation. The nature of each of these is discussed in more detail in Ref. (6). Because of the wide variety of scrubbers, and the many possible functional mechanisms, it is difficult to develop a comprehensive classification of types. In the foregoing table scrubbers have been classified into several categories according to similar structural features. Actually, performance capabilities within each category may be widely different. Scrubbers in which the gas simply enters and leaves a chamber where one or more spray nozzles are mounted have been termed "chamber scrubbers". The chamber may be large to slow down the gas, or it may be in the form of an ejector to speed them up. The venturi scrubber (Fig. 9a), which has recently received wide attention because of its high potential collection efficiency, would fall into this group. Scrubbers which utilize centrifugal action due to tangential or vanned gas inlets, as in Fig. 9b, have been termed "cyclone scrubbers". Those in which gas velocity is used to secure liquid contacting and which do not conveniently fall into one of the other classes have been termed "neutral scrubbers" as in Fig. 9c. Scrubbers termed "mechanical types" are those in which an externally driven motor is employed for contacting purposes, as in Fig. 9d.

A coarse packed bed, either granular or fibrous (Fig. 9e), over or through which a liquid is circulated in addition to the gas, is termed a "packed scrubber". In "film scrubbers" a liquid is circulated over the scrubber elements. The liquid is not contacted with the gas other than at the surface of the element, but serves to keep the collecting surface free

of particles and to prevent re-entrainment of deposited particles. All units which do not fall conveniently into one of the above categories have been listed simply as miscellaneous. The design and performance of scrubbing equipment are quite different, depending on whether a gaseous or particulate (dust or mist) pollutant is to be removed. The same scrubber will usually not be adequate for both functions. It is usually advantageous to have the air flow concurrently to the absorbing liquid when dealing with gaseous pollutants. The types of scrubbers applicable to the problem are, therefore, limited. For very soluble gases at low concentration, such as hydrogen chloride vapors, concurrent contacting would probably be adequate. The principles of operation and design of scrubbers for removing gaseous pollutants are covered in detail in Section (10) of Ref. (6). The equilibrium relationships between the gaseous pollutant and the scrubbing liquid, the temperature and pressure, and the retention or contact time may all play an important role. Towers filled with ceramic or other packing are frequently used although they may be subject to plugging if much particulate matter is also present. Grid-packed towers have successfully overcome this difficulty.

Scrubbers are indicated as a potential means for the collection of particulate contaminants if: (1) It is permissible or desirable to add liquid to the air stream from the standpoint of the process, health, and safety; (2) the particulate matter is very fine (predominately under 10 microns diam.); (3) a very high collection efficiency is required; (4) the gas must be cooled; and (5) vapors or gaseous matter must also be removed from the air stream. A scrubber will usually not be applicable if an inertial separator, such as a cyclone, will perform satisfactorily. This is because scrubbers will usually run higher in cost. Scrub-

bers are normally competitive with cloth collectors (bag filters), although they may be used to handle conditions where bag filters are not applicable because of temperature, moisture conditions, explosion hazards, etc. Problems that must receive special consideration in applying scrubbers include: (1) corrosion due to the addition of the scrubbing liquid; (2) liquid entrainment in the air stream leaving the scrubber; and (3) disposal or recovery of the sludge or slurry from the scrubber.

In removing particulate pollutants, counter-current operation usually has no particular advantages (or disadvantages) over concurrent operations, except in special cases where other functions, such as concentration of liquid solutions, are to be performed simultaneously. Because so many commercial types are available and because comparative operating and economic data are scarce, it is not possible to give any specific broad recommendations. The author is aware of research, currently being prepared for publication, which indicates that the controlling factor in the collection efficiency of scrubbers on particulate contaminants is the overall pressure drop, and furthermore that the type and geometry of the scrubber is of only secondary importance. In many cases a relatively small increase in pressure drop may result in a large increase in collection efficiency.

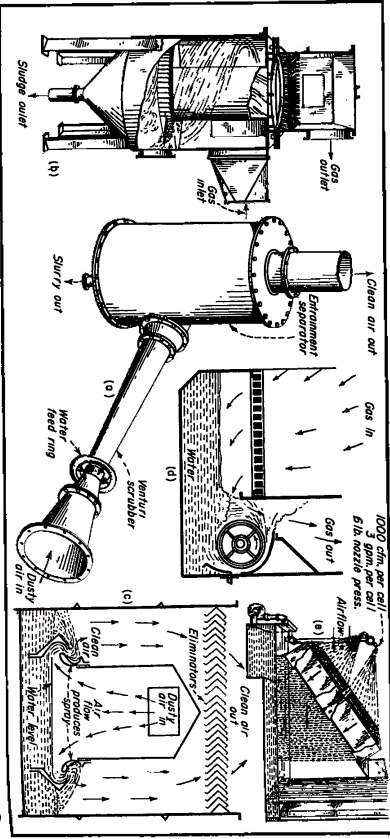


Fig. 9—Group of typical scrubbers: (a) Pass-Airway venturi scrubber (Chemical Construction Corp.); (b) Hydro-cyclone (Whiting Corp.); (c) Type N Rotocyclone (American Air Filter Co.); (d) Centrifuge (Schering Industries); (e) Capillary Cell scrubber (Chemical Construction Corp.); for illustrations of other types see Ref. (6).

Many commercial types

Scrubbers are normally competitive with cloth collectors (bag filters), although they may be used to handle conditions where bag filters are not applicable because of temperature, moisture conditions, explosion hazards, etc. Problems that must receive special consideration in applying scrubbers include: (1) corrosion due to the addition of the scrubbing liquid; (2) liquid entrainment in the air stream leaving the scrubber; and (3) disposal or recovery of the sludge or slurry from the scrubber.

Precipitators Stop Dust and Fumes

Versatility in recovery of fine aerosols of both liquid and solid contaminants means many jobs for the precipitator.

WAYNE T. SPROULL, Acting Director of Research, Western Precipitation Corp., Los Angeles, Calif.

In a recent article, A. J. Haegey, Smith gives some interesting data regarding air pollution in the Los Angeles area, which he estimates to be roughly 62.5 square miles. On days when the atmospheric inversion layer extends to, say, 1,000 ft. elevation (which is a common occurrence), there is a stagnant reservoir of air over the city which weighs about 650 million tons. This large but limited reservoir soon becomes polluted by waste matter from the city. If this waste matter consisted entirely of acrolein, for example, he estimates that 80 tons of it would be nucleable to the inhabitants, 3,500 tons would cause them to shed tears involuntarily, and about 180,000 tons of it would be lethal in 10 min.

Extensive studies have indicated that, in the Los Angeles area, organic material in the air—such as that released by incomplete combustion of oil, gasoline, trash, etc.—reacts with ozone or perhaps other contaminants like nitrogen oxides. This occurs under the influence of sunlight forming an aerosol which is responsible for a large fraction of the smog

Scrubbers properly designed are capable of giving a collection efficiency in excess of 99 percent. The pressure drop or power consumption required, however, will depend on the particle size of the particular dust involved. Normally the water circulation rate in dust scrubbers per 1,000 cu ft. of air handled per min., is in the range of 2 to 10 gpm., although certain types may run as high as 200 gpm. The water consumption or makeup rate will depend on the evaporation losses, on the concentration of dust present in each specific case, and on the amount of recirculation that can be employed. With certain types of units, practical operating considerations may preclude recirculation.

REFERENCES

1. A. C. S. Symposium on Atmospheric Contamination and Pollution, Ind. Eng. Chem., 43, 338-356 (1951).
2. American Energy Commission, "Handbook on Air Pollution," U.S. Gov. Printing Office, Washington, D. C., 1950.
3. J. H. P. van den Hul, "Air Pollution," U.S. Gov. Printing Office, Washington, D. C., 1950.
4. "Manufacturing Chemists Association," "Handbook on Air Pollution," (in preparation), pp. 187-195 (1948).
5. E. Perry, J. H. P. van den Hul, "Air Pollution," U.S. Gov. Printing Office, Washington, D. C., 1950.
6. United States Technical Conference on Air Pollution, May 8-9, 1950, Washington, D. C. (Proceedings of the University of Michigan, School of Public Health, "Atmospheric Pollution," 1950, pp. 11, 49, 1950).
7. "Atmospheric Pollution," U.S. Gov. Printing Office, Washington, D. C., 1950.

actually observed over the city on days when there is an atmospheric inversion layer. The figures cited in the paragraph above indicate that atmospheric pollutants in industrial areas must be escaping in very large quantities in order to have become such a nuisance, not to say health menace.

If such processes contribute a major share of urban smog, it is seen that only a portion of the pollutants which ultimately annoy the people and injure plant life originally entered the atmosphere in the same chemical state as they have when they do the damage. Thus the collection (by precipitators, for example) of all aerosols entering the air from factory chimneys, etc., may still not prevent aerosols from forming in the air and causing smog. Nevertheless, some of the dust and fume which is visible in the air in industrial neighborhoods quite commonly escapes as dust or fume from the mills and factories. Among these, for example, are cement plants, as well as steam power plants, open hearth furnaces, and the like. In collecting pollutants of this type to prevent smog, one of the

THE COLLECTION EFFICIENCY OF CYCLONE TYPE PARTICLE COLLECTORS —A NEW THEORETICAL APPROACH

David Leith
and
William Licht

The concept of a continual back-mixing of the uncollected particulates in the gas stream is applied to the conventional cyclone having tangential inlet. This is coupled with the determination of an appropriate average residence time for the gas in the cyclone to derive a new equation for cyclone efficiency.

This is shown to depend upon three dimensionless parameters: C , a cyclone design number depending upon the physical shape (but not size); ψ , a modified type of impaction parameter depending upon the entering conditions; and n , the exponent in the modified form of the vortex law for tangential velocity distribution. It is possible to calculate all of these numbers for any proposed design and operation and to predict grade-efficiency relationships a priori. The new theoretical equation is tested against published data and gives excellent agreement. It predicts the general nature of the grade-efficiency curves better than any method heretofore available. It may also be used in reverse to determine the cyclone parameters experimentally from a single grade efficiency curve. The implications of this theoretical model for improved and optimized cyclone design are also discussed.

Previous attempts to develop a theoretical model for the collection efficiency of a cyclone type particulate collector have not met with much success. The experimentally determined grade-efficiency curves for standard gas cyclones are always concave downward and approach 100% efficiency almost asymptotically. Some theoretical models so far proposed give a curve which is S-shaped; others predict a sharp critical value for the smallest particle size which may be collected completely. (Some examples are shown in Figures 12 and 13).

The principal reason for these discrepancies seems to be a failure to take into account that turbulence and flow in the gas stream cause a continual back-mixing of the

Department of Chemical and Nuclear Engineering, University of Cincinnati, Cincinnati, Ohio. D. Leith is with Ammonia Purification Technology, Inc., P. O. Box 71, Riverside, California 92502.

suspended (uncollected) particles in the gas. A new approach, incorporating the concept of back-mixing, is presented herein. Coupled with the determination of an appropriate average residence time of the gas in a cyclone, it leads to a very good agreement with such published experimental data as are adequate for checking. This will be illustrated with reference to conventional cyclone design using a tangential inlet as shown in Figure 1. Certain other refinements in what might be called the classical mathematical model of cyclone collection are also involved in the new approach.

PARTICLE MOTION IN CYCLONE

To begin with, it is necessary to have an equation giving the radial component of the trajectory of an individual particle moving in a gas which is spinning under

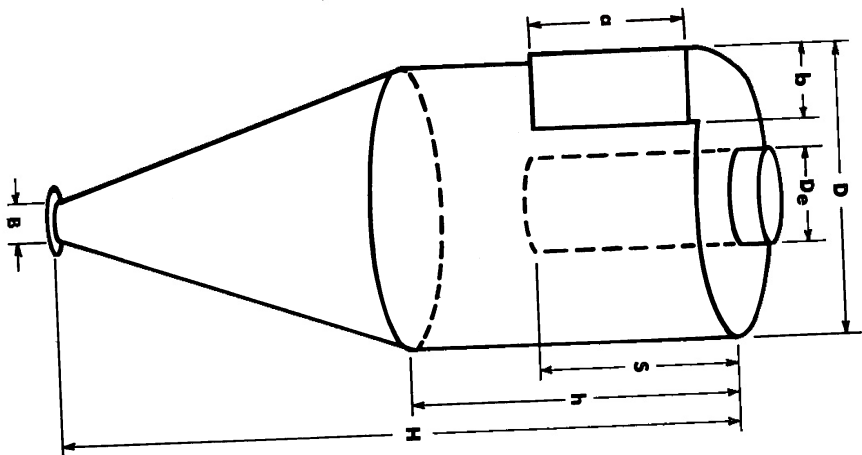


Fig. 1. Cyclone with tangential gas inlet.

the conditions inside a cyclone. A differential equation describing this motion may be set up by making a force balance on the particle with the following assumptions:

- (i) The particle is spherical in shape.
- (ii) The motion of a particle is not influenced by the presence of neighboring particles.
- (iii) The drag force radially on the particle is given by Stokes' Law.
- (iv) The radial velocity of the gas is zero.
- (v) The tangential velocity component of the particle is

the same as that of the gas stream, that is, there is no slip in the tangential direction between the particle and the gas.

- (vi) The tangential velocity component is related to the radial position by a modified form of the equation for a free vortex in an ideal fluid:

$$u_r R^n = \text{constant}$$

In the ideal free vortex law $n = 1$, but experimental observations (1 to 5) show that in a cyclone n may range between 0.5 and 0.9 according to the size of the cyclone and the temperature. Alexander (3) gives the following empirical equations:

$$n = \frac{(12D)^{0.14}}{2.5} = \frac{(D_r')^{0.14}}{2.5} \quad (1)$$

$$\frac{1-n}{1-n_2} = \left(\frac{T_1}{T_2}\right)^{0.13} \quad (1a)$$

A chart for n prepared by Caplan (6) based upon these equations is available. This may be used to estimate a value of n which might be expected to arise. No other way of predicting n has been found. However, as will be shown, values of n may be deduced from experimental grade-efficiency data.

Under the above assumptions the force balance yields

$$\frac{d^2R}{dt^2} + \frac{18\mu}{d^2\rho_p} \frac{dR}{dt} - (u_r)^2 R^{2n} \frac{1}{R^{2n+1}} = 0 \quad (2)$$

in which $u_r R^n = u_{r2} R_2^n = \text{constant}$, and where R_2 may be taken as the radius of the cyclone wall. For simplicity it will be assumed that it would be satisfactory to take u_{r2} as equal to the average velocity of the gas in the inlet duct, that is,

$$u_{r2} = \frac{Q}{ab}$$

Strictly speaking, the tangential velocity of the vortex at the cyclone wall boundary must be zero. However, the boundary layer, a region in which the captured particles slide down the cyclone wall toward the duct outlet, must be thin. Little error is introduced by setting $R = R_2$ when $u_r = u_{r2}$ as defined above.

Equation (2) is not readily solvable, even for the ideal case where $n = 1$. An approximate solution can be obtained by arbitrarily neglecting the second-order derivative. This is equivalent to saying that the particle moves radially outward with a constant velocity, which is obviously inconsistent with the resulting approximate equation:

$$\frac{dR}{dt} = \frac{d_r^2 (u_{r2})^2 \rho_p (R_2)^{2n+2}}{18\mu} \frac{1}{R^{2n+1}} \quad (3)$$

Integration yields

$$t = \frac{9\mu}{\rho_0(n+1)} \left(\frac{R_2}{R_1} \right)^{2n+2} \left[\left(\frac{R_1}{R_2} \right)^{2n+2} - \left(\frac{R_2}{R_1} \right)^{2n+2} \right] \quad (4)$$

if the particle travels from R_1 to R in time t . If the particle just reaches the cyclone wall in time t , then $R = R_2$ and

$$t = \frac{9\mu}{\rho_0(n+1)} \left(\frac{R_2}{R_1} \right)^{2n+2} \left[1 - \left(\frac{R_1}{R_2} \right)^{2n+2} \right] \quad (5)$$

This equation is a more general form of those developed by Davies (7) and Strauss (8) and reduces to them if n is taken to be unity. It also becomes equivalent to the equation derived by Umney (9) as cited by Daniels (10) if again n is unity, and if in the Umney development no slip is assumed between the particle and the tangential component of the gas velocity. All of these solutions involve the same approximation of neglecting the second-order term in the differential equation.

The error involved in making this approximation can only be estimated by performing numerical solutions to the complete differential equation (2). One specific example of this has been worked out by Mehta (11) in the case where $n = 0.5$. He performed a numerical solution of the complete differential equation for a typical set of operating conditions similar to those of Stairmand's tests (12), and compared it with the approximation given by Equation (4). He found that the two solutions approached each other and gave virtually the same result after t had attained about 1/20 of the time required for the particle to reach R_2 . At shorter times the approximate solution tended to overestimate the time of travel. Further investigation of this point for a variety of conditions is highly desirable, although as will be seen below, the approximate equation (5) does appear to work out well in the back-mixing model.

GAS FLOW IN CYCLONE

Next the pattern of gas flow in a cyclone must be considered. Since there is a core zone of low pressure extending along the axis of the cyclone below the exit duct, the gas must gradually move radially inward. Ter Linden's measurements (5) show that it does so at a linear velocity which is relatively constant, regardless of radial position or elevation. As a volume of gas passes vertically down the cyclone it is then gradually drawn off into the central core at a constant rate, proportional to the inward radial velocity. Different parcels of gas introduced into the cyclone at the same time may thus have different residence times within the unit, depending upon the level at which they are introduced and upon how soon after entry they are drawn off.

For simplicity, it is desirable to determine an average residence time for all of the gas stream, such as will account for the collection obtained. This may be done as follows: The total average residence time may be taken to

equal the average time required for gas to descend from the average level of entrance to the level of the bottom of the exit pipe, plus the average time in residence below this point. The average minimum residence time can be calculated by assuming all the gas enters the cyclone at the mid point of the entrance duct. With this assumption,

$$t_{\text{min avg}} = \frac{\pi(S-d/2)(D^2 - D_2^2)}{4Q} = \frac{V_c}{Q} \quad (6)$$

where

$$V_c = \frac{\pi(S-d/2)(D^2 - D_2^2)}{4} \quad (7)$$

The additional time of residence will vary from zero to a maximum corresponding to the lowest point of descent of the gas into the conical cyclone body, with the maximum additional time being taken as one-half of this maximum.

The lowest point of descent of gas is not necessarily the actual bottom of the cyclone as measured by very long glass cyclones that the gas vortex will have a well-defined stable turning point at some distance below the bottom of the exit duct which is less than $(H - S)$. He calls this the natural length l of the cyclone and gives an empirical formula for it, as:

$$l = 2.3 D_2 \left(\frac{D_2}{D_0} \right)^{1/3} \quad (8)$$

It is noteworthy that this natural length is, according to Alexander, independent of the gas flow rate.

The maximum additional residence time of gas not drawn off until reaching the tip of the vortex will be

$$t_{\text{max}} = \frac{V_m}{Q} \quad (9)$$

where V_m is the effective volume of the lower portion of the cyclone at the natural length, where the vortex turns. This effective volume is equal to the total volume of the cyclone from the level of the exit duct down to the level of the natural length, minus the volume of the central core of the cyclone where the gas stream is swept upwards and out of the particle-separating vortex. Taking the diameter of the central core to be equal to that of the gas exit duct gives

$$V_m = \frac{\pi D_2^2}{4} (h - S) + \frac{\pi (l + S - h) D_2^2}{4} \quad (10)$$

$$d = D - (D - B) \left[\frac{S + l - h}{H - h} \right] \quad (10')$$

where

However, the core diameter, as a fraction of the exit pipe diameter has been variously given as 1/3, 2/3, and 1 by Stairman (12), Ter Linden (5), and Barth (13) respectively.

A practical cyclone should have a physical length $(H - S)$ near its natural length l . If the cyclone body is longer than l , that is, $(H - S) > l$, the space at the bottom of the cyclone, below the vortex turning point, will be wasted. If the cyclone body is shorter than l , that is, $(H - S) < l$, the full separating potential of the cyclone will not be realized. In this case t_{max} will be determined simply by the total lower volume of the cyclone minus that of the central core. That is, V_m would be replaced by V_m which is

$$V_m = \frac{\pi D_2^2}{4} (h - S) + \frac{\pi D_2^2}{4} (H - h) \left[1 + \frac{B + B^2}{D + D^2} \right] - \frac{\pi D_2^2}{4} (H - S) \quad (10b)$$

The average total residence time of the gas in a cyclone will then be taken as

$$t_{\text{avg}} = \frac{1}{Q} \left[V_c + \frac{V_m}{2} \right] = \frac{K_c D^2}{Q} \quad (11)$$

where

$$K_c = \frac{(V_c + V_m/2)}{D^3} \quad (12)$$

Here K_c is a dimensionless constant for a given cyclone design. That is, it depends only upon the relative proportions of the various dimensions. For cyclones which are geometrically similar in all respects it is independent of the size. The magnitude of K_c is an indication of the relative effective volume a given design provides, in which separation of particles from gas may take place.

The shape of any cyclone of the type under discussion is completely specified by the values of a set of seven basic dimensionless geometric ratios which may be expressed in terms of D as follows:

$$\frac{D_2}{D}, \frac{a}{D}, \frac{b}{D}, \frac{S}{D}, \frac{h}{D}, \frac{H}{D}, \frac{B}{D}$$

with reference to Figure 1. The appropriate values in this set also fix ratios l/D and d/D . Hence the value of K_c is determined by these seven design parameters which may in principle all be chosen independently. From experience certain limits are usually placed upon these choices for example, $\frac{D_2}{D} < \frac{S}{D}$, $\frac{a}{D} < \frac{h}{D}$, $\frac{b}{D} < \frac{H}{D}$, etc. However within such limitations, the designer of a cyclone is free to select values of these ratios such as to accomplish whatever objective he may have in mind. If this is to maximize average residence time, then the ratios should be selected so as

to give the largest value of K_c . The effect of this upon collection efficiency will be shown below.

It is now evident that assumption (iv) underlying differential equation (2) is not fulfilled for that portion of the cyclone below the bottom of the exit duct. Correction could be made for the effect of the constant inward radial gas flow velocity (u_r) upon the drag force on the particle. This would lead to a modified differential equation:

$$\frac{d^2 R}{dt^2} + \frac{18\mu}{(d_p)^3 \rho_p} \frac{dR}{dt} - (u_r r_p)^2 (R_2)^{2n} \frac{1}{R^{2n+1}} + \frac{18\mu u_r}{(d_p)^2 \rho_p} = 0 \quad (13)$$

In this, u_r might be estimated as

$$u_r = \frac{Q}{\pi D_2 l} = \frac{u_r D_2}{\pi D_2 l} \quad (14)$$

The importance of this correction will depend not only upon the magnitude of the additional constant term in (13) but also upon what proportion of the total dust collection takes place below the bottom of the exit duct, that is, upon how much larger is the average residence time than the minimum residence time. The net effect would tend to reduce the calculated collection efficiency. It has been neglected in this new approach because the measured values of u_r (5) are low and in fact tend toward zero at the wall where collection takes place.

PARTICLE DISTRIBUTION AND COLLECTION

No data have been reported on the actual distribution of particles within a cyclone. However, it is clear that three mechanisms, at least, will tend to cause back-mixing of uncollected particles: (1) As the gas below the exit duct moves radially inward to be drawn off, it will tend to drag particles with it. (2) Turbulence and eddies within the unit will aid in the back-mixing of particles. (3) Also, particles have been observed (14) to bounce from the wall of a cyclone back into the gas stream.

It will be postulated that drag force, turbulent mixing, and particle bouncing or re-entrainment, are sufficiently prevalent to ensure that a uniform concentration of uncollected dust is maintained in the gas flowing through any horizontal cross section of a cyclone, that is, that back-mixing is complete.

Consider a horizontal cross section of a cyclone as shown in Figure 2. In time dt , all particles a distance dR or less from the cyclone wall will move to the wall and be collected. Meanwhile the particles will travel a distance $Rd\theta$ tangentially and dL vertically. The number of particles removed dn_r will be

$$-dn_r = \frac{d\theta}{2} [R_2^2 - (R_2 - dR)^2] c dL \quad (15)$$

where c is the number concentration of particles. The

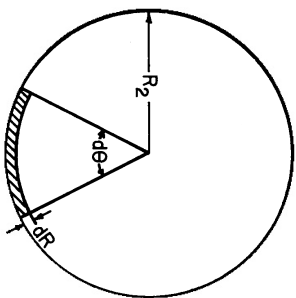


Fig. 2. Cross section of a cyclone.

total number of particles in the sector* from which particles are removed is

$$n' = \frac{d\theta}{2} R_2^2 c \, dL \quad (16)$$

The fraction of particles removed in time dt is therefore

$$\frac{dn'}{n'} = \frac{2R_2 dR - (dR)^2}{R_2^2} \approx \frac{2dR}{R_2} \quad (17)$$

neglecting the second-order differential.

In order to relate the fraction of particles collected to the average residence time, it is necessary to express equation (17) in terms of time. This may be done through Equation (4), which was developed to show the relationship between time and the radial position of a single particle in a vortex. A system of uncollected particles, evenly distributed across the cross section of such a vortex, will have its center of mass at the vortex center. If the system of uncollected particles is instantaneously, continuously, and completely redistributed by back-mixing, as postulated, the center of mass of the uncollected particle system will always remain at the vortex center, even though the total number of uncollected particles is decreasing with increasing gas residence time.

The rate at which the uncollected particle system moves toward the vortex wall as a function of the time the system has spent within the vortex, may then be obtained by saying that the radial position of the uncollected particle system is at the vortex center, $R_1 = 0$ at zero time and differentiating (4) to obtain

$$\frac{dR}{dt} = \frac{\rho_p}{18\mu} \left(\frac{d_p u_{T2}}{R_2} \right)^2 \left[\frac{\rho_p (n+1)}{9\mu} \left(\frac{d_p u_{T2}}{R_2} \right)^2 \right]^{-1/(n+2)} \quad (18)$$

*It is true, of course, that in the upper part of the cyclone, corresponding to volume V_1 , the particle system cannot physically be distributed all the way into the center because of the presence of the outlet duct. Since V_1 is usually less than V_2 , however, this correction has been neglected.

Combining Equations (17) and (18):

$$\int_{n_0}^{n'} \frac{dn'}{n'} = - \int_0^t \frac{\rho_p}{9\mu} \left(\frac{d_p u_{T2}}{R_2} \right)^2 \left[\frac{\rho_p (n+1)}{9\mu} \left(\frac{d_p u_{T2}}{R_2} \right)^2 \right]^{-1/(n+2)} dt \quad (19)$$

Integrating up to the average residence time $t_{\text{avg}} = \frac{K_1 D^3}{Q}$, as given by Equation (11), yields

$$\eta = \frac{n_0 - n'}{n_0} = 1 - \exp - \frac{2 \left[\frac{\rho_p}{9\mu} \left(\frac{d_p u_{T2}}{R_2} \right)^2 (n+1) \right]^{1/(n+2)} K_1 D^3}{Q} \quad (19a)$$

Noting that $Q = n_0 (db)^*$, this equation may be displayed in a more meaningful form by defining dimensionless parameters as follows:

$$\Psi = \frac{\rho_p d_p^2 u_{T2}}{18\mu D} (n+1)$$

a centrifugal inertial impaction parameter, reflecting operating conditions within the cyclone.

$$C = \frac{8K_1}{K_2 K_3}$$

$$K_4 = \frac{a}{D} \quad K_5 = \frac{b}{D}$$

a cyclone design number, reflecting the physical shape of the cyclone.*

Equation (19a) then becomes

$$\eta = 1 - \exp - 2[C\Psi]^{1/(n+2)} \quad (20)$$

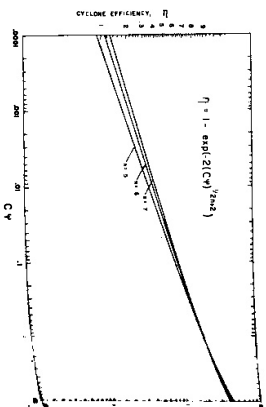


Fig. 3. Generalized cyclone efficiency curve.

If the inlet duct to the cyclone is circular in cross-section with diameter D_1 , instead of rectangular, replace $(db)^$ by D_1^2 , and $K_1 K_2 K_3$ by $K_1 = \frac{1}{4} (D_1/D)^2$.

which is the new theoretical equation for collection efficiency based upon the back-mixing postulate. Equation (20) is plotted in general form in Figure 3.

CHARACTERISTICS OF NEW EQUATION

Equation (20) states that the efficiency of collection is determined primarily by only two dimensionless parameters. One C depends only upon the shape of a cyclone as fixed by the seven size ratios and is independent of its size or of any operating conditions. The other Ψ is fixed by the nature of the gas-solid system (particle size, particle density, composition of gas), the temperature and velocity of operation, and the size (diameter) of the cyclone. The model thus confirms statements made by Hawksley et al. (15) to the effect that efficiency is some function of the group here called Ψ , and that geometrically similar cyclones (that is, having the same value of C) operating with the same value of Ψ have the same efficiency.

A grade-efficiency curve for any proposed cyclone and set of operating conditions may be calculated by the detailed procedures given in Appendix A. It will be found to have the same general shape as the experimentally determined curves illustrated in Figures 12 and 13. The second derivative of efficiency with respect to particle size, $d^2\eta/dp^2$ is always negative, so that the curve is everywhere concave downward. It will rise from $\eta = 0$ at $d_p = 0$ to approach $\eta = 1$ asymptotically. It will have no critical particle size.

The grade-efficiency curve may be rectified by plotting $\log[-\ln(1-\eta)]$ vs $\log d_p$. Letting $A = \frac{C\Psi}{d_p^2}$ in Equation (20), the straight-line equation is

$$\log[-\ln(1-\eta)] = \log 2A^{1/(n+2)} + \frac{1}{n+1} \log d_p \quad (21)$$

The slope of this log-log plot will depend only upon n , while the ordinate intercept (corresponding to $d_p = 1$) will then be determined by A . Care must be taken with units, for example, if d_p is plotted in microns, A must be in microns⁻².

The equation indicates that operation of a given cyclone will be more efficient at higher flow rates, or upon particles of greater density, and less efficient at higher temperatures. All other factors being held constant, a cyclone of larger body diameter will be less efficient. A long thin cyclone will tend to be more efficient than a short fat one at the same operating conditions. All of these effects (which are well-known qualitatively) may be predicted quantitatively by calculating the way in which they influence the values of the parameters Ψ and C . It is evident that collection efficiency will tend to be maximized by the use of a set of the seven design ratios which maximizes the value of C .

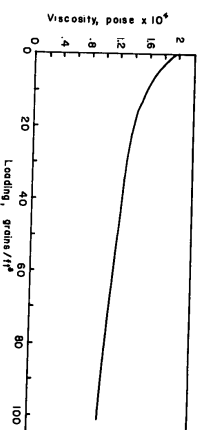


Fig. 4. Apparent viscosity of air as a function of dust loading.

It is sometimes desired to compare the size of particles which will be collected with equal efficiency under different operating conditions. This may readily be done through the parameter Ψ . If Ψ' and Ψ'' represent two sets of conditions, then for equal efficiency $\Psi = \Psi'$ for the two sets. Hence

$$\frac{d_p}{d_p'} = \left[\frac{\rho_p'}{\rho_p} \times \frac{u_{T2}'}{u_{T2}} \times \frac{\mu}{\mu'} \times \left[\frac{D_1'(n'+1)}{D_1(n+1)} \right]^{1/2} \right]^{1/2}$$

Thus the particle size, for equal collection efficiency, is inversely proportional to the square root of the density of the dust, and of the inlet velocity or flow rate, and directly proportional to the square root of the viscosity of the gas and of the diameter of the cyclone body. These relationships are in agreement with those proposed by Sairmand (12).

It should be emphasized that if all of the concepts and assumptions used in developing Equation (2) are correct, the performance of a cyclone may be predicted a priori, that is, without performing any tests upon it.

The important effect of dust-loading (that is, concentration of dust in the inlet air) does not appear explicitly in the equation. It is known that higher loading produces higher efficiency. This may be due in part to agglomeration of colliding particles producing an effectively larger equivalent particle diameter. If so, this effect could be accounted for in the Ψ -term. Further, Sproull (16) has shown that the apparent viscosity of dusty air is substantially lower than that of clean air, as shown in Figure 4. This effect, too, would be accounted for by the Ψ -parameter. Further work is needed on this question.

TESTING THE NEW EQUATION

Data of sufficient completeness for testing the ability of Equation (20) to predict grade-efficiency curves, are very scarce for tangential inlet cyclones of the design shown in Figure 1. Sairmand (12) and Peterson and Whitty (17) have reported laboratory tests performed with dusts of constant density, but varying particle sizes, entrained in air streams fed to cyclones. Fractional efficiency curves were developed from an analysis of the particles separated from the air streams by the cyclones. Sairmand used a typical dust composed of particles with

TABLE 1. SUMMARY OF DATA COMPILED FROM EXPERIMENTAL CYCLONES

Term	Stairmand (12)	Peterson and Whitty (17)	von Ebbenhorst-Tengberg (19)
Dimensions of Cyclone (in.)			
D	8	12	11
Inlet height	4	7	9.25
Outlet height	1.6	2.5	1.55
Outlet length	4	7*	4.7
Exit diameter	12	16	11.6
Cylinder height	32	38	5.8
Overall height	3	6	16.8
Dust outlet diameter	3	4	3.8
Calculated			
H - S	19.8	21.6	22.0
V ₁	28	31	20.0
V ₂	75.5	298	473
V ₃	556	1470	2290
V ₄	—	—	—
V ₅	—	—	810
K ₂	0.692	0.997	0.660
Operating Conditions—all taken to be at 20° C.			
Type particle	Dust	Clay, and plaster	—
Particle density—g./cu. cm.	2.0	1.6	1.6
Loading—g./cu. ft.	—	0.3	10
Throughput—cu. ft./min.	133	610	10
* Assumed value			

a wide range of sizes. Peterson and Whitty used mono-disperse aerosols and determined the cyclone efficiency for each particle size. Details of the test conditions are given in Table 1.

Efficiency predictions calculated for the tests of Stairmand and Peterson and Whitty are compared with their experimental values in Figures 5 and 6. The agreement is seen to be excellent, within about 4% overall. A more sensitive examination of these data, made by replotting the grade-efficiency curves on log probability paper, reveals that such lack of agreement as there is, occurs mainly for the very small and the very large particles. This may well be due to re-entrainment of the small particles (less than 1 to 2 microns) and to bouncing from the

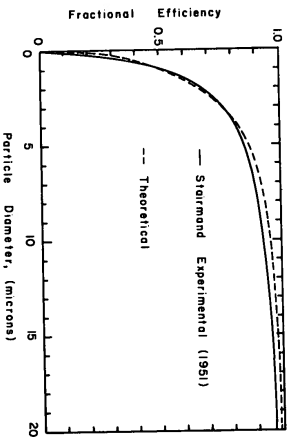


Fig. 5. Comparison of new theoretical efficiency prediction with experimental data of Stairmand (1951).

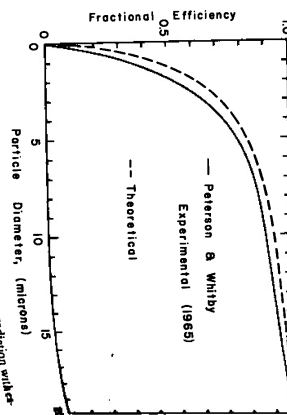


Fig. 6. Comparison of new theoretical efficiency prediction with experimental data of Peterson & Whitty (1965).

cyclone wall, such as has been observed by Mori et al. (8), of coarse particles. These effects are of course not taken into account in the development of the theoretical equation.

Data are also available from von Ebbenhorst-Tengberg (19) who has plotted cyclone efficiency against the quantity $d_p \sqrt{\frac{\rho_p u_{12}^2}{\mu D}}$, which will be called T . As μ , and ρ_p are unobtainable it is not possible to convert these data to standard grade-efficiency curves. However, sufficient information is available to calculate the cyclone design number C , and ψ is seen to be the product of T^2 by $\left(\frac{n+1}{18}\right)$. The theoretical efficiency of these cyclones can

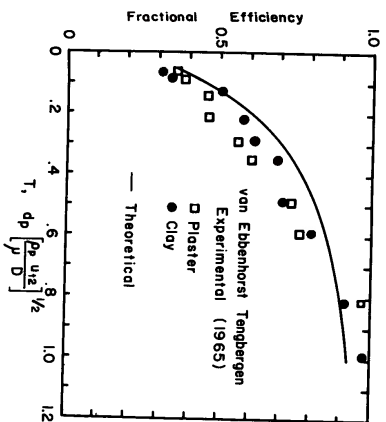


Fig. 7. Comparison of new theoretical efficiency prediction with experimental data of von Ebbenhorst-Tengberg (1965).

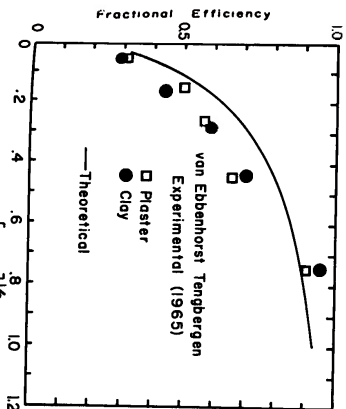


Fig. 8. Comparison of new theoretical efficiency prediction with experimental data of von Ebbenhorst-Tengberg (1965).

can be calculated and compared with the experimental data, as shown in Figures 7 and 8, which are for cyclones of the same design but different diameters. The scatter in the data makes it difficult to give a positive statement regarding the agreement, but it appears to be generally within about 10% except for the higher end of the range T . It happens that these cyclones, as constructed, are smaller than their natural length, as shown in Table 1. Consequently, they are not as efficient as they might be.

In the calculation of C (and K_2) the value of V_n in Equations (11) and (12) must be replaced by V_n . This results in lower values for C . However the effect is not very great in these cases, as the values of V are not very much larger than those of $(H - S)$.

All four sets of these data were also tested by means of the log-log plot corresponding to Equation (2). The plots are shown in Figures 9, 10, and 11. In the case of von Ebbenhorst-Tengberg data, the plot is modified by replacing $\log d_p$ with $\log T$ the modified equation being

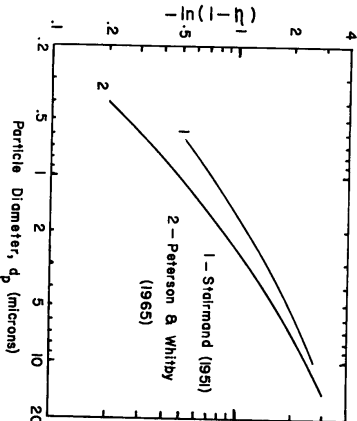


Fig. 9. Rectified plot of Stairmand data, and Peterson & Whitty data.

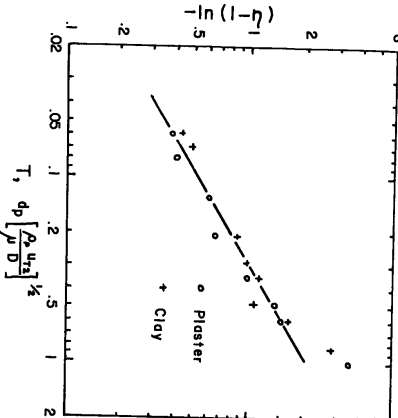


Fig. 10. Rectified plot of Tengberg data—11 in. cyclone.

$$\log[-\ln(1-\eta)] = \log_2 \left[C \left(\frac{a+1}{18} \right)^{1/(a+2)} + \frac{1}{n+1} \right] \log T \quad (22)$$

Although there is some curvature to the plots of the Stairmand and the Peterson and Whitley data, reasonable straight lines may be drawn in all four cases. The values of n obtained by measuring the slope of each of these lines are shown below and compared with the value of n calculated from Equation (1) which was used in the preparation of the predicted grade-efficiency curves shown in Figures 5 to 8.

Source of Data	n (plot)	n (Equation (1))
Stairmand	0.94	0.54
Peterson and Whitley	0.51	0.58
Tengberg (11 in.)	0.43	0.56
Tengberg (18 1/2 in.)	0.64	0.60

The agreement is good except in the case of the Stairmand data.

From the value of the ordinate intercept, that is, where $d_p = 1$ micron or $T = 1$ on each of these log-log plots, a value of C may also be calculated and compared with that obtained from the cyclone dimensions as given by Equation (19). These compare as follows:

Source of data	C (plot)	C (Equation (19))
Stairmand	42.8	55.2
Peterson and Whitley	34.9	39.2
Tengberg (11 in.)	17.4	23.8
Tengberg (18 1/2 in.)	8.78	23.8

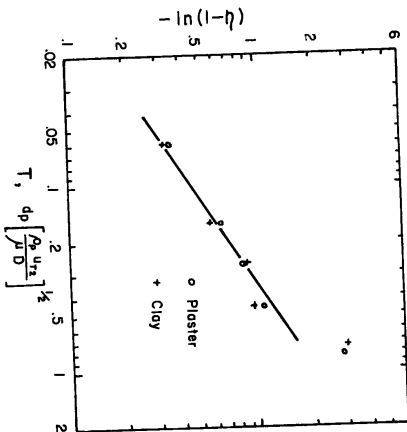


Fig. 11. Rectified plot of Tengberg data—18 1/2 in. cyclone.

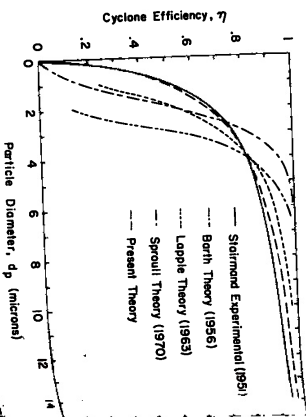


Fig. 12. Comparison of experimental Stairmand data with theoretical predictions by other methods.

These comparisons tend to indicate that the average residence time has been somewhat overestimated. There are many other published grade-efficiency curves which may be tested by the log-log plot method, even though insufficient information is given to calculate predicted curves by Equation (20). For example those given by Swift (20) have been found to give good straight lines. However this type of testing is difficult to carry out with precision because most of the published curves are drawn to small scale which is difficult to read, and the original raw data are not quoted.

COMPARISON WITH OTHER EQUATIONS

To indicate how the results obtained with the new equation compare with several other published methods of predicting grade-efficiency curves, the Stairmand data and the Peterson and Whitley data were also calculated according to the methods of Lapple (21), Barth (13), and Sproull (22). There is insufficient information to do this for the Tengberg data.

The comparative results are given in Figures 12 and 13. It is seen that the other methods give curves which are not only farther off from the experimental but also show a point of inflection in curvature which is not present in the experimental curves tested here.

Although these comparisons are certainly limited in scope, the new equation does give clear promise of providing a more accurate representation of grade-efficiency curves than any other method proposed. This is established a preliminary confirmation of the premises upon which it is based, that is, the concept of back-mixing of the uncollected particles coupled with the determination of an appropriate average residence time for the gas stream. The model is based upon the fundamental geometry and mechanics of the cyclone with very little recourse to any empiricism.

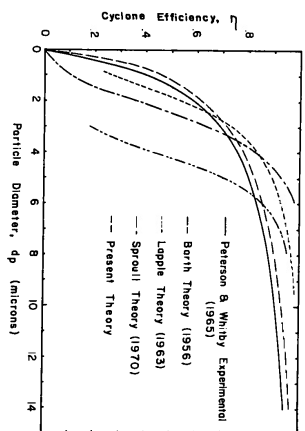


Fig. 13. Comparison of experimental Peterson & Whitley data with theoretical predictions by other methods.

OPTIMIZING CYCLONE DESIGN

Equation (20) may be used to optimize the design of a cyclone. Maximum collection efficiency will be obtained by using the largest possible value of the product $(C\psi)$. As was pointed out above, C may be maximized independently by appropriate choice of the set of seven geometric ratios which specify the cyclone shape. For a given set of operating conditions, the size of the cyclone may then be selected so as to maximize ψ independently. However, the pressure drop across the cyclone must also be taken into account. One criterion for optimum operation would be to maximize the ratio of collection efficiency to pressure drop. If a suitable equation for ΔP may be found, then it could be coupled with Equation (20) to determine that combination of design and operation which would produce a maximum value of $\eta/\Delta P$. The overall performance of cyclones operated in series may also be predicted by applying the equation to each cyclone separately, with the feed to the second cyclone taken as the outlet stream from the first. Such combinations may then be optimized.

It is planned to deal with these topics in detail in future papers, as well as to test the applicability of this model to centrifugal separators of different types of design, for example, scroll inlet or helical inlet cyclones.

NOTATION

Any consistent set of units may be used, except as noted

- B = outlet duct diameter for dust
- C = cyclone design number
- D = body diameter
- D_o = gas outlet diameter
- D_c = diameter of cyclone body, ft.
- D_i = diameter of cyclone body, in.
- H = overall cyclone height

- $K_o = a/D$
- $K_i = b/D$
- K_c = cyclone volume constant, see Equation (12)
- \dot{Q} = gas throughput-volume of gas/time flowing through cyclone
- R = radial distance from vortex center
- R_1 = radial position of particle at beginning of time period t
- R_2 = distance from vortex center to vortex wall, $D/2$
- S = outlet length
- T = Tengberg group, $d_p \sqrt{\rho_g \mu_g} / \mu D$
- T_1, T_2 = absolute temperatures
- V_{in} = volume of cyclone at natural length, see Equation (10)
- V_1 = annular shaped volume above exit duct to mid-level of entrance duct
- V_H = volume of cyclone below exit duct
- a = inlet height
- b = inlet width
- c = concentration of particles, number per volume
- d = diameter of cyclone at point where vortex turns, see Equation (10)
- d_p = particle diameter
- h = height of upper cylindrical body of cyclone
- l = natural length—distance below gas outlet where vortex turns
- n = vortex exponent
- n' = number of particles
- t = time for particle within vortex to go from R_1 to R_2
- t_{avg} = average minimum residence time of gas in cyclone
- t_{max} = maximum additional residence time of gas below exit duct level
- t_{tot} = average total residence time
- u_g = velocity of gas stream radially inward, see Equation (14)
- u_T = tangential velocity of particle
- u_{T2} = tangential velocity of particle at cyclone wall
- η = cyclone separation efficiency, by number of particles
- θ = sector angle
- ρ_p = density of particle
- μ = viscosity of gas
- ψ = cyclone inertial impaction parameter

LITERATURE CITED

1. Prockar, F., *Glenns Ann.*, **107**, 43 (1930).
2. Shepherd, C. B., and C. E. Lapple, *Ind. Eng. Chem.*, **31**, 972 (1939).
3. Alexander, R. Mck., *Proc. Austral. Inst. Min. Met.* (N.S.), **152**, 202 (1949).
4. First, M. W., paper presented at ASME Con. (1949).
5. ter Linden, A. J., *Proc. Inst. Mech. Eng.*, **160**, 233 (1949).
6. Caplan, Knowlton, in: *Air Pollution III* A. C. Stern (ed.), 2nd ed., p. 359, Academic Press, New York (1968).
7. Davies, C. N., *Proc. Inst. Mech. Eng.*, **1**, 185 (1952).
8. Stevens, W., *Industrial Gas Cleaning*, Chap. 6, Pergamon Press, New York (1966).

9. Umaney, L. E. R., "Theory and Design of an Improved Centrifugal Air Cleaner," Nat. Gas Turbine Estab. Rept. No. R-33 (1948).
10. Daniels, T. C., *Engineer*, **203**, 358 (1957).
11. Reith, D.J., private communication to the authors (1970).
12. Sarrin and C. J., *Trans. Inst. Chem. Engrs.*, **29**, 356 (1951).
13. Barth, Walter, *Brennstoff-Warme-Kraft*, **8**, 1 (1956).
14. Jost, T., *Trans. Inst. Chem. Engrs.*, **23**, 640 (1957).
15. Hawley, F. G., W. S. Badrich, and J. H. Blackett, "Measurement of Solids in Fine Gases," British Coal Utilization Research Assn., Leatherhead, England (1965).
16. Sproull, W. T., *Air Pollution Control Technol.*, **14**, 439 (1966).
17. Peterson, C. M., and K. T. Whitey, *ASHRAE J.*, **42** (1965).
18. Mori, Y., S. Akita, and S. Tanaka, *J. Chem. Eng. (Japan)*, **1**, 92 (1968).
19. van Ebbenhorst Tengbergen, H. J., *Staub*, **25**, 44 (1965).
20. Swift, Peter, *Steam Heating Engr.*, **38**, 453 (1969).
21. Lapple, C. E., "Predicting Efficiency of Cyclones," Air Pollution Eng. Manual, USPHS 99-A-P-40, p. 95 (1967).
22. Sproull, W. T., *Air Pollution and its Control*, p. 62, Exposition Press, Jericho, N. Y. (1970).

APPENDIX A. SUMMARY OF STEPS TO CALCULATE GRADE-EFFICIENCY CURVE

(Numbers refer to equations in text)

$$\eta = 1 - \exp - 2(C\psi)^{1/(2n+2)} \quad (20)$$

$$C = 8K_c/K_s/K_b$$

$$\psi = \frac{\rho_p^2 \eta_{r_2} (n+1)}{18\mu D}$$

$$n = \frac{(12D)^{0.14}}{2.5} \quad (1)$$

$$\frac{1-n_1}{1-n_2} = \left(\frac{T_1}{T_2}\right)^{0.3} \quad (1a)$$

1. Calculate n from Equation (1) using (1a) for temperature correction if the cyclone is to be operated at elevated temperatures.
2. Calculate the natural length l and compare this with the value of the dimension $(H-S)$.

$$l = 2.3D \left(\frac{D^2}{4b}\right)^{1/3} \quad (8)$$

(A) If $l < (H-S)$, calculate V_{H1} :

$$V_{H1} = \frac{\pi D^2}{4} (H-S) + \frac{\pi D^2}{4} \frac{(l+S-h)}{3} \left(1 + \frac{d}{D} + \frac{d^2}{D^2}\right) - \frac{\pi D^2 l^2}{4} \quad (10)$$

$$d = D - (D-b) \left(\frac{S+l-h}{H-h}\right) \quad (10a)$$

(B) If $l > (H-S)$, calculate V_{H1} :

$$V_{H1} = \frac{\pi D^2}{4} (H-S) + \frac{\pi D^2}{4} \frac{(H-h)}{3} \left(1 + \frac{B}{D} + \frac{B^2}{D^2}\right) - \frac{\pi D^2 (H-S)}{4} \quad (10b)$$

3. Calculate the K_c using either V_{H1} or V_H as determined above.

$$K_c = \frac{V_H + V_{H1}/2}{D^3} \text{ or } \frac{V_H + V_{H1}/2}{D^3} \quad (11)$$

$$V_2 = \frac{\pi(S-d/2)(D^2-D^2)}{4} \quad (7)$$

4. Calculate the cyclone design number C

$$C = \frac{8K_c}{K_s K_b} \quad K_2 = a/D \quad K_3 = b/D$$

5. Calculate the cyclone inertial impaction parameter ψ for a single particle size using cyclone diameter, air flow rate, air viscosity, and particle density as specified:

$$\psi = \frac{\rho_p^2 \eta_{r_2} (n+1)}{18\mu D}$$

6. Using the values of C , ψ , and n determine the collection efficiency, using either Equation 20 or Figure 5.

7. Repeat the calculation of ψ for a series of particle sizes and determine the efficiency for each size considered.

8. Plot the efficiency vs the particle size to obtain a grade-efficiency curve.

THE PROBLEM OF SMOKE FORMATION AND CONTROL

Bimal K. Biswas
and
Robert H. Essenhigh

Control of smoke by preventing formation would appear to be feasible or present with only a very limited number of fuels, as in some premixed gases and fuel oil flames. The alternative to prevention is combustion. This presents problems due to the varied natures of smokes: at one end of the spectrum of compositions the main constituent is carbon particles whose reactions have been very fully studied though interpretation is still open to debate; at the other end of the spectrum the composition is dominated by condensable vapors of a tarry nature, such as coal or solid waste volatiles, about which there is no record of prior investigations establishing the kinetics of rates of combustion other than the preliminary report on this present investigation (3)]. In this paper, experiments on the continuing investigation of smoke from computer card clippings are described. The method of experiment is the stirred-reactor device based on countervortex flow described previously (1 to 3). Greatly improved methods of determining smoke supply rates have allowed determination of the kinetic constants of combustion, found to be a second-order reaction. A first- or pseudo first-order reaction, proportional to the smoke concentration alone, is ruled out by the existence of an unstable intersection on a back plot of the appropriate Semenov/Vulfs graph. Stable intersections are obtained for a second-order reaction, with the rate proportional to the oxygen concentration as well as to the smoke concentration. The activation energy determined from the relevant Arrhenius plot is 16.5 kcal, which is typical of values frequently given for CO combustion. The result is in line with the common postulate that CO is the slow step in hydrocarbon combustion.

fuels, partly on account of the lack of knowledge of the mechanisms of soot and smoke formation, and partly on account of the essentially empirical nature of the practical devices utilizing prevention.

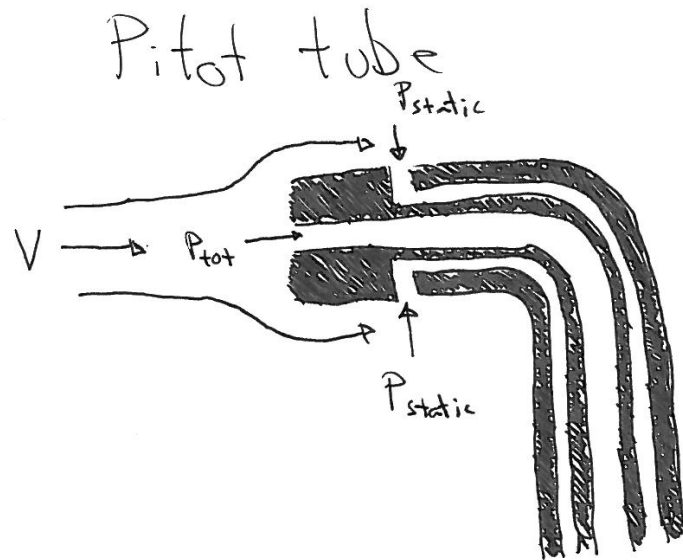
BACKGROUND

To set the combustion problems in context it is convenient to consider first, in brief outline, the circumstances of smoke formation and emission. Smoke may be described as the visible component in

This paper on the formation and control of smoke is concerned primarily with the problem of smoke elimination by combustion. To that end, we describe in this paper further experiments on combustion of smoke, extending those already published (1 to 3). Control through preventing formation is practiced in certain instances, as discussed below, but for reasons to be given we do not at present see prevention as a practical possibility with most

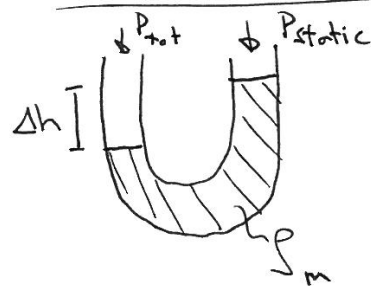
Combustion Laboratory, Pennsylvania State University, University Park, Pa. 16802.

Appendix E - Pitot Calculations



$$P_{tot} = P_{static} + P_{dyn} = P_{static} + \frac{1}{2} \rho_g V^2$$

$$\Rightarrow V = \sqrt{\frac{2(P_{tot} - P_{static})}{\rho_g}}$$



$$P_{tot} - P_{static} = \Delta h \rho_m g$$

$$V = \sqrt{\frac{2 \Delta h \rho_m g}{\rho_g}}$$